

**siRNA-nanocarriers Induce Fluorescent Protoporphyrin-IX by  
Silencing of Ferrochelatase -a New Tool for Tumor Imaging**

**Inaugural-Dissertation  
to obtain the academic degree  
Doctor rerum naturalium (Dr. rer. nat.)**

**Submitted to the Department of Biology, Chemistry and Pharmacy  
of Freie Universität Berlin**

**By**

**Kayiu Wan**

**From Guangdong, China**

**December, 2008**



**Germany**

The experiments presented in this thesis were carried out during the period of January 2005-October 2008 at AG Kemmner, Max-Delbrück-Centrum für Molekulare Medizin, Berlin, Germany, and Physikalisch-Technische Bundesanstalt, Department of Biomedical Optics, Berlin, Germany, as well as at AG Experimental Pharmacology, Max-Delbrück-Centrum für Molekulare Medizin, Berlin, Germany, under supervision of PD Dr. Wolfgang Kemmner and Prof. Dr. Rainer Haag.

**1st Reviewer:** PD Dr. Wolfgang Kemmner

**2nd Reviewer:** Prof. Dr. Rainer Haag

**Date of defense:** April 29, 2009

“No man is an island” *John Donne*

## Acknowledgements

First of all, I would like to thank my supervisors, Prof. Dr. Rainer Haag, Freie Universität Berlin, Germany, and PD Dr. Wolfgang Kemmner, Max-Delbrück-Centrum für Molekulare Medizin, Berlin, Germany, for permitting me to study and to do research in Germany. I am especially appreciative for their constant supervision and for sharing their knowledge with me in many ways as well as for their providing the intellectual and professional guidance for my dissertation during the course of my doctoral work throughout the years.

I would also like to express my gratitude to PD Dr. Thomas Moesta for his constant support, his kindness and helpfulness.

My special thanks go to Dr. Bernd Ebert, Dr. Steffen Rüttinger, and Dr. Rainer Macdonald, Physikalisch-Technische Bundesanstalt, Department of Biomedical Optics, Berlin, Germany, for their cooperation and excellent technical support in PpIX-determination, Two-photon excitation microscopy, and *in vivo* PpIX fluorescence detecting. Furthermore, I would like to thank Dr. Reinhard Zeisig, AG Experimental Pharmacology, Max-Delbrück-Centrum für Molekulare Medizin, Berlin, Germany, for his excellent technical support in preparation of folate-PEG cationic liposomes, and Ursula Klamm for the determination of ferrochelatase-enzyme activity.

I would like to acknowledge the technical help from my colleagues. They have been extremely helpful to me throughout the course of my doctoral studies. Virtually, I performed none of the work described here entirely on my own. I am indebted to the efforts of many who have provided assistance and support to me, namely Dr. Marion Fehlker, Dr. Christian Astrosini, Jan Voigt, Sabine Grigull, and Claudia Roefzaad. I would like to thank them for their kindness and support.

Thanks also to the former and present fellow students, and friends in Germany: Pia Forberich, Celine Kretschmer, and Susann Forster, for being so nice to me.

Finally, I would like to express my deep and heartfelt appreciation to my family, although no words can ever declare how much I adore them. My special appreciation goes to my lovely parents, Qieyue Wan and Liying Li, my son Chingyu Wan, my wife

Siuling Chan, and all my siblings, with whom I had so many interesting and valuable discussions throughout the research project. Many thanks for being so considerate and tolerant throughout the years. I do love you! Thank you for your love and support.

This study was financially supported by the Deutsche Forschungsgemeinschaft grant DFG Mo534/4.

Kayiu Wan

December 2008

## TABLE OF CONTENTS

<b>Acknowledgments</b>	i
<b>Table of Contents</b>	iii
<b>Zusammenfassung</b>	v
<b>Abstract</b>	vi
<b>1 Introduction</b>	1
1.1 The diagnostic window for detecting early malignancies	1
1.2 Carcinogenesis	2
1.3 PpIX-mediated fluorescent imaging technique	3
1.4 ALA-induced-PpIX photodetection and its limitations	5
1.5 Heme metabolism	9
1.6 Ferrochelatase	12
1.7 The mechanisms involved in selective accumulation of PpIX in tumor	12
1.8 RNAi	14
1.9 Delivery of siRNA molecules <i>in vivo</i>	18
1.9.1 The biodistribution characteristics of chemically synthesized siRNAs	18
1.9.2 Non-viral vectors used for delivery of siRNA <i>in vivo</i>	20
1.9.3 Enhanced permeability and retention effect	22
1.9.4 Folate-PEG cationic liposomes	22
1.9.5 Dendritic polyglycerol-based cationic polymers	24
1.10 Aims of the thesis	25
<b>2 Materials and methods</b>	26
2.1 Laboratory equipment	26
2.2 Chemicals and reagents	26
2.3 Patients' tissue samples	28
2.4 Tissue preparation, RNA extraction and cDNA synthesis	28
2.5 Cell culture	28
2.6 Extraction and purification of RNA from cultured cells and cDNA synthesis	29
2.7 Quantitative real-time TaqMan PCR	30
2.8 PpIX determination	30
2.9 Determination of ferrochelatase enzyme activity	31
2.10 Preparation of siRNA and transfection <i>in vitro</i>	31
2.11 Two-photon microscopy	32
2.12 Preparation of PEG cationic liposomes and folate-PEG cationic liposomes	34
2.13 Preparation of the siRNA-carrying PG-based nanoparticles	35
2.14 Fluorescent microscopy	35

2.15 Confocal microscopy	36
2.16 PpIX-mediated fluorescent imaging for detecting tumors <i>in vivo</i>	36
2.17 Data evaluation	38
<b>3 Results</b>	39
3.1 Expression of heme metabolism relevant enzymes in colorectal tissues	39
3.2 FECH mRNA expression in different parts of the gastrointestinal tract	41
3.3 FECH expression correlates with the potential to accumulate PpIX	43
3.4 Silencing of FECH-expression by siRNA-treatment <i>in vitro</i>	43
3.5 PpIX accumulation in LS174T cells treated with FECH-siRNA	44
3.6 PpIX accumulation after combined FECH-siRNA and ALA treatment	45
3.7 Two-photon microscopy for intracellular PpIX fluorescence imaging	46
3.8 Visualization of the process of cationic liposomes mediated uptake of siRNAs	50
3.9 Silencing efficacy of FECH-siRNA transfected by folate-PEG cationic liposomes	53
3.10 Preliminary results for detecting millimeter-sized tumors in the mouse model	55
<b>4 Discussion</b>	59
4.1 Relationship between FECH expression and PpIX formation	59
4.2 Tumor targeting delivery of siRNAs mediated by nonviral vehicles	61
4.2.1 Transfection efficiency	61
4.2.2 Tumor selectivity	64
4.2.3 Biocompatibility	67
4.3 The diagnostic application potential of the siRNA-based inhibitor of FECH for early cancer detection	68
<b>5 Prospects and future research directions</b>	73
<b>List of references</b>	75
<b>Abbreviations</b>	89

## Zusammenfassung

**Einführung:** Während der Entwicklung verschiedener Karzinome zeigt sich bereits früh eine selektive und endogene Anhäufung des fluoreszenten Vorläufermoleküls von Häm, des Protoporphyrin IX (PpIX), im Tumorgewebe. Der Nachweis der durch PpIX ausgelösten Fluoreszenz könnte daher als eine neue Methode zur Diagnose früher Tumorstadien verwendet werden. Allerdings ist bisher nicht geklärt, was die erhöhte PpIX Fluoreszenz in Karzinomen induziert.

**Resultate:** Quantitative RT-PCR Untersuchungen zeigten eine Minderexpression der Ferrochelatase (FECH), eines wichtigen Enzyms der Hämsynthese, das die Bildung von PpIX aus Häm katalysiert, in Magen-, Kolon- und Rektumkarzinomen. Nach Einsatz der RNA-Interferenz-Technik mit siRNA zum Knock-down der FECH-Expression in LS174T kolorektalen Zellen war eine um das 20-fache erhöhte Fluoreszenz der PpIX nachweisbar. Dies konnte in vergleichbaren Versuchen auch für MDA-MB-435-Zellen gezeigt werden. Wurden die Zellen außerdem zusätzlich zur FECH-siRNA mit dem Substrat der Hämsynthese, der Aminolävulinsäure (ALA), behandelt, konnte eine dramatische Erhöhung der PpIX-Anhäufung um einen Faktor 50 im Vergleich zu Zellen, die nur mit ALA behandelt wurden, erreicht werden. Diese *in-vitro*-Ergebnisse wurden inzwischen in *in-vivo*-Experimenten bestätigt. Eine kombinierte Behandlung von xenotransplantierten Mäusen mit einer in Folat-PEG-kationischen Liposomen verpackten oder an Dendritic-Polyglycerol-kationischen gebundenen FECH-siRNA zusammen mit ALA ermöglichte den Nachweis von millimetergroßen Karzinomen der Nackt-Mäuse anhand der PpIX-abhängigen Fluoreszenz bei 630 nm nach Bestrahlung mit Laserlicht der Wellenlänge 405 nm. Weder eine Behandlung mit siRNA oder ALA allein führte zu vergleichbaren Fluoreszenzemissionen.

**Schlussfolgerung:** Eine experimentell induzierte Minderexpression des Ferrochelatase-Enzyms führt zu einer dramatischen Erhöhung der PpIX-Fluoreszenz in verschiedenen Tumorzelllinien. Diese Ergebnisse unterstützen die Hypothese, dass die Minderexpression der Ferrochelatase die beobachtete endogene PpIX-Fluoreszenz in humanen Karzinomen verursacht. Die *in-vivo*-Versuche zeigen, dass eine Gabe von FECH siRNA in Verbindung mit einer sehr geringen Dosis von ALA verwendet werden kann, um millimetergroße Karzinome im Maus-Modell zu identifizieren. Neben den diagnostischen Möglichkeiten, die sich daraus eröffnen, könnte diese Methodik den Weg zu einer neuen Art der photodynamischen Therapie von Karzinomen ebnen, bei der die Dosis an ALA sehr gering gehalten werden kann, um unerwünschte Nebenwirkungen zu vermeiden.

## Abstract

**Background:** Selective and endogenous accumulation of Protoporphyrin IX (PpIX), a fluorescent precursor of heme, is one of the early events associated with the development of human carcinomas. Previous investigations of our group demonstrated preferential accumulation of PpIX in gastrointestinal malignant tissues. However, the reason for this accumulation has not been clarified yet. PpIX-mediated fluorescent imaging might be a new approach for visualization of early cancers.

**Results:** A significant down-regulation of ferrochelatase (FECH) expression in gastric, colonic, and rectal carcinomas was determined by quantitative RT-PCR of human tissue samples. Experimentally-induced knock down of FECH expression in LS174T cells by using RNA-interference (RNAi) technique led to an accumulation of PpIX of more than 20-fold compared to untreated cells. Similarly, silencing of FECH in MDA MB 435 cells showed a considerable enhancement of PpIX accumulation. Incubation of LS174T cells with the substrate of heme-synthesis, aminolevulinic acid (ALA) in a concentration of 0.1 mM did not induce significant accumulation of PpIX. However, if cells were treated with siRNA followed by ALA, a dramatic enhancement of PpIX accumulation by a factor of 50 was achieved compared to cells treated only with ALA. These findings were further confirmed by *in vivo* experiments in nude mice xenotransplanted with human mammary carcinoma cell lines. Application of a single dose of 5mg/kg ALA alone did not result in sufficient fluorescence for *in vivo* detection of the xenografted tumors. However, if mice were treated with siRNA followed by ALA, PpIX-dependent fluorescence hotspots were detected at the sites of the millimeter-sized tumors in nude mice.

**Conclusion:** Functional application of siRNA alone leads to a dramatic enhancement of PpIX accumulation in colorectal cancer cells and human mammary carcinoma cells, supporting the hypothesis that down-regulation of FECH expression plays a crucial role for selective accumulation of PpIX in cancerous tissues. *In vivo* application of siRNA-based inhibitor of FECH in conjunction with a very low dose of ALA leads to a significantly higher endogenous PpIX level at the site of the xenografted tumor, which provides a promising new modality for detecting the millimeter-sized tumor in the mouse model. Either siRNA encapsulated within folate-PEG cationic liposomes or bound to polyglycerol-based nanocarriers worked well in this regard. This approach may facilitate early tumor diagnosis. Moreover, it may pave the way to a new kind of specific photodynamic therapy for cancerous diseases as the routinely applied high concentrations of ALA which have a number of undesired side effects can be reduced by using FECH-siRNA.

## 1 Introduction

### 1.1 The diagnostic window for detecting early malignancies

Early detection of cancer has been, and will continue to be the best way to significantly improve therapeutic outcome. Early cancer diagnosis aims to find primary tumor prior to metastasis. Unfortunately, in clinical practice, solid tumors are diagnosed at a rather late stage, when more than half of all patients had already developed metastases. For example, approximately 30% of breast-cancer patients had presented with clinically detectable metastases at the time of initial diagnosis, and a further 30-40% of patients had harbored occult metastases<sup>1</sup>. Thus, less than one third of newly diagnosed solid tumor patients can be cured by local therapeutic modalities alone<sup>2</sup>. Approximately 70% of patients are beyond the hope of a complete surgical extirpation or radiation cure.

Invasion and metastasis are the most insidious and life-threatening aspects of cancer<sup>3</sup>. The ability of malignant cells to invade through normal tissues and to metastasize to distant sites throughout the body is the main cause of death in cancer patients<sup>4</sup>. The most critical pathologic turning point in cancer is the establishment of metastasis. Approximately 90% of all cancer patients die from metastases<sup>5, 6, 7</sup>.

Conventional anatomic imaging techniques typically detect cancers when they are one centimeter or greater in diameter, at which point they already consist of  $>10^9$  cancerous cells (including circulating and microscopic metastatic deposits)<sup>8</sup>. Endoscopy can provide high-resolution imaging of the entire hollow organs surface. However, flat epithelial cancerous lesions and carcinoma *in situ* remain frequently unchanged in color or morphology<sup>9</sup>. Thus, early malignancies can easily be missed during ordinary white-light examinations as their small size and appearance can be similar to that of normal tissues under white-light illumination.

Carcinogenesis is usually a long-term pathological process. A wide range of research, including both, basic studies and clinical trials, provided numerical evidence to support that a substantial diagnostic window exists during carcinogenesis for detecting early malignancies. The acquisition of the invasive and angiogenic phenotype may extend back over a period of 10 years, which offers a window for early detection of tumor prior to metastasis. This important window can be defined as the period in the course of which transition from a hyperproliferative state to acquisition of the capacity for invasion and metastasis occurrence takes place<sup>10</sup>.

## 1.2 Carcinogenesis

Cancer is a malignant cellular disorder which represents a large and complex group of related but distinct diseases, characterized by uncontrolled multiplication and disorganized growth of affected cells. Genetic alterations are responsible for cancer development and progression. Cancer results when cells accumulate a variety of genetic defects of the proto-oncogenes, tumor suppressor genes, and DNA repair genes which are involved in the control of cell growth and division. That will lead to uncontrolled cellular multiplication. Cancerous cells manifested a significant disruption of the normal, orderly and regulated cycle of cell replication, with the capacity to invade other tissues, either by direct growth into adjacent tissue through invasion or by implantation into distant sites by metastasis.

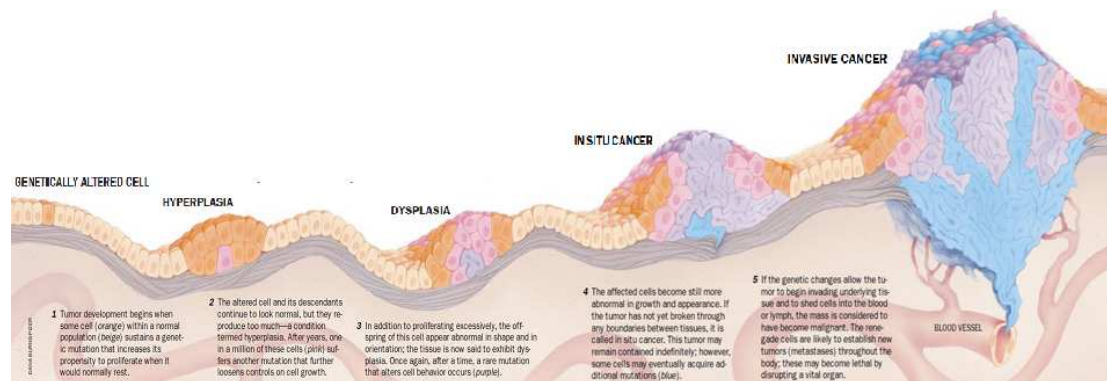


**Figure 1.1 Schematic description of cancerogenesis in an epithelium**

(Reproduced from: Weinberg RA, *Sci Am* (1996), 275: 62-70)

According to currently accepted theories of carcinogenesis, this is assumed to be a multistep process in which genetic alterations accumulate, ultimately producing the neoplastic phenotype<sup>11</sup>. Tumor development begins when some cell within a normal population sustains a genetic mutation that increases its propensity to proliferate when it would normally rest<sup>12</sup>. Firstly, acquired genetic susceptibility enables stepwise selection of variant sublines of cancer cells. During this time interval, these cells undergo several modifications. As a result of chronic irritation, these cells may differentiate towards a phenotype better adapted to the prevailing environment. Thereafter, hyperplasia and metaplasia occur. Hyperplasia takes place if the cell population is capable of replication. Metaplasia is a reversible change in which one adult cell type is replaced by another adult cell type. In this type of cellular adaptation, cells sensitive to a particular stress are replaced by other cell types that better withstand the adverse environment. In case adverse environment is a carcinogen and is not removed, over time, the epithelia are modified further and are eventually characterized by an increasing degree of cellular and nuclear atypia, which is called dysplasia. This step is no longer reversible.

The following step is the carcinoma *in situ* (CIS). At this stage, the entire epithelial layer is replaced by atypical cells. CIS is an early form of carcinoma defined by the absence of invasion of surrounding tissues. In other words, if the neoplastic cell growth has not yet broken through any boundaries between tissues (for instance the basement membrane), it is called a carcinoma *in situ* (CIS). As the neoplastic cells proliferate in their normal habitat, they are named “*in situ*”<sup>13</sup>. Most forms of CIS have a real potential to turn into invasive carcinoma, if left untreated long enough. It is not known which fraction of carcinomas *in situ* evolve towards invasive lesions, but it is believed that almost all invasive lesions have evolved from an earlier carcinoma *in situ*.

### **1.3 PpIX-mediated fluorescent imaging technique**

In fact, cancerous tissue often shows differences not only in its genetic mutations, but also in its biological behaviors such as biochemical alterations. Therefore it can result in its optical characteristics.

Cancer metabolic alterations are often associated with or prior to the onset of disease<sup>14, 15</sup>. Biochemical alterations and morphological changes associated with pre-cancer perturb tissue absorption, scattering and fluorescence properties. Thus, optical spectroscopy can probe pre-cancerous changes<sup>16</sup>.

PpIX mediated fluorescent imaging technique can act as a promising molecular optical imaging tool for the detection of malignancies at their earliest stages. Selective accumulation of PpIX in cancerous tissues has been proved to be one of the early events associated with carcinogenesis<sup>17</sup>. The general property of PpIX loading by tumor cells, either following ALA dosing or without administration of exogenous ALA, has stimulated numerous basic research and clinical studies for potential diagnostic and therapeutic uses<sup>18, 19, 20, 21</sup>. After the application of appropriate wavelength and moderate intensity light to excite PpIX, localized fluorescent hotspots could be observed at the location where the disease was endoscopically visible. In this way, the tiny cancerous lesions, such as dysplasia, carcinomas *in situ*, and macroscopically indiscernible premalignancies, could be observed by PpIX-mediated fluorescent-imaging approach.

In contrast to conventional anatomical diagnostic imaging, molecular imaging (MI) technique sets forth to probe the molecular abnormalities that are the basis of disease rather than to image the final effects of these molecular alterations<sup>22, 23</sup>.

Molecular imaging includes all imaging methods applied in the identification, characterization and assessment *in vivo* of biological processes which occur at the cellular and molecular level <sup>24</sup>. The most recent definition of molecular imaging has been put forth by a task force organized by the Radiological Society of North America (RSNA) and the Society of Nuclear Medicine (SNM). To quote: “Molecular imaging techniques directly or indirectly monitor and record the spatiotemporal distribution of molecular or cellular processes for biochemical, biologic, diagnostic, or therapeutic applications” <sup>25</sup>.

In general, molecular and biochemical alterations occur prior to major structural tissue changes. To probe the molecular and biochemical alterations by optical molecular imaging approach allows finding the primary tumor prior to morphological structures changes.

Profio <sup>26</sup> and Kinsey <sup>27</sup> pioneered the development of dedicated fluorescence instrumentation using photoelectronic detectors. This initiated clinical and animal model studies of haematoporphyrin derivative-mediated photodynamic therapy (PDT) by Dougherty and coworkers <sup>28</sup>. By means of ultraviolet irradiation, Harris <sup>29</sup> observed red fluorescence in ulcerated human oral carcinoma. Endogenous porphyrin that is not associated with microorganisms has also been speculated to cause red fluorescence in oral cancer <sup>19</sup>. The porphyrin-fluorescence features in human cancer in comparison with non-cancerous tissues were investigated recently. Onizawa *et al.* reported that autofluorescence in human oral cancer correlated with the progression of lesions, and that fluorescent substances such as protoporphyrin were produced in association with the cancerous tissue. The autofluorescence in human oral cancer was mostly dependent on protoporphyrin IX, coproporphyrin, and related compounds <sup>20</sup>. Moesta *et al.* examined the colorectal resection specimens, lymphatic and liver metastases from 33 colorectal cancer patients, a total of 1053 palpable mesenteric nodes were fluorimetrically characterized *ex vivo*. PpIX was identified as the predominant fluorophore in primary tumors and their metastases <sup>21</sup>.

Compared to other exogenous photosensitizers, PpIX is one of the intermediate products in heme-cycle, which naturally exists in the body. The hematoporphyrin is the most labile of the natural porphyrins derived from PpIX. PpIX serves as both: fluorescent marker for photodynamic diagnosis (PDD) as well as photosensitizer for photodynamic therapy (PDT) <sup>30, 31, 32, 33, 34</sup>.

Chemically, PpIX is best characterized as a lipophilic structure. In an aqueous

environment, it appears in formation of dimmers<sup>33</sup>. Excited at 405 nm light, the PpIX-related fluorescence in tissue has a dual peak, at approx. 635 and 705 nm, emission in the red region<sup>34</sup>.

PpIX-mediated optical molecular imaging provides the possibility of *in situ* detection of millimeter-sized cancer foci or micrometastases, *e.g.*, the tiny tumors in peritoneal cavity, which were beyond the detection threshold of many other conventional diagnostic imaging techniques, were observed by using PpIX-mediated fluorescent imaging approach. ALA-induced PpIX was also used as a photosensitizer for selective destruction of ovarian micrometastases by photodynamic therapy in an animal model<sup>35, 36, 37, 38, 39, 40, 41</sup>.

Alterations in tissue composition between normal and malignant tissue form a basis for the diagnostic potential for neoplastic tissue<sup>42</sup>. Krieg *et al.* suggested that the research of tumor-cell selectivity of PpIX fluorescence should focus on the mechanisms responsible for an altered PpIX metabolism to find tumor-specific target molecules<sup>43</sup>.

#### **1.4 ALA-induced-PpIX photodetection and its limitations**

To detect malignancies by PpIX-dependent autofluorescence certainly poses advantages because it does not require any treatment or staining of the tissues. However, tumor-specific PpIX autofluorescence is rather weak *in vivo*. Thus, administration of exogenous photoactive compounds might improve the sensitivity considerably and achieve greater diagnostic accuracy for detecting cancers.

Berlin studied the pharmacokinetics of ALA in humans and rats by radio-labelled ALA in 1956<sup>44, 45</sup>. ALA is a naturally occurring, 5-carbon amino acid. It is easily dissolved in water and in a large variety of solvents and emulsions. At a pH around 5, ALA is chemically stable, but can react non-enzymatically to several condensation products at higher pH values<sup>46</sup>.

The last step in the heme-synthetic route involves conversion of PpIX (a photosensitizing species) to heme (a nonphotosensitizing agent). The investigators have also found that exogenous administration of ALA could induce the cellular PpIX accumulation<sup>47, 48</sup>. In 1986, Pottier first reported that using ALA induced PpIX to obtain red fluorescence excitation and emission spectra *in vivo* and developed a sensitive spectrophotofluorometry system that permitted the rapid and non-invasive determination of fluorescence-emission spectra in the skin of living non-anesthetized

animals<sup>32</sup>. The selective photodynamic destruction effect of the ALA-induced PpIX was experimentally introduced by Malik in 1987 in the treatment of erythroleukemic cells *in vitro*. They present a specific method for erythroleukemic cell inactivation<sup>49</sup>. Based upon their own data on ALA-mediated PpIX production in the skin of mice<sup>50</sup>, Divaris *et al.* discovered a selective tumor localization of endogenous porphyrins induced by ALA. An elevated PpIX concentration can be obtained through the heme-cycle following administration of ALA. The fully clinical application potential of the method was recognized by Kennedy and Pottier, who started to treat cancers in the skin of humans by administering the ALA topically<sup>51, 52</sup>.

It is well documented that ALA-induced PpIX is accumulated more in tumor cells than in normal cells, *e.g.*, in skin<sup>53</sup> and various organs, such as brain<sup>54, 55</sup>, oral cavity<sup>56, 57</sup>, esophagus<sup>58, 59, 60</sup>, gastrointestinal tract<sup>61, 62</sup>, colon<sup>48</sup>, lungs<sup>63</sup>, ovary<sup>36, 39</sup>, cervix<sup>64, 65</sup>, bladder<sup>66, 67, 68, 69, 70, 71, 72</sup>, and leukemic cells<sup>49, 73, 74, 75</sup>.

In 1999, 20%  $\delta$ -aminolevulinic acid (Levulan<sup>R</sup>) was approved by the US Food and Drug Administration (FDA) for a topical treatment of actinic keratoses (AKs) in combination with blue light. Actinic keratoses can develop into skin cancer. When a malignant change does occur, the cancer is called a squamous cell carcinoma. This unique system uses a combination of ALA topical solution and blue light to target AKs. 20%  $\delta$ -aminolevulinic acid is the only FDA-approved formulation of the topical treatment ALA-PDT system for actinic keratoses<sup>76</sup>. However, none of the currently used ALA or other photosensitizers is clinically approved by FDA for photodynamic diagnosis (PDD).

ALA-induced PpIX has been assessed experimentally for diagnosis and treatment of various medical indications. However, the limited local bioavailability of ALA has widely prevented its use in daily clinical practice, and a significant hurdle remained to the development of this technique as a routine clinical diagnostic tool is the non-negligible neurotoxic effects of exogenous ALA after systemic administration.

Regula *et al.* measured the plasma ALA concentrations during oral administration of ALA in 13 patients with gastrointestinal cancers. The mean plasma ALA concentration in 11 patients 6 hours after a fractionated dose of 30 mg/kg was 63 $\mu$ mol/L, the ALA levels in 2 other patients 6 hours after a dose of 60 mg/kg were 116 and 205 $\mu$ mol/L, respectively<sup>77</sup>. Information is now available to show that the mean normal plasma level of ALA is 92nmol/L<sup>78</sup>. The mean plasma concentration of ALA in the asymptomatic carriers of the acute intermittent porphyria

was 1.7  $\mu\text{mol/L}$  <sup>79</sup>.

It has been reported that doses of exogenous ALA, ranging from 30 to 1000 mg/kg, were used in the ALA-induced PpIX mode. Obviously, applying a high dose of exogenous ALA for PDD/PDT may lead to much higher plasma ALA levels in those who received the examination or treatment than that of healthy individuals and even porphyric patients. Besides the risk of prolonged skin photo-toxicity, these high doses of ALA are known to produce a number of neurotoxic manifestations and in this case, ALA is generally considered to be the most likely neurotoxic compound <sup>80, 81, 82, 83, 84, 85, 86, 87, 88</sup>. This may be in part due to the fact that ALA is somewhat similar in structure to the neurotransmitter G-Aminobutyric acid (GABA) <sup>89, 90</sup>.

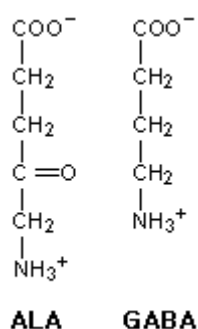


**Figure 1.2 Chemical structures of ALA and GABA**

(Reproduced from: Albert C, Quarterly Journal of Medicine 1987, 241: 377-392)

After blocking nerve transmission by tetrodotoxin in isolated rabbit duodenum, ALA 0.2-0.8  $\times 10^{-3}$  M can inhibit muscle tone and both spontaneous and induced contractions <sup>91</sup>. ALA can have a direct effect on rabbit gut smooth muscle. This may be partly due to direct effects of ALA on the alpha adrenergic receptors <sup>92</sup>. GABA is an inhibitory neurotransmitter in both spinal cord and cerebral cortex <sup>93, 94</sup>. ALA can mimic GABA action by increasing chloride ion conductance in the crayfish stretch receptor neurones <sup>95</sup>.

ALA has also been shown to impede  $\text{Na}^+$ ,  $\text{K}^+$ -ATPase activity in rabbit brain preparations <sup>96</sup>. Since inhibition of sodium-potassium pump can influence neuromuscular transmission by increasing neurotransmitter release, ALA is believed to act as a GABA agonist.

ALA was undetectable in most samples of normal cerebrospinal fluid (CSF). However,

the exogenous ALA may penetrate across the blood-brain barrier <sup>97, 98, 99</sup> and the central nervous system itself may synthesize porphyrins from exogenous ALA and, the reactive oxygen species (oxygen radicals) are generated during ALA autoxidation. Therefore, much care should be taken in clinical trials of systemic ALA administration, particularly for the patients with porphyria or severe diseases of the liver and kidneys, because acute attacks of hepatic porphyrias with neurovisceral symptoms are always associated with high urinary excretion of ALA <sup>100</sup>, thus, elevated ALA is considered responsible for neurological symptoms, and ALA is toxic to the brain.

In patients receiving oral administration of ALA in doses of up to 60 mg/kg, transient nausea and vomiting were noticed in 15-30% of them, and 25-30% developed temporary changes in various liver-function tests <sup>77, 101</sup>. Gorchein and Webber found that the maximum plasma ALA levels in 2 patients with acute intermittent porphyria were only 9 and 12  $\mu\text{mol/L}$ , but with severe neurogenic dysfunction, including respiratory paralysis, quadriplegia, and extensive autonomic abnormalities <sup>78</sup>. Infusion of haematin was given to decrease the ALA levels, but there had been no obvious clinical benefit. Thus, they doubted that uncertainties still exist for the plasma ALA levels in relation to the pathogenesis of the neurological manifestations in those patients with acute intermittent porphyria. However, this could be explained by inter-individual susceptibility to the effects of haematin and/or ALA on account of genetic or other interacting factors.

Wide range and abundance of evidence supports that ALA does have effects on the nervous system. The accumulation of ALA revealed definite neurotoxic effects *in vivo* and is responsible for the neurological manifestations. Therefore it is generally considered to be the neurotoxic compound <sup>80, 81, 82, 83, 84, 85, 86, 87, 88, 96</sup>.

The neurotoxic symptoms can be life-threatening in some cases, especially if the muscles that control breathing become paralyzed. To ensure safer clinical practice, the application of a lower dose of exogenous ALA is now a universally accepted concept in the way of using ALA to induce PpIX for fluorescent imaging detection. Thus, there is a tremendous incentive for developing more sensitive modalities which can achieve efficient enhancement of intracellular PpIX and avoid or reduce the undesired side effects of exogenous ALA thereby obtain safer, greater meaningful information and more diagnostic accuracy for detecting cancers at their earlier stages.

## 1.5 Heme metabolism

The biosynthesis of heme in mammalian cells involves co-operation between mitochondrial and cytoplasmic compartments. The first step and the last 3 steps occur within mitochondria, the rest 4 intermediate steps are cytoplasmic.

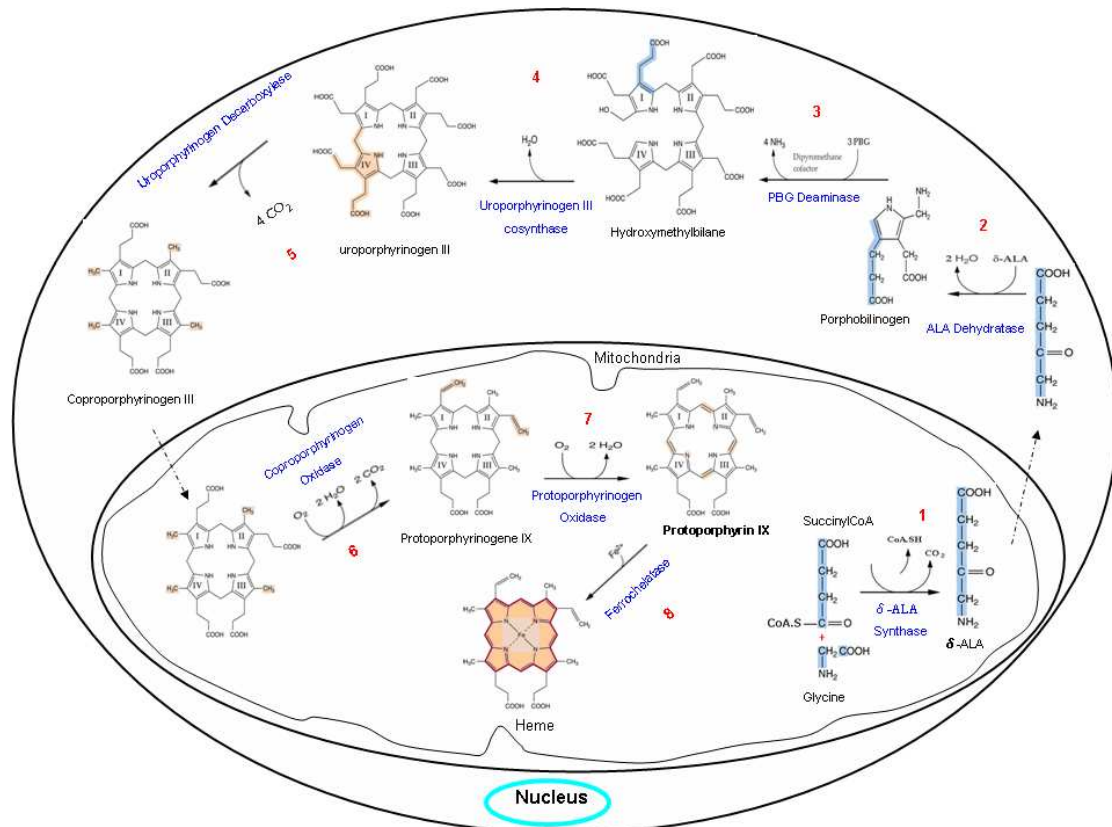


**Figure 1.3 The Heme Biosynthesis Pathway**

The first step begins with the condensation of succinyl-coenzyme A and glycine to form δ-aminolevulinic acid, which catalyzes by δ-Aminolevulinic synthase (1). Then the products are transported to cytoplasm. ALA dehydratase induces the condensation of 2 molecules of ALA to yield porphobilinogen (2). Porphobilinogen deaminase catalyzes successive condensations of 4 molecules of porphobilinogen to release hydroxymethylbilane (3). Uroporphyrinogen synthase converts hydroxymethylbilane to uroporphyrinogen III (4). Uroporphyrinogen decarboxylase removes four acetic acid carboxyl groups from uroporphyrinogen to produce the coproporphyrinogen, and then the coproporphyrinogen will be transported into mitochondria (5). Coproporphyrinogen oxidase decarboxylates and oxidizes 2 of the 4 propionic side chains of the coproporphyrinogen to form the protoporphyrinogen IX (6). Protoporphyrinogen oxidase removes 6 hydrogens from protoporphyrinogen IX to produce the protoporphyrin IX (7). The final step is the incorporation of ferrous iron into protoporphyrin IX to form heme, which catalyzed by Ferrochelatase (8).

Heme synthesis begins with condensation of succinyl-coenzyme A and glycine to form  $\delta$ -aminolevulinic acid (ALA), which catalyzed by  $\delta$ -Aminolevulinic synthase (ALAS). Using isotopic tracers, it was initially found that N & C atoms of heme are derived from glycine and acetate <sup>102, 103</sup>. It was later determined that the labeled acetate enters Krebs Cycle as acetyl-CoA, and the labeled carbon becomes incorporated into succinyl-CoA, the more immediate precursor of heme.

ALAS is in the mitochondria, where the substrate, succinyl CoA, is produced. In vertebrates, there are two ALAS isoenzymes: ALAS1 is the housekeeping enzyme, which is required for cytochromes synthesis and is inhibited by heme. ALAS2 is an erythroid isozyme, which is required for hemoglobin synthesis and is not inhibited by heme. The enzyme is located on the matrix side of the inner mitochondrial membrane <sup>104, 105</sup>.

The next enzyme in the pathway, ALA dehydratase also called porphobilinogen synthase, is located in the cytosol and induces the condensation of two molecules of ALA to yield porphobilinogen (PBG) with the elimination of two water molecules. Porphobilinogen is the first pathway intermediate that includes a pyrrole ring <sup>106</sup>.

The porphyrin ring is formed by condensation of four molecules of porphobilinogen. Porphobilinogen deaminase (PBGD) catalyzes successive condensations of porphobilinogen, releases the tetrapyrrole hydroxymethylbilane. Uroporphyrinogen III synthase converts the linear tetrapyrrole hydroxymethylbilane to the macrocyclic uroporphyrinogen III. Both enzymes are located in the cytosol, and the action of PBGD is the rate-limiting step. The combined action of PBGD and uroporphyrinogen III synthase condenses four molecules of PBG in a head-to-tail manner and cyclizes the tetrapyrrole chain to form uroporphyrinogen III <sup>107</sup>.

A series of decarboxylations and oxidations have to take place before iron can be inserted into the tetrapyrrole ring. The first part of this process is performed in the cytosol by uroporphyrinogen decarboxylase. This enzyme removes four acetic acid carboxyl groups from uroporphyrinogen to form coproporphyrinogen <sup>106</sup>.

The last three enzymatic reactions take place in the mitochondrion. Coproporphyrinogen III is now exposed to coproporphyrinogen oxidase which is situated in the intermembrane space of the mitochondria. The enzyme decarboxylates and oxidizes the propionic side chains in ring A and B to vinyl groups, and protoporphyrinogen IX is formed <sup>108, 109, 110</sup>.

The next step is the oxidation of the tetrapyrrole ring by removal of six hydrogens from protoporphyrinogen IX to produce protoporphyrin IX, catalyzed by protoporphyrinogen oxidase. The enzyme is embedded in the inner mitochondrial membrane with its active site on the matrix side of the membrane <sup>111</sup>. It is an oxygen-dependent enzyme with high substrate specificity.

The last step of heme synthesis is incorporation of ferrous iron into PpIX, which takes place in the mitochondria catalyzed by ferrochelatase (EC 4.99.1.1) and the eukaryotic enzyme is located in the inner mitochondrial membrane facing the matrix of the mitochondrion <sup>112</sup>. Ferrous iron ( $\text{Fe}^{++}$ ) is added to protoporphyrin IX via ferrochelatase to yield heme. Eukaryotic ferrochelatase is synthesized in the cytosol and then imported into the mitochondria.

85% heme comes from erythrocytes, the rest from a turnover of cytochromes p450s and immature erythrocytes, *i.e.*, most of the heme is from the degradation of hemoglobin. Since in the steady state 6 - 8 grams of hemoglobin are synthesized daily, 6 - 8 grams must also be degraded. After approximately 120 days in the circulation, red blood cells are taken up and are degraded by the reticuloendothelial system, particularly in the liver and spleen. This gives rise to about 300 milligrams of heme. As heme is not reutilized, it has to be degraded and excreted. Although heme is not recycled, its iron is conserved. Normally, senescent and damaged erythrocytes are sequestered by the spleen, which processes them in a manner that preserves their iron content. The microsomal heme oxygenase system of the reticuloendothelial cells starts degradation of heme.

Degradation of heme is catalyzed by Heme Oxygenase (HO) (EC 1.14.99.3). HO is the first and the rate-limiting enzyme in the catabolism of heme to yield equimolar amounts of biliverdin, carbon monoxide (CO) and free iron <sup>113, 114</sup>. The source of bilirubin is from degradation of heme. In the presence of NADPH and  $\text{O}_2$ , the enzyme add hydroxyl group to the methenyl bridge between two pyrrole rings with a concomitant oxidation of ferrous iron ( $\text{Fe}^{++}$ ) to Ferric iron ( $\text{Fe}^{+++}$ ). In the second reaction biliverdin reductase reduces the central methene bridge of biliverdin, producing bilirubin. Bilirubin is transported to the liver by binding non-covalently to albumin. In the hepatocyte, the solubility of bilirubin is increased by adding two molecules of glucuronic acid, which catalyzed by bilirubin glucuronyl-transferase. The major product is bilirubin diglucuronide. Bilirubin diglucuronide is actively transported against a concentration gradient into the bile canaliculi and finally excreted via feces and/or urine.

## 1.6 Ferrochelatase

Human ferrochelatase (EC4.99.1.1) is encoded by a single gene. The chromosomal localization of the human ferrochelatase gene has been mapped to chromosome 18q21.3<sup>115, 116</sup>. Ferrochelatase is an iron sensor in mitochondria<sup>117, 118</sup>. It is the terminal enzyme of the heme synthetic pathway<sup>119</sup>. The function of ferrochelatase is to catalyze ferrous iron into protoporphyrin IX to form heme. Mammalian ferrochelatase utilizes ferrous iron as the physiological metal substrate. The enzyme is capable of utilizing several other divalent metals (*e.g.* Zn<sup>++</sup> Co<sup>++</sup> and Ni<sup>++</sup>) as substrates as well<sup>120, 121</sup>, and there are a wide variety of IX isomer porphyrins *in vitro*. Certain other divalent metals such as Mn<sup>++</sup>, Cd<sup>++</sup>, and Hg<sup>++</sup> are inhibitors<sup>122</sup>. Ferric ion is not used as a substrate<sup>123</sup>.

Decreased ferrochelatase activity leads to an accumulation of precursor porphyrins within cells, particularly in those tissues (*e.g.*, liver and bone marrow) where there is a high rate of heme synthesis. The excess production of protoporphyrin results in the disease protoporphyria<sup>124</sup>. As with most mitochondrial proteins, eukaryotic ferrochelatase is nuclear encoded, synthesized in the cytoplasm as a precursor form, and subsequently processed to the mature protein during translocation to the matrix side of the inner mitochondrial membrane in an energy-requiring step that involves proteolytic processing of the precursor form of the protein to its mature form<sup>125, 126</sup>. Animal ferrochelatases possess a [2Fe-2S] cluster<sup>127</sup>. Recombinant human ferrochelatase was produced and purified as previously described<sup>128</sup>.

## 1.7 The mechanisms involved in selective accumulation of PpIX in tumor

Heme is formed physiologically out of its precursor PpIX. Under physiologic conditions, heme synthesis is regulated in a negative feedback control of the ALA synthase by free heme, *i.e.*, the amounts of the intermediate products between ALA and heme are regulated initially by ALA synthase. Increasing concentration of heme will create a feedback mechanism and further down-regulate intracellular ALA production from succinyl-CoA and glycine. However, the negative feedback mechanism can be overcome by an excess amount of ALA applied exogenously. That is, if a high amount of ALA is applied to the synthesis pathway exogenously, this negative feedback mechanism can be set out of control, consequently leads to accumulation of fluorescent porphyrins, mainly PpIX in tissues of epithelial origin and their malignant counterparts<sup>48</sup>. Following the addition of excessive amounts of exogenous ALA, ferrochelatase will not be able to immediately convert all of the produced PpIX into heme. Therefore, PpIX accumulates temporarily in the cells and renders them photosensitive and fluorescent features.

There have been many attempts to elucidate the molecular mechanisms of tumor-selective PpIX accumulation by studying various aspects of heme metabolism. In general, it is thought to be induced by increased cellular uptake of ALA, increased PpIX synthesis, reduced PpIX conversion or all <sup>43</sup>.

One theory is that there exists an increased cellular uptake of ALA and retention of the ALA-derived PpIX. The mechanisms may involve a higher tumor cellular uptake of ALA through an active transport mechanism, a disturbed efflux of PpIX, and the poorly organized vascular architecture of tumors <sup>129, 130, 131, 132, 133, 134, 135, 136, 137</sup>. That is to say, the success of ALA-mediated accumulation of PpIX in cancerous cells depends on an efficient ALA uptake leading to an efficient conversion of ALA into PpIX, and a low PpIX efflux.

In contrast, Krieg *et al.* using excess ALA on colon cancer and fibroblast cell lines indicated that the metabolism of PpIX determines tumor-specific PpIX fluorescence, whereas ALA uptake is not significantly different among cell lines <sup>43</sup>. The recent attempt to improve uptake of ALA by increasing lipophilicity of ALA through esterification of the molecule leads to improved membrane permeability <sup>138, 139</sup>. Brunner using different ALA esters on several carcinoma cell lines showed an earlier maximum of PpIX accumulation, whereas no significant improvement in tumor selectivity was found when compared with ALA after treating cells with a dose of ALA esters 0.6 mmol/L <sup>140</sup>. These findings indicated a more important role of PpIX metabolism in tumor cell selectivity.

Another theory suggested that there could be an increased PBGD activity at a normal or marginally increased FECH activity, *i.e.*, a faster rate of conversion of ALA to PpIX <sup>141, 142, 143, 144, 145</sup>.

An alternative hypothesis suggests that an increased PpIX formation is combined with a reduced PpIX conversion in the heme synthetic pathway. The latter seem to be the consequences of reduced FECH-enzyme activity and/or an insufficient intracellular availability of iron. Those contribute to accumulation of PpIX after ALA application <sup>130, 143, 146, 147, 148, 149, 150</sup>. Taketani *et al.* (2000) suggested that the FECH activity was under the control of intracellular iron and possibly correlated with formation of the Fe/S cluster at the C-terminal region. The role of the Fe/S cluster was confirmed by observations that the activity of *E. coli* ferrochelatase, which lacks a Fe/S cluster, was insensitive to desferrioxamine when expressed in Cos7 cells <sup>117</sup>. Iron is essential in a wide variety of cellular processes including cell proliferation, viability,

and DNA synthesis. The iron is utilized as a cofactor by heme, aconitase, cytochromes <sup>151</sup>, and ribonucleotide reductase <sup>152</sup>. Tumor cells may have an increased demand for iron to meet their rapid division. It is possible that the competition for iron by other metabolic pathways results in its lowered availability for FECH.

Although the decreased ferrochelatase activity was reported in some types of human cancers, and selective accumulation of PpIX in tumor was suspected to be related to lowered FECH enzyme activity, as far as we know, no unequivocal evidence has been obtained for the involvement of the down-regulation of FECH expression correlating directly with the accumulation of PpIX in tumor tissues.

### **1.8 RNAi**

RNA interference (RNAi) is a recently described mechanism for inhibiting gene expression, which lead to post transcriptional gene silencing (PTGS) after endogenous production or artificial introduction into a cell of double-stranded RNA with sequences complementary to the targeted gene <sup>153</sup>. Whereas the transcription of the gene is normal, the translation of the protein is prevented by selective degradation of its encoded mRNA. The functional mediators of RNAi are small interfering RNA (siRNA) <sup>154</sup>. The discovery of RNAi related previous work on PTGS in plants to the activity of dsRNA. In the case of plants, it has been known for a long time that transgenes can induce their own silencing and simultaneously silence the homologous endogenous gene by a process known as co-suppression <sup>155, 156</sup>. Rich Jorgensen and colleagues tried to deepen the purple color of the petunia by introducing a pigment-producing gene. Instead of the expected deep purple color, many of the flowers appeared variegated or even white. This was named “co-suppression”, since both the introduced exogenous gene and the homologous endogenous gene were suppressed simultaneously.

Several sets of observations indicate that co-suppression might be initiated in at least two distinct ways. There is strong evidence from plant systems that RNA products, rather than simply the presence of multiple genomic copies of DNA sequences, can trigger co-suppression in some cases <sup>157</sup>. In plants, transgenes can be silenced at both the transcriptional and post-transcriptional levels. The mechanism responsible for PTGS is the selective degradation of mRNAs triggered by double-stranded RNA.

It was not until 1990s that RNA was showed to trigger gene silencing in an inheritable manner. The first evidence that dsRNA could lead to gene silencing came from investigations of *Caenorhabditis elegans* (*C. elegans*) in 1995. Both sense and

antisense RNAs were proved to be effective at silencing homologous target genes when injected separately. Guo and colleagues used antisense RNA to shut down expression of the *par-1* gene in order to assess its function. As expected, injection of the antisense RNA disrupted expression of *par-1*, surprisingly, injection of the sense-strand control did too<sup>158</sup>. This resulting was a puzzle until three years later.

The seminal discovery following this was made by Fire and Mello, who demonstrated that the combination of sense and antisense RNAs together was substantially more effective at producing interference than either strand individually. This experimentally-induced PTGS, the first report of the use of RNAi as a tool in biology was very potent and remarkably. Both the individual sense and antisense RNA preparations separately had only marginal interference activity, requiring a very high dose of injected RNA to produce any observable effect. In contrast, a sense-antisense mixture caused potent interference with endogenous gene activity<sup>159</sup>. Electrophoretic analysis indicated that the injected mixture material was predominantly double-stranded RNA. The dsRNA was gel-purified from the annealed mixture and was found to retain potent gene silencing effect. Thus, the dsRNA was proved to be the key trigger of the gene silencing.

Tuschl *et al.* reported that RNAi-induced silencing was realized via degradation of messenger RNA, which is promoted by dsRNA but not single-stranded RNA<sup>160</sup>. RNAi is triggered by dsRNA which induces the effective degradation of target mRNA through the generation of a sequence-specific nuclease activity. Hammond *et al.* termed this enzyme “RNA-induced silencing complex” (RISC)<sup>161</sup>. This enzyme contains an essential RNA component. After partial purification, the sequence specific nuclease co-fractionates with a discrete, 25-nucleotide RNA species which may confer specificity to the enzyme through homology to the substrate mRNAs<sup>161, 162</sup>.

Zamore *et al.* (2000) and Bernstein *et al.* (2001) used the *Drosophila* in vitro system to examine the the molecular mechanism during the RNAi reaction, they found that the cell extracts contained the ability to process long dsRNA into 21 to 23-nt effector RNAs termed “small interfering RNAs” (siRNAs)<sup>163, 164</sup>.

Quickly, the molecular details of the assembly of RISC were elucidated. RISC is a sequence-specific, multicomponent nuclease that destroys target mRNA. It was shown to contain Dicer, the Argonaute-2 (Ago-2) protein and ~22-nt siRNA.

Dicer is a member of the RNase III family of nucleases that speciacally cleave double

stranded RNAs<sup>164</sup>. Dicer and Ago-2 might physically interact, perhaps through their shared PAZ domains<sup>165</sup>. It is likely that the interaction between Ago-2 and Dicer facilitates the incorporation of siRNAs into RISC complexes and then the sense strand of siRNA is peeled away, leaving the antisense strand in RISC as the sequence specific target guider for cleavage of the complementary target mRNA in the cytoplasm.

Over the last few years, a more thorough understanding of the mechanism of action and intracellular pathways of RNAi has developed. However, a significant hurdle remains to be overcome in the development of RNAi as a research and therapeutic tool, i.e., double stranded RNA molecules longer than 30bp in length, in most of mammalian cells can cause non-specific gene silence.

In response to viral infection or long dsRNA, the mammalian cells could secrete interferon. Long dsRNA can activate protein kinase R (PKR) and 2', 5' adenylylase synthetase (2,5AS). PKR can phosphorylate elongation initiation factor 2 $\alpha$  (eIF2 $\alpha$ ) to block all protein synthesis<sup>166, 167</sup>. The biologically active 2,5AS molecules can bind to and convert RNase L, a ubiquitous 2,5AS-dependent endoribonuclease, from its inactive monomer to its active dimer form, which induces non-specific mRNA degrading in the infected cells<sup>168</sup>. Interestingly, dsRNA less than 30bp in length do not activate the PKR and 2,5AS. If long dsRNAs are chopped into small interfering RNAs, these siRNA molecules will induce sequence specific gene silencing in mammalian cells.

The first evidence that synthetic siRNAs can mediate RNAi in mammalian cells was provided by Elbashir and co-workers in 2001 when the chemically synthesized small dsRNAs 21-23 nucleotides in length was shown to be able to mediate cleavage of the target RNA in a short span of time<sup>169</sup>. The PKR activation was not effectively triggered by these short dsRNA oligos. This finding opened the floodgates and followed by a flood of papers that described RNAi technology in mammalian systems. These small dsRNA oligos are creating new dimensions in the field of molecular biology. Its applications are surprisingly numerous.

In general, three different approaches are employed in generating siRNAs: (1) *In vitro* transcription; (2) Endogenous expression; and (3) Chemical synthesis.

During *in vitro* transcription reactions, the siRNAs were prepared using T7 RNA polymerase. The *in vitro* transcription approach is limited by specific sequence

requirements. T7 RNA polymerase starts transcription at the final G in the promoter sequence. The polymerase then transcribes the opposite strand 3'→5'. Thus, the first base in the copy will be a G. That is, all siRNAs produced by this method will start with a 5'-G residue and require a 3'-C residue at the terminal to allow annealing with the complementary RNA<sup>170</sup>. Since the efficacy of siRNAs that targeted to different regions of a gene varies dramatically, the number of the small dsRNA molecules that can act as the effective candidate siRNAs generated by this method could be limited.

Endogenous expression: Viral vectors have recently been applied to RNAi. Viral vectors are typically very efficient. They take advantage of viruses that have evolved over millions of years to develop as sophisticated vehicles to transfer nucleic acid into mammalian cells. Vectors derived from viruses by the use of recombinant DNA techniques are most favored because they can efficiently deliver nucleic acid into a variety of cells directly *in vivo*. Despite of their high transfer efficiency, viral vector systems are still associated with biosafety concerns. The use of viral vectors for tumor targeting delivery of siRNAs is limited due to the limitations in tumor-tissues selectivity, the potential of random integration into the host chromosome and subsequent activation of proto-oncogenes. Other challenges include the difficulty of preparing, the costs of manufacturing, etc. Recombinant viral vectors are generally rendered replication defective to minimize pathogenicity while preserving the gene transfer capabilities of the native virus. However, there still exists the possibility that other versions of impurities with replication-competent may reside in vector preparations or the viral vector could revert to a wild-type virion. Therefore, they are potentially hazardous for the patients and their environment. Furthermore, viruses are inherently immunogenic. It is possible that the immunogenic properties of viral vectors could initiate serious innate humoral immune response to the expressed viral proteins and lead to difficulty with repeat administrations. A relatively fit 18-year-old patient with an inherited enzyme deficiency, died 17 September 1999, 4 days after a genetically altered adenovirus was injected into his liver for human gene therapy<sup>171</sup>. Retroviral vectors would have unique advantages over synthetic vectors in terms of persistency. However, a significant safety concern is that the genomic integration carries the grave risk of insertional mutagenesis and potential carcinogenesis. Retroviral vectors work by integrating parts of the viral genome into the host which can introduce insertional mutations. Clinical trials have been halted after two pediatric patients undergoing experimental gene therapy using retroviral vectors for x-linked severe immune deficiency syndrome (x-SCID) developed leukemia<sup>172, 173, 174</sup>.

Plasmid vectors have been developed to express short hairpin RNAs (shRNAs) that

can be subsequently converted into siRNAs *in vivo*. In the case of using shRNA expression plasmid vector for *in vivo* RNAi activation, one of the disadvantages of this endogenous expression construct is difficult to transfect due to the tissue and cellular barriers. While most rapidly dividing cells are easily transfected using shRNA expression plasmids, these plasmid vectors are not easily transfected into non-dividing cells. Assuming that a plasmid based shRNA expression vector can overcome multiple tissue barriers to enter into the target cell, further intracellular barriers await, *i.e.*, endosomal trap and nuclear entry. In the absence of cell division, plasmid vectors cannot easily be introduced into the nucleus, where the DNA is transcribed. In addition, the process of cloning a DNA sequence, which encoded the expression of a shRNA, into plasmid constructs and the need for verification of the cloned sequence are often time-consuming.

Chemical synthesis is a direct means of generating siRNAs. Advantages of chemically synthesized siRNA include the precise control of the actual amount and purity of siRNA, the possibility to characterize the siRNA, and the ability to introduce modifications into the siRNA to enhance its efficacy and target specificity or label the siRNA with a fluorescent probe to monitor quantitatively their interactions within living cells. The siRNA duplex requires a 3'-hydroxyl group and a 5'-phosphate group for functional activity<sup>175</sup>. The steps of chemical synthesis of siRNAs include the generation of two homologous strands, ensuring that both sense and antisense strands consist of 19 nucleotides with 2-nt overhangs at 3' end, and annealing of the strands to form a duplex<sup>169</sup>. The disadvantages of synthetic siRNA include its transient gene silencing and high cost, particularly very large quantities of siRNA required for *in vivo* studies. However, the cost of chemically synthesized siRNA has already reduced significantly over the past few years, and it appears that there could be a trend that will continue. Hopefully, cost should finally not be a barrier to the use of this valuable tool. Chemically synthesized siRNA mediated RNAi has become widely used for a variety of applications from functional genetic analysis to drug discovery. Today it is one of the most commonly used techniques to reduce levels of a particular gene to study its function, elucidate a drug target, or analyze a particular cellular pathway<sup>176</sup>.

## **1.9 Delivery of siRNA molecules *in vivo***

### **1.9.1 The biodistribution characteristics of chemically synthesized siRNAs**

Delivery of siRNA appears to be more efficient than plasmid DNA, possibly due to the smaller size of siRNA. Furthermore, efficient nuclear entry is required for plasmid but not if synthetic siRNA is involved, *i.e.*, the nuclear import, which is a significant barrier to the delivery of plasmid vector, is not required for siRNA. Hence the future

for *in vivo* applications of synthetic siRNA looks bright. For transfection of siRNAs, although delivery of these RNA oligos into cultured cells can be achieved by most delivery agents, their applications *in vivo* remain a major challenge. Clearly, shortcomings in one will adversely affect the success of the other. Realization of the full potential of the RNAi will depend significantly on the development of efficient *in vivo* delivery carriers. An effective siRNA *in vivo* delivery system need to overcome a multitude of biological barriers to enable the RNA oligos to reach their action site.

The *in vivo* fate of a siRNA molecule is determined by both the physicochemical properties of the siRNA and the anatomical and physiological characteristics of the body. Rapid clearance of siRNAs by the renal system may be one of the most important factors that can govern the biodistribution of siRNAs in the body. Santel *et al.*<sup>177</sup> used Cy3-labeled siRNAs to investigate the biodistribution characteristics of systemically administered lipoplexed siRNAs and naked siRNAs. They found that naked siRNA molecules are rapidly excreted through the kidney 5 min after intravenous injection, whereas there were no detectable signals in other organs (pancreas, heart, lung, liver, and spleen). These observations suggest that unmodified exogenous siRNAs should be excreted rapidly by kidney following their systemic administration. Water *et al.*<sup>178</sup> also demonstrated that after intravenous administration of naked <sup>111</sup>In-siRNA, the <sup>111</sup>In-DTPA-siRNA rapidly distributed throughout the body, and a large amount was delivered to the kidneys and excreted into the urine. One hour after injection, the amount of siRNA present in the kidneys was about 40 times higher than in the other organs (liver, brain, intestine, muscle, lung, spleen, and blood). The *in vivo* biodistribution characteristics of naked siRNAs might be explained by their physicochemical properties (polyanion charges and molecular weight).

In a healthy organism, the renal threshold is in the range of 30-50 kDa to avoid leakage of body proteins into the bladder<sup>179</sup>. Thus, molecules with a molecular weight of less than 30 kDa are susceptible to glomerular filtration and are excreted into the urine. The molecular weight of duplex of siRNA (21 nucleotides) for RNAi is approx. 15,000, and therefore the kidneys are assumed to play an important role in the disposition of siRNAs circulating in the vasculature<sup>178</sup>. In bloodstream, naked siRNA is rapidly removed from the circulation after intravenous administration. Most of the injected dose is excreted renally within minutes and taken up by liver Kupffer cells, which make a very small percentage of the administered dose of siRNA available, this small percentage of siRNA is additionally subject to nuclease degradation within a

short period of time. Thus, cellular uptake of naked siRNA seems to be inefficient<sup>180</sup>.

### **1.9.2 Non-viral vectors used for delivery of siRNA *in vivo***

Delivery of DNA/siRNA by using non-viral approaches is considered to have far fewer drawbacks. Synthetic delivery systems can in principle overcome the limitations of viral vectors, although their delivery efficiency needs to be improved.

The most concrete structural evidence currently available for use in the rational design of nonviral DNA delivery systems is the crystal structure of the nucleosome core particle of chromatin. Luger *et al.* have revealed the structure of a natural DNA histone complex by X-ray analysis<sup>181</sup>. In the nucleus, DNA is wrapped around the outside of the histone to form nucleosomes, much like thread wound around a spool. This protein structure with cationic amino acids on the surface can now act as a model for the rational design of polycationic vectors for DNA/siRNA transfection.

Polymers with positively charged amine groups are materials that electrostatically bind DNA/RNA to form tight complexes (polyplexes). The resulting particles usually range in size from a few tens to several hundred nanometers in diameter. These complexes mediate cellular entry and protect the delivered nucleic acid molecules by sterically blocking the access of DNase/RNase. Polyplexes are typically toroidal or spherical structures<sup>182, 183</sup>. Each polyplex particle most often contains several DNA molecules along with many polymer chains.

Nucleic acid-polymer complexes are internalized via adsorptive pinocytosis or receptor-mediated endocytosis. In either case, these DNA/siRNA-containing complexes might remain localized in the endosomes, failed to escape into cytoplasm. Endosomes are acidified rapidly to pH value of 5-6 due to the actions of ATPase proton-pump enzymes in the vesicles membrane. These complexes can subsequently be trafficked into lysosomes. Lysosomes are acidic organelles, containing various degradative enzymes. Lysosomes are further acidified to a pH value of ~4.5<sup>179</sup>. Therefore, the delivered DNA/siRNA molecules will encounter a hostile environment.

Endo-lysosomal escape is an essential prerequisite for successful *in vivo* application of RNAi technique. Only siRNA-containing complexes can escape rapidly into the cytoplasm, where the RNAi machinery is located, and furthermore, the siRNA molecules are also able to liberate from the complexes can silence the mRNA of interest.

Sørensen *et al.*<sup>184</sup> demonstrated that intraperitoneal injection of DOTAP liposome siRNAs-TNF $\alpha$  complex inhibited lipopolysaccharide-induced TNF $\alpha$  gene expression. They found that the development of sepsis in mice following a lethal dose of lipopolysaccharide injection was significantly inhibited by pre-treatment of the animals with anti-TNF- $\alpha$  siRNAs. Landen *et al.*<sup>185</sup> reported that DOPC-encapsulated siRNA targeting the oncoprotein EphA2 was highly effective in reducing *in vivo* EphA2 expression as measured by both Western blot assay and immunohistochemistry. Zimmermann *et al.* used a liposomal formulation of SNALP to evaluate systemic delivery of siRNAs directed towards apolipoprotein B (ApoB), 80% silencing of liver Apob mRNA and ApoB-100 protein was achieved with a single 1mg/kg dose of SNALP-formulated Apob-specific siRNA<sup>186</sup>. Torchilin *et al.*<sup>187</sup> successfully delivered siRNA into lung-tumor cells by encapsulating siRNAs into liposomes additionally bearing arginine octamer (R8) molecules attached to their outer surface. The siRNA-loaded R8-liposomal complexes remained intact in the blood serum even after 24-h incubation, and showed very high transfection efficiency in all three tested lung tumor cell lines. This offers the potential for *in vivo* siRNA delivery application. Santel *et al.* developed a liposomal system that consists of cationic and fusogenic lipids for siRNA delivery. They used siRNA molecules to knock-down endothelia-specifically expressed genes CD31 and Tie2 and found that the corresponding mRNA and protein levels were significantly reduced after systemic application of siRNA. To evaluate the effect of the liposomal system on siRNA biodistribution *in vivo*, they injected 1.88 mg/kg of complexed Cy3-siRNA intravenously in mice. Fluorescently labeled siRNA-lipoplexes were taken up by the endothelial cells in different vascular beds, mainly liver, heart, lung, spleen, and kidney, showing a profound delay in the clearance rate<sup>177</sup>.

In the case of liposomal system for *in vivo* delivery of siRNA, one of the most important challenges is to overcome the clearance of liposomes caused by opsonization. In general, liposomes are rapidly recognized and removed from the circulation by the reticuloendothelial system (RES)<sup>188, 189</sup>. Macrophages recognize liposomes as foreign particles through a process known as opsonization. The liposomes are labeled by attaching serum proteins, so-called opsonins, which enhance the clearance of liposomes<sup>189</sup>. These labeled liposomes are recognized by the macrophages and then the liposomes are taken up and destroyed.

The cationic surface of liposome is able to interact with biomolecules or nontarget cells. Cationic liposomes have long been known to interact with serum proteins in the extracellular matrix, leading to aggregation or release of nucleic acids from the

complexes even before reaching the target cells. Small and large molecules found in serum such as oleic acid and heparin can disrupt the structural integrity of lipoplexes by displacing nucleic acids and lipid components leading to heavily impaired transfection efficiency<sup>190</sup>. In order to minimize their interaction with serum proteins or complement system, many liposomal vectors have been coated with a polymer called polyethylene glycol (PEG). These PEG-liposomes are known as stealth liposomes.

### **1.9.3 Enhanced permeability and retention effect**

Enhanced permeability and retention effect (EPR effect) results from a combination of the increased vascular permeability and the decreased lymphatic drainage caused by the lack of functional lymphatic vessels in tumor tissue<sup>191, 192, 193</sup>. In general, low-molecular-weight compounds diffuse into both normal and tumor tissue through the endothelia layer of capillaries. However, continuous capillaries with tight junctions are the most common type of capillaries in normal tissues. Thus, macromolecules cannot pass through the capillary walls in most normal tissues. In contrast, tumor vasculature is known to contain a high number of immature vessels. These fenestrated vessels are leaky to circulating macromolecules, and favor the movement of large-molecular-weight diagnostic and therapeutic agents across tumor vessels<sup>179</sup>. Under these circumstances, together with insufficient lymphatic drainage, macromolecules are retained in the interstitial space of solid tumors. This feature has been termed “enhanced permeability and retention effect”.

### **1.9.4 Folate-PEG cationic liposomes**

Besides ensuring the good nuclease stability and reducing renal filtration, using strategies that provide an active targeting manner to the intended tissues would be helpful to improve the efficiency and specificity of siRNAs *in vivo* delivery.

The strategies that could allow active targeting involve the surface functionalisation of siRNA carriers with ligands that are selectively recognized by receptors on the surface of the cells of interest, or by conjugating them with monoclonal antibodies against characteristic components of the area of interest. Since ligand–receptor or antigen-antibody interactions can be highly selective, these interactions could allow a more precise targeting of the site of interest and promote specific cellular uptake via receptor-mediated endocytosis.

For example, by incorporating liposome with a ligand such as folic acid, this can target to the tumor-cell surface over expressed folate receptor (FR). The competitive

dominance of the liposomes which conjugated with receptor-specific ligand is their active targeting delivery ability. Here, the aim is active targeting to a desired site and then triggers receptor-mediated internalization of the entire siRNA-carrying lipoplexes into the cell interior, not just passive targeting of the tumor tissue by extravasating into the tumor interstitial space through the leaky vessels. Thus, more siRNA molecules are expected to be delivered into tumor cells.

The human  $\alpha$  isoform folate receptor ( $\alpha$ hFR) is a glycosylphosphatidylinositol-linked transmembrane protein with high affinity for folic acid.  $\alpha$ hFR is an important molecule in the cellular uptake of folates and folate analogues. It is usually considered as an essential component in the maintenance of cellular folate homeostasis. Internalization of folates by  $\alpha$ hFR involves receptor-mediated endocytosis<sup>194</sup>. Expression of the  $\alpha$ hFR is very low in most adult normal tissues. In contrast,  $\alpha$ hFR is a cellular surface marker for numerous solid tumors and myeloid leukemias. High levels of the expression of  $\alpha$ hFR have been reported in several tumor types. For example, among the different cell types of the normal ovary,  $\alpha$ hFR expression was detected only in germinal epithelium. However, high  $\alpha$ hFR mRNA levels were observed in all of the serous cystadenocarcinomas examined<sup>195</sup>. Other cancers with a high level of  $\alpha$ hFR expression relative to their normal counterparts include breast, brain, lung, and colorectal cancers<sup>195, 196, 197, 198, 199, 200, 201</sup>.

Folate receptor is an attractive molecular target for tumor-targeted drug delivery with macromolecular carrier system. Folate-mediated tumor targeting represents a popular approach that has been used to deliver diagnostic and therapeutic agents to folate receptor expressing tumors<sup>202, 203, 204, 205</sup>. Reddy *et al.* reported that the overall tumor transfection efficiency of widespread intraperitoneal cancers can be significantly enhanced using folate-targeted techniques<sup>206</sup>. Christopher *et al.* found that folate liposomes can effectively deliver oligonucleotides into folate receptor-positive tumor cells<sup>207</sup>. Liposomal daunorubicin as well as doxorubicin were delivered into various tumor cells via the folate receptor were also reported<sup>208 209</sup>. Xing *et al.* used folate receptor  $\beta$  - targeted liposomal doxorubicin (F-L-DOX) combined with receptor induction using all-trans retinoic acid (ATRA). They found that the cytotoxicity of F-L-DOX in leukemic cells was superior to that of liposomal doxorubicin, exhibited a strong dependence on FR expression<sup>210</sup>. Folate-targeted liposomes have been suggested as delivery vehicles for targeting tumors with haptens for tumor immunotherapy<sup>211</sup> and also been used for boron neutron capture therapy<sup>212</sup>.

Folate receptor constitutes a useful target for tumor-specific drug delivery. Folic acid

molecules can also be covalently linked to cationic polymers to confer potential tumor target specificity to these drug-carriers for delivery of siRNA. Kim *et al.* used antisense oligodeoxynucleotide (AS-ODN), siRNA, and shRNA expressing plasmid for inhibition of green fluorescent protein (GFP) expression. They conjugated above three nucleic acids with Polyethylenimine (PEI) and PEI-polyethylene glycol-folate (PEI-PEG-FOL). Among the three inhibitory nucleic acids, the PEI-PEG-FOL/siRNA complex exhibited the most dose-effective and fastest gene silencing effect for folate receptor positive human oral carcinoma KB cells <sup>213</sup>. In this study, we plan to utilize folate-PEG cationic liposome as one of the vehicles for delivery of FECH-siRNA *in vivo*.

### 1.9.5 Dendritic polyglycerol-based cationic polymers

Hyperbranched polymer represents a polymer which may be obtained by reaction especially between multifunctional monomers. The resulting structures are imperfect and polydisperse. Hyperbranched polymers are often random copolymers which have a plurality of branch points and multifunctional branches, leading to further branching with polymer growth. The degrees of branching (DB) of hyperbranched polymers is lower (DB = 53–60 %) as compared to perfect dendrimers (DB = 100 %). The core-shell architecture of hyperbranched polymers is less pronounced in comparison with perfect dendrimers.

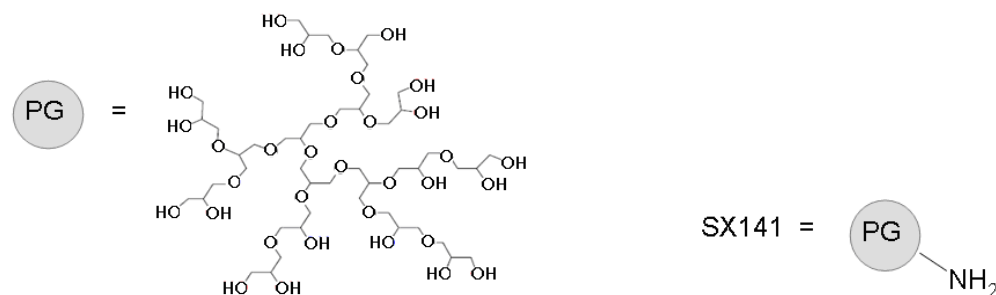


**Figure 1.4**

**Hyperbranched PG**

**PG-based cationic polymer**

(The depicted structure is a small fragment of the large polymer, the technical data was kindly provided by Professor Rainer Haag)

Hyperbranched polyglycerol (PG) is one important hyperbranched polymer and is considered a possible alternative to the structurally perfect dendrimers. Due to the similar physicochemical properties, dendrimers and hyperbranched polymers are referred to as dendritic polymers in the literature. The use of hyperbranched polymers instead of perfect dendrimers is justified by their similar properties, better accessibility and lower costs, which are all extremely important for large-scale synthesis <sup>214</sup>. Dendritic PG is globular structure in solution. In contrast to dendrimers

which contain only dendritic and terminal units, hyperbranched polyglycerols usually consist of dendritic, linear, and terminal units.

Hyperbranched PG possesses an inert polyether scaffold. Each branch ends in a functional hydroxyl-group, which renders hyperbranched PG a highly functional material. The high functionality coupled with the versatile and well-investigated reactivity of hydroxyl-functions is the basis for a variety of derivatives<sup>215</sup>. PG-PEG and PG-PEG-Folate recently were prepared and investigated as potential drug-delivery systems<sup>216</sup>. PG can also be used as core unit and functionalized with amine groups. Such polymers can be applied in DNA/siRNA transfection. In this study, we are interested in the application potential of the polyglycerol-based nanocarriers for delivery of siRNAs to tumors.

### **1.10 Aims of the thesis**

The objectives of the thesis focus on:

- (1) the investigation of the relationship between FECH expression and PpIX formation
- (2) the assessment of the possibility of utilizing folate-PEG cationic liposomes and PG-based cationic polymers as the vehicles for delivery of siRNAs to tumor
- (3) the evaluation of the diagnostic application potential of the siRNA-based inhibitor of FECH for early cancer detection

## **2 Materials and methods**

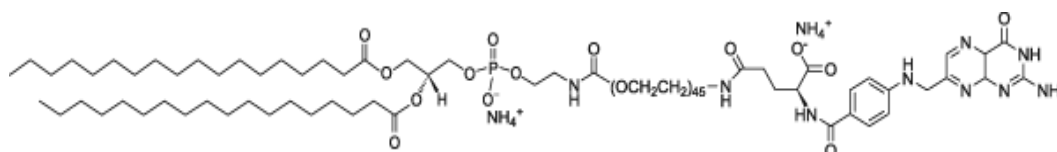
### **2.1 Laboratory equipment**

Taqman 7000 SDS Cycler, Applied Biosystems (Weiterstadt, Germany); Eppendorf Bio-photometer (Eppendorf AG, Hamburg, Germany); MMI CELLCUT<sup>®</sup> laser microdissection system (MMI Molecular Machines & Industries GmbH, Germany); Reversed-phase RP18 column HPLC (Shimadzu, Duisburg, Germany); Fluorimeter (Merck, Darmstadt, Germany); Optical parametric oscillator (OPO, GWU-Lasertechnik, Erfurtstadt, Germany); Q-switched Nd:YAG laser (GCR-230, Spectra-Physics Inc., USA); Inverted microscope stand (Zeiss Axiovert 35M, Carl Zeiss, Oberkochen, Germany); Mode-locked titanium: sapphire (Ti:Sa) laser (MaiTai, Spectra-Physics, Mountainview, CA); Closed loop galvanometer scanner (GSI Lumonics, Moorpark, CA, USA); Water immersion objective (N.A. 1.2, Carl Zeiss, Oberkochen, Germany); Avalanche photo detector (SPCM – AQR – 14, Perkin Elmer Inc., Santa Clara, CA, USA); PC plug-in counter board (pci-6602, National Instruments, Munich, Germany). Rotary evaporator (Büchi, Essen, Germany), LiposoFAST<sup>™</sup> Basic system (Avestin, Ottawa, Canada), high-performance thinlayer chromatography (Automated Multiple Development System and Linomat IV; CAMAG, Muttenz, Switzerland), Coulter Counter N4 plus (Coulter Electronics, Hialeah, USA), OLYMPUS BX 50 fluorescence microscope (Olympus Corporation, Japan); Leica TCS SP5 confocal microscope (Leica Microsystems GmbH, Wetzlar, Germany), fluorescence imaging system (Physikalisch-Technische Bundesanstalt, Berlin, Germany), EMCCD-Camera (electron multiplied CCD-Camera, IXON, manufacturer Andor Technology, Belfast, Northern Ireland).

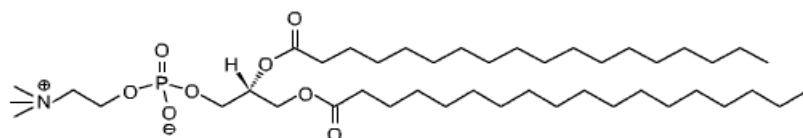
### **2.2 Chemicals and reagents**

DEPC-water and all real-time PCR chemicals were, unless otherwise stated, from Applied Biosystems (Weiterstadt, Germany). Agarose was obtained from BioWhittaker Molecular Applications (Rockland, ME, USA). M-MLV Reverse Transcriptase, RNasin, RNaseH, and dNTP were purchased from ProMega (Mannheim, Germany). RNeasy RNA-extraction Kit, QIAshredder Kit, One-Step RT PCR Kit, QiaEx-II gel extraction Kit, chemically synthesized siRNAs, Cy3-labeled siRNAs, and TransMessenger kit were purchased from Qiagen (Hilden, Germany). Phenol/Chloroform and other chemicals were purchased from Roth (Karlsruhe, Germany). Sucrose was obtained from Serva (Heidelberg, Germany). Protoporphyrin IX disodium salt, zinc acetate, Triton X-100, BSA,  $\delta$ -aminolevulinic acid (ALA), and 4',6-Diamidino-2-phenylindole dihydrochloride hydrate (DAPI) were purchased from Sigma-Aldrich (Munich, Germany); Dulbecco's Modified Eagle's Medium, fetal calf serum, phosphate buffered saline, antibiotics, and glutamine from GIBCO, Life Tech

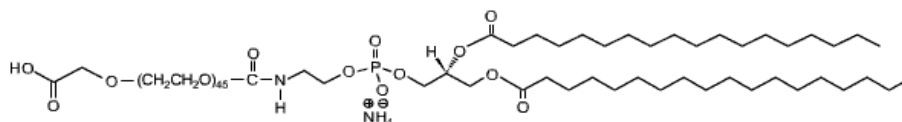
(Eggenstein, Germany). Fluorescent mounting media antifade reagent (DAKO, CA, USA). 1,2-Dioleoyl-3-Trimethylammonium-Propane(DOTAP), 1,2-Distearoyl-*sn*-Glycero-3-Phosphocholine(DSPC), 1,2-Distearoyl-*sn*-Glycero-3-Phosphoethanolamine-N-[Carboxy(PolyethyleneGlycol)2000](DSPE-PEG), 1,2-distearoyl-*sn*-glycero-3-phosphoethanolamine-N-[folate(polyethylene-glycol)-2000] (DSPE-PEG-Folate), and cholesterol were purchased from Avanti Polar Lipids(Alabaster, AL, USA). Polyglycerol-based SX141 nanoparticles were kindly provided by Professor Rainer Haag. The degree of functionalisation (DF) of SX141 is nearly 100 % according to the technical data sheet.



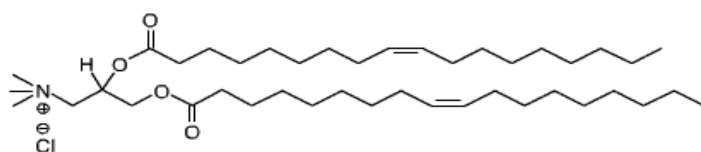
1, 2-distearoyl-*sn*-glycero-3-phosphoethanolamine-N-[folate(polyethylene glycol)-2000] (DSPE-PEG-Folate)



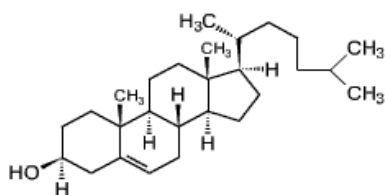
1, 2-Distearoyl-*sn*-Glycero-3-Phosphocholine(DSPC)



1, 2-Distearoyl-*sn*-Glycero-3-Phosphoethanolamine-N-[Carboxy(Polyethylene Glycol)2000] (DSPE-PEG)



1, 2-Dioleoyl-3-Trimethylammonium-Propane(DOTAP)



Cholesterol

**Figure 2.1 Chemical structures of lipids and cholesterol used in this thesis**

### **2.3 Patients' tissue samples**

Patients had been treated in the Department of Surgery and Surgical Oncology, Robert-Roessle-Klinik in Berlin, Germany. Carcinoma tissues were excised carefully from tumor specimens. Non-malignant mucosa was also scraped off at a distance of over 50 mm from the tumor margin. Tissue was snap-frozen in liquid nitrogen by the Tumorbank service of the Robert-Roessle-Klinik. Carcinomas were classified and characterized according to the World Health Organization's UICC (Union Internationale Contre le Cancer) system. Normal tissue refers to peritumoral tissue verified to be free of any pathologic traits. All patients had been treated surgically between 1999 and 2001. In each case, a comprehensive histopathological and clinical record is available. Patient specimens were collected after informed consent and only used after ethics-committee approval (Charité, Berlin). For quantitative RT-PCR studies, a panel of 18 cases with esophageal carcinomas, 20 cases with gastric carcinomas, 15 cases with colonic carcinomas, and 15 cases with rectal carcinomas along with their non-malignant counterparts, were examined. Tumor stages were equally represented.

### **2.4 Tissue preparation, RNA extraction and cDNA synthesis**

Cryo-sections from tumor and normal tissue specimens were transferred into RLT-Buffer containing 140  $\mu$ M  $\beta$ -mercaptoethanol and frozen at  $-80^{\circ}$  C. In order to assure absence of tumor cells in normal tissue and sufficient tumor content in cancer specimens, all tissue specimens were evaluated by a pathologist. Only specimens containing more than 60% epithelial cells, but no Peyer's patches or necrotic areas were further processed. RNA was isolated using QIAshredder and RNeasy Kits. Integrity of isolated mRNA was checked by  $\beta$ -Actin One-Step RT PCR, and RNA concentration was determined photometrically. About 3  $\mu$ g of RNA were applied for cDNA synthesis. In the presence of 4  $\mu$ M random hexamer primer, RNA was incubated for 10 min. at  $70^{\circ}$  C, afterwards the mixture was kept on ice for another 10 min. After addition of M-MLV-Buffer, 8 U/ $\mu$ L M-MLV Reverse Transcriptase, 0.8 U/ $\mu$ L RNasin, 0.1  $\mu$ g/ $\mu$ L BSA and 1.25 mM dNTP and 1 h incubation at  $37^{\circ}$  C, twice the volume of absolute ethanol was added. Following 30 min. at  $-40^{\circ}$  C, samples were spun down in a centrifuge at 15,000 g at  $4^{\circ}$  C for 20 min. and washed once with 70% ethanol. Finally, cDNA was reconstituted in 50  $\mu$ L DEPC water and frozen at  $-20^{\circ}$  C.

### **2.5 Cell culture**

MDA-MB-231, MDA-MB-435 breast cancer cell lines, and LS174T, SW480, HT29, colorectal cancer cell lines originating from the American Type Culture Collection (ATCC), were grown in Dulbecco's modified Eagle's medium (DMEM)

supplemented with 10 % FBS, 2 mM glutamine, 0.6 µg penicillin/ ml (equivalent to 100 Units) and 0.1 mg streptomycin / ml medium. Subconfluent adherent cells were harvested by a mixture of trypsin (0.05%) and EDTA (0.02%), rescued with their own medium and washed with phosphate buffered saline (PBS).

## **2.6 Extraction and purification of RNA from cultured cells and cDNA synthesis**

About  $1 \times 10^6$  cells were trypsinized from the cell-culture vessel, total RNA purification from the harvested cells using QIAGEN RNeasy Mini Kit according to manufacture's instructions: Aspirated medium, and washed cells with PBS. Aspirated PBS and added trypsin to trypsinize the cells, after cells detach from the cell-culture vessel, added medium (containing serum to inactivate the trypsin), transferred cells to an RNase-free polypropylene centrifuge tube, and pelleted by centrifugation at  $300 \times g$  for 5 min. Completely aspirated supernatant. Added 350 µl of Buffer RLT (ensured that  $\beta$ -ME is added to Buffer RLT before use), vortexed or pipeted to mix, ensured that no cell clumps were visible before proceeding to next step; pipeted the lysate directly onto a QIAshredder spin column placed in a 2 ml collection tube, and centrifuged for 2 min. at maximum speed, added 350 µl of 70% ethanol to the homogenized lysate, and mixed well by pipetting. Did not centrifuge, then applied up to 700 µl of the sample, including any precipitate that may have formed to an RNeasy mini column placed in a 2 ml collection tube. Closed the tube gently, and centrifuged for 15 s at  $\geq 8000 \times g$  ( $\geq 10,000$  rpm), discarded the flowthrough, added 700 µl Buffer RW1 to the RNeasy column. Closed the tube gently, and centrifuged for 15 s at  $\geq 8000 \times g$  ( $\geq 10,000$  rpm) to wash the column, discarded the flow-through and collection tube, transferred the RNeasy column into a new 2 ml collection tube, pipeted 500 µl Buffer RPE onto the RNeasy column, closed the tube gently, and centrifuged for 15 s at  $\geq 8000 \times g$  ( $\geq 10,000$  rpm) to wash the column, discarded the flow-through, added another 500 µl Buffer RPE to the RNeasy column, closed the tube gently, and centrifuged for 2 min. at  $\geq 8000 \times g$  ( $\geq 10,000$  rpm) to dry the RNeasy silica-gel membrane. To elute, transferred the RNeasy column to a new 1.5 ml collection tube, pipeted 50 µl RNase-free water directly onto the RNeasy silica-gel membrane, closed the tube gently, and centrifuged for 1 min. at  $\geq 8000 \times g$  ( $\geq 10,000$  rpm). RNA concentration was determined by using Eppendorf Bio-photometer. Approx. 3 µg of RNA were applied for cDNA synthesis. In the presence of 4 µM random hexamer primer, RNA was incubated for 10 min. at 70° C, afterwards the mixture was kept on ice for another 10 min. After addition of M-MLV-Buffer, 8 U/µL M-MLV Reverse Transcriptase, 0.8 U/µL RNasin, 0.1 µg/µL BSA and 1.25 mM dNTP and 1 h incubation at 37° C, twice the volume of absolute ethanol was added. Following 30 min. at -40° C, samples were spun down in a centrifuge at 15,000 g at 4° C for 20 min.

and washed once with 70% ethanol. Finally, cDNA was reconstituted in 50  $\mu$ L DEPC water and frozen at -20° C.

## 2.7 Quantitative real-time TaqMan PCR

For all genes, Assays-on-Demand (ABI) primer and probes were employed. For quantitative analysis of gene expression, 100 ng of cDNA were used per well. All reactions were carried out threefold. After mixing with the appropriate volume of TaqMan Universal PCR Master Mix, quantitative real-time PCR was run in a MicroAmp Optical 96-Well Reaction Plate using the ABI 7000 Sequence Detection System. Thermal cycle conditions were as follows: 95° C for 10 min., initially, then 40 cycles of 95° C for 15 s and 60° C for 1 min. In order to analyze expression data according to the  $\Delta\Delta C_t$  method<sup>217</sup>,  $C_t$  values were exported from the ABI Prism 7000 SDS Software into Microsoft Excel (Seattle, WA).  $C_t$  values of a cDNA stock from the cell line LS174T were used as calibrator. Thereby, gene expression in a sample under investigation is reported as a multiple of cell line expression. This expression is achieved by employing the equation

$$\text{Relative Amount} = 2^{-(\Delta C_{t_{\text{Sample}}} - \Delta C_{t_{\text{Calibrator}}})}$$

wherein  $\Delta C_t$  stands for the difference between  $C_t$  values of gene of interest and housekeeper  $\beta$ -Actin.

## 2.8 PpIX determination

PpIX Fluorescence in homogenized centrifuged pellets from cell culture was quantitatively determined by time-resolved fluorescence spectroscopy. PpIX fluorescence was excited with an optical parametric oscillator (OPO, GWU-Lasertechnik, Erftstadt, Germany), pumped by the third harmonic ( $\lambda = 355$  nm,  $E_{\text{pulse}} = 100$  mJ) of a Q-switched Nd:YAG laser (GCR-230, Spectra-Physics Inc., USA). The OPO was tuned to provide laser radiation at  $\lambda = 505$  nm to excite PpIX-fluorescence. The energy and duration of output pulses amounted typically to 50  $\mu$ J and 3 ns, respectively. The laser beam was coupled into a 600  $\mu$ m hard clad silica fiber used for illumination of cell samples. The fluorescence light was collected by the same fiber and a dichroic beam splitter served to separate reflected laser light from fluorescence. Approx. 5 % of the remaining fluorescence intensity were separated by a quartz plate and coupled into a hard clad silica fiber, approx. 5 m long, whereas the main fluorescence intensity (90 %) was focused into a second fiber, 1 m long. In this way, fluorescence in the first channel was delayed with respect to the second channel by approx. 20 ns, which allowed simultaneous recording of prompt and delayed fluorescence intensity. For this purpose, the ends of both fibers were attached one above the other to the entrance slit of an imaging polychromator

equipped with an intensified CCD-camera (Model ICCD-576, Princeton Instruments Inc, Trenton, USA.). The intensifier was gated by an electrical pulse (-180 V) of approx. 10 ns duration derived from a high-voltage (HV) pulse generator synchronized with the laser pulse. The HV pulse generator was triggered by a pulse provided by the power supply of the Nd:YAG laser and appropriately delayed by means of a digital delay generator. In this way, immediate and delayed fluorescence intensities were recorded. Furthermore, two long pass filters were applied ( $\lambda_{50\%} = 550$  nm) to cut off the remaining scattered excitation light from emitted fluorescence light. For quantification, we calculated the normalized fluorescence intensity of the main PpIX-fluorescence band at  $\lambda = 633$  nm. A factor of 18 corresponded to the ratio of the transmitted and reflected fluorescence intensity by the quartz plate.

## 2.9 Determination of ferrochelatase enzyme activity

FECH activity was determined as described by van Hillegersberg *et al.*<sup>147</sup> with minor modifications. Briefly, approx.  $5 \cdot 10^7$  frozen cells were powdered in 500  $\mu$ l ice-cold H<sub>2</sub>O using a tissue-homogenizer (Braun, Germany). Then, 50  $\mu$ l of the homogenate were added to 100  $\mu$ l buffer A, consisting of 25 mM Tris/HCl, 0.1 % Triton X-100, 1.75 mM palmitic acid, pH 8.2. Protein content in the supernatant was determined using the BioRad protein assay. 50  $\mu$ l of a 250  $\mu$ M protoporphyrin solution in 0.01 N KOH were added, and the reaction was started by addition of 50  $\mu$ l 200  $\mu$ M zinc acetate. After 60 min. at 37°C, the reaction was stopped by addition of 1 ml dimethylsulfoxide:methanol (30:70). After centrifugation at 16000 x g for 5 min., 100  $\mu$ l supernatant were injected into a reversed-phase RP18 column HPLC (Shimadzu, Duisburg, Germany) with acetone/methanol/water/formic acid (560:240:200:2), 1 ml/min as the mobile phase. Zinc-Protoporphyrin was detected using a fluorimeter (Merck, Darmstadt, Germany) with an excitation  $\lambda = 415$  nm and an emission wavelength  $\lambda = 580$  nm. One unit of activity was defined as the amount of enzyme catalyzing the formation of 1  $\mu$ mol product/min. The activity of the enzyme was given in nU/mg protein.

## 2.10 Preparation of siRNA and transfection *in vitro*

All siRNA-molecules were designed according to standard procedures and obtained from Qiagen (Hilden, Germany). Three different sequences were used: siRNA-sequence FECH-510, 5'-gauucaagagcaguaccgc-3', covering the FECH mRNA, transcript variant 1, with accession NM\_001012515.1 between nucleotides 510-528, and FECH mRNA, transcript variant 2, with accession NM\_000140.2 between nucleotides 492-510, respectively; siRNA FECH-1140, 5'- gaauauccucuugguaccg -3',

covering the FECH mRNA, transcript variant 1, with accession NM\_001012515.1 between nucleotides 1140-1158, and FECH mRNA, transcript variant 2, with accession NM\_000140.2 between nucleotides 1122-1140, respectively; siRNA FECH-2107, 5'- guacaguguucaugauacg -3', covering the FECH mRNA, transcript variant 1, with accession NM\_001012515.1 between nucleotides 2107-2125, and FECH mRNA, transcript variant 2, with accession NM\_000140.2 between nucleotides 2089-2107, respectively. The following siRNA sequence was used as negative control: 5'- gaccaugggacucaagag -3'. The negative control siRNA was compared with NM\_001012515.1 and/or NM\_000140.2 sequences. Results showed that no significant similarity was found, *i.e.*, the negative control siRNAs exhibit no target mRNA in the transcripts of both NM\_001012515.1 and NM\_000140.2.

For siRNA-treatment, the TransMessenger kit (Qiagen) was used. Cell seeding density in 6-well plates was always  $2 \times 10^5$  cells per well. Transfection experiments were performed 24 hours after seeding, siRNA in a final concentration of 50 nM. Briefly, 0.44  $\mu$ g siRNA was mixed with buffer and enhancer and incubated at room temperature for 5 minutes. Thereafter, 2.2  $\mu$ l TransMessenger were added, and the entire solution was mixed by pipetting up and down. Then, the complexes were incubated for 10 min. at room temperature to allow transfection-complex formation to take place. During this time, the growth medium was gently aspirated and cells were carefully washed. DMEM medium 600  $\mu$ l (without serum or antibiotics) were added into the no-siRNA & no-transfection reagent control wells, and 500  $\mu$ l/well DMEM medium (without serum or antibiotics) were added into the other wells. Then, 100  $\mu$ l of the transfection complexes were added into the corresponding wells. Cells were incubated with the transfection complexes for 4 h under their normal growth conditions. Washed cells with 2ml PBS, and then 1000-2000  $\mu$ l DMEM medium (containing serum and antibiotics) per well were added. A second siRNA-treatment was conducted on day 5. Cells were harvested at day 6. All experiments were performed at least threefold.

### **2.11 Two-photon microscopy**

Experiments were carried out on a two-photon excitation confocal equipment established in Physikalisch-Technische Bundesanstalt, Department of Biomedical Optics, Berlin by utilizing an inverted microscope stand (Zeiss Axiovert 35M, Carl Zeiss, Oberkochen, Germany). In short, the system consisted of a mode-locked titanium: sapphire (Ti: Sa) laser (MaiTai, Spectra-Physics, Mountainview, CA) that generated pulses with a duration of approx. 100 fs at a repetition rate of 80 MHz. After having passed beam-neutral density filters and a beam expander, the excitation

light was directed to a dichroic mirror that was highly reflective in the near infrared and transparent below 725 nm (725DCX SP, AHF, Germany). Thus, the laser beam was coupled into the optical epi-illumination path of the microscope. To allow imaging, we incorporated a two-dimensional laser-beam scanner consisting of two mirrors driven by a closed loop galvanometer scanner (GSI Lumonics, Moorpark, CA, USA). A tube lens and a 10x magnification ocular (both Carl Zeiss) acted as relay-lens system between the scanner mirrors and the objective. Finally, the excitation light was focused into the sample by a 63x C-apochromat, water immersion objective (N.A. 1.2, Carl Zeiss, Oberkochen, Germany). The fluorescence radiation was collected by the same microscope objective and then passed scan lenses and scanning mirrors. Since for two-photon excitation the excited fluorescence light was of shorter wavelength than the excitation light, the generated fluorescence signal passed the dichroic beam-splitter mentioned above. To further suppress scattered excitation light, an additional short pass (700 SP, AHF) was incorporated into the detection path. Although in two-photon microscopy no confocal aperture is needed for axial sectioning its inclusion in the detection path reduces the contribution of scattered out-of focus fluorescence and residual ambient light and, hence, increases the signal/background ratio. Therefore, the fluorescence intensity was imaged by an achromat ( $f = 600$  mm) onto an adjustable aperture, the diameter of which was set to 1.8 mm. The overall magnification was measured to be about 1,530 for the 63x magnification objective. Light passing the confocal aperture was spectrally filtered for analysis by a long pass filter with 50% transmission at 595 nm and two band pass filters ( $535 \pm 17.5$  nm and  $635 \pm 20$  nm) (AHF Analysentechnik AG, Tuebingen, Germany). The light of each path was focused onto an avalanche photo detector (SPCM – AQR – 14, Perkin Elmer Inc., Santa Clara, CA, USA), which converted the detected photons into standard TTL pulses. The pulses were counted by a PC plug-in counter board (pci-6602, National Instruments, Munich, Germany). Measurement of excitation spectra (not shown) in the tunable range of the excitation laser (760-920 nm) yielded a PpIX excitation maximum at  $\lambda = 760$  nm. The one-photon excitation maximum of PpIX was located at approx. 400 nm. As expected<sup>218</sup>, the two-photon excitation maximum was slightly blue-shifted compared to the one-photon excitation spectrum. Images of 200x200 pixels were acquired by line scans at  $\lambda = 760$  nm. The excitation power measured at the sample position was  $0.8 \pm 0.1$  mW. The inter-pixel distance selected amounted to 0.98  $\mu\text{m}$  corresponding to a total field of view of 197 x 197  $\mu\text{m}$ . The exposure time per pixel was varied between 0.25 ms and 1.25 ms according to the overall fluorescence intensity of the sample to assure good detection statistics with the lowest possible excitation power. Total data acquisition times, therefore, varied between 10 and 50 s.

## 2.12 Preparation of PEG cationic liposomes and folate-PEG cationic liposomes

Liposomes were prepared by the lipid film/hydration technique as described previously by Huwyler *et al.* with a minor modification<sup>219</sup>. Briefly, cationic liposome formulations composed of DOTAP, cholesterol, DSPC, DSPE-PEG-Folate or DSPE-PEG. The properties of liposomes were indicated in Table 2.1 & Table 2.2. A mixture from stock solutions of above lipids in a round-bottomed flask was dried to a thin lipid film in a rotary evaporator (Büchi, Essen, Germany). The flask containing the thin lipid film was then placed under vacuum for 1 hour to remove residual organic solvent and the lipid film was dried thoroughly. After that, the dried layer was hydrated with a glucose solution (5%, w/v) to a final concentration of 5mM of DOTAP, then the flask was shaken in 53 °C warm water-bath for 10-15 min. until the lipid suspension became even and uniform. Multilamellar vesicles were obtained by 12 hours of shaking. Large unilamellar vesicles (LUV) were prepared by extruding the resulting multilamellar vesicles 20 times repeatedly through polycarbonate membranes of 100 nm pore size using the LiposoFAST™ Basic System (Avestin, Ottawa, Canada). The lipid content and liposomal composition of the preparations were determined by high-performance thinlayer chromatography (Automated Multiple Development System and Linomat IV; CAMAG, Muttenz, Switzerland). Vesicle size determination was performed by dynamic light-scattering measurements with a Coulter Counter N4 plus (Coulter Electronics, Hialeah, USA). Mean particle size distribution (based on solid sphere weight results) is given as polydispersity index (PI) - varying from 0 (entirely monodisperse) to 1 (completely polydisperse suspension).

**Table 2.1** Composition and properties of Folate-PEG-cationic liposomes

Liposome composition	DOTAP : cholesterol : DSPC : DSPE-PEG-Folate
Molar ratio	5 : 4.7 : 5 : 0.3
Suspension media	aqueous 5% glucose solution
Mean size (diameter)	105 ± 48nm
Polydispersity index	0.22

**Table 2.2** Composition and properties of PEG-cationic liposomes

Liposome composition	DOTAP : cholesterol : DSPC : DSPE-PEG
Molar ratio	5 : 4.7 : 5 : 0.3
Suspension media	aqueous 5% glucose solution
Mean size (diameter)	104 ± 22nm
Polydispersity index	0.04

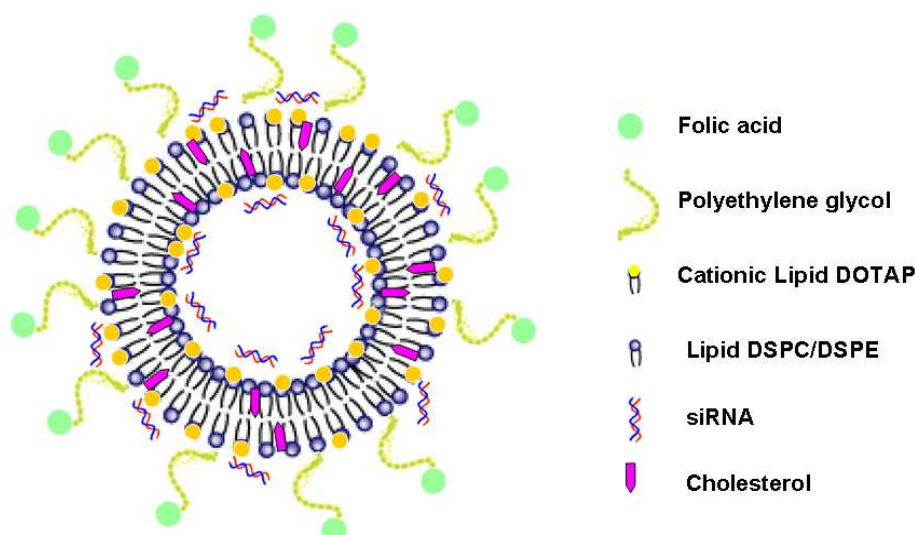


**Figure 2.2** Schematic structure of the folate-PEG cationic liposome-siRNA complex depicted in this thesis

### 2.13 Preparation of the siRNA-carrying PG-based nanoparticles

The protocol described by professor Rainer Haag was followed. SiRNAs were encapsulated in the SX141 nanoparticles in a 1:8 molar ratio. Briefly, to prepare the stock solution of siRNA, 2970 $\mu$ g FECH-1140 siRNA were added to 1 ml buffer. Solution of PG-based nanoparticle was prepared by dissolving SX141 in phosphate-buffered saline (PBS). For intratumor injection, we used the concentration of siRNA at a dose of 0.067 nmol per gram of body weight, and the SX141 at a dose of 0.536nmol per gram of body weight. Animals were administered in an intratumor injection of total volume 50 $\mu$ l siRNA-SX141 mixture per mouse/day.

### 2.14 Fluorescent microscopy

MDA MB 231 cells were seeded in 8-well chamber slide at a cells-plating density of  $1 \times 10^4$  /well. Cells were grown in standard culture conditions before transfection. 24h after seeding, PEG cationic liposomal complex or folate-PEG cationic liposomal complex containing siRNA labeled with the fluorophore Cy3 (50nM), as well as naked Cy3-siRNA (50nM) and no-siRNA & no-liposomes control media were placed separately in the 8-well chamber slides. After 4 h incubation with the transfection media, the cells were washed twice with PBS, and then fixed with 4% paraformaldehyde in PBS for 10 min. at room temperature. The cells were washed with PBS again and nuclei were stained with 300 nM 4',6-diamidino-2-phenylindole dihydrochloride hydrate (DAPI; D8417, Sigma) for 10 min. After that, cells were washed twice with PBS. Finally, the fluorescent mounting media antifade reagent (DAKO, CA, USA) was applied and a cover slip was added above the slide to prepare for microscopy.

The cells were viewed by using an Olympus BX50 microscope (Olympus Corporation, Japan) modified for fluorescence capabilities, 100 Watt Epifluorescence Illumination applied in conjunction with transformer OLYMPUS U-RFL-T. Fluorescence within the cells was visualized using a filter-cube UVF: U-MWU; TPF: U-MWIB set. Digital pictures were captured by using an Olympus Soft Imaging Solutions ColorView II digital camera, flanged onto the microscope. Acquired fluorescence images then were transferred to the computer. The camera was controlled by the analySIS image analysis software (Software Imaging Solutions for Life Science Microscopy<sup>®</sup>, Olympus Soft Imaging Solutions GmbH, Germany). This software enabled acquisition, processing and visualization of fluorescence images. Photography was similar to other fluorescent techniques, fluorescence from both the DAPI (blue) and the cy3 (red) could be acquired and recorded separately and later recombined in a merged false color image.

### **2.15 Confocal microscopy**

MDA MB 435 cells were seeded in 8-well chamber slide at a cells-plating density of  $1 \times 10^4$  /well. Cells were grown in standard culture conditions before transfection. 24h after seeding, FECH-siRNA (50nM) in folate PEG cationic liposome-siRNA complex was applied to the chamber slide and incubated for 4 h; Folate PEG cationic liposome alone without siRNA treatment was used as negative controls. After incubation, cells were washed with PBS and replaced with their own medium. A second siRNA treatment was conducted on day 4. Cells fluorescence capabilities were viewed at day 6 by confocal microscopy: at day 6, the slides were washed twice with PBS, and the cells were fixed with 4% paraformaldehyde in PBS for 10 min. at room temperature. Afterwards, cells were re-washed twice with PBS. Finally, the fluorescent mounting media antifade reagent (DAKO, CA, USA) was applied and a cover slip was added above the slide. Slides were viewed under Leica TCS SP5 confocal microscope for fluorescence capabilities.

### **2.16 PpIX-mediated fluorescent imaging for detecting tumors *in vivo***

Mice were used for all experiments and all animal procedures were approved by the regional authorities according to German animal-care regulations. The female nude mice used in the present experiments were 6 to 7 weeks of age and weighed approx. 20 g at initiation of the experiments. Human mammary carcinoma MDA MB 435 cells ( $1 \times 10^7$ /mouse) were inoculated in the right/left inguinal fat pad of nude mice at day 0. Then the animals were kept for another 2 - 3 weeks to allow the development of tumors with a size of approximately 3 mm in diameter. Tumor-bearing mice were randomized for the studies. The nude mice bearing xenograft tumors were assigned to

7 different groups as follows:

Group A (2 mice) animals were injected intratumorally at day 16, day 18, and day 21 with 50  $\mu$ l folate-PEG cationic liposomes without FECH-siRNAs serving as control.

Group B (4 mice) animals were injected intratumorally at day 16, day 18, and day 21 with 50 $\mu$ l folate-PEG cationic liposomes plus an intratumoral injection of ALA at different drug concentrations: 5mg (1mouse), 10mg (1mouse), and 15 mg/kg (2mice), at day 22.

Group C (3 mice) animals were injected intratumorally at day 16, day 18, and day 21 with 50  $\mu$ l folate-PEG cationic lipoplexes containing FECH-1140 siRNAs at a dose of 0.067 nmol/gram of body weight.

Group D (5 mice) animals were injected intratumorally at day 16, day 18, and day 21 with 50  $\mu$ l folate-PEG cationic lipoplexes containing FECH-1140 siRNAs at a dose of 0.067 nmol/gram of body weight plus an intratumoral injection of ALA at a single dose of 15 mg/kg at day 22.

Group E (3 mice) animals were injected intratumorally at day 16, day 18, and day 21 with 50  $\mu$ l siRNA carrying-SX141 nanoparticles (encapsulated with a dose of 0.067nmol/gram of FECH-1140 siRNAs) plus an intratumoral injection of ALA at a single dose of 5 mg/kg at day 22.

Group F (3 mice) animals were injected intratumorally at day 16, day 18, and day 21 with 50  $\mu$ l siRNA carrying-SX141 nanoparticles (encapsulated with a dose of 0.067 nmol/gram of FECH-1140 siRNAs) plus an intratumoral injection of ALA at a single dose of 10 mg/kg at day 22.

Group G (3 mice) animals were injected intratumorally at day 16, day 18, and day 21 with 50  $\mu$ l siRNA carrying-SX141 nanoparticles (encapsulated with a dose of 0.067 nmol/gram of FECH-1140 siRNAs) plus an intratumoral injection of ALA at a single dose of 15 mg/kg at day 22.

Tumors in xenografted human tumor model of nude mice were detected at day 22 by probing the emission of PpIX fluorescence. Images were acquired by using a non-invasive intravital fluorescence imaging system (Physikalisch-Technische Bundesanstalt, Berlin, Germany), which consisted of a LED (Luxeon 1W, center

wavelength 505nm) as excitation light source and an EMCCD-Camera (electron multiplied CCD-Camera, IXON, manufacturer Andor Technology, Belfast, Northern Ireland). For detection, a camera with a 50mm Nikon objective and 2 long pass filters (550 nm omega optical inc., Brattleborough, USA) were used. Due to the broad emission spectrum of LED, we used a 550 nm short pass filter in front of it.

### **2.17 Data evaluation**

All *in vitro* experiments were repeated with at least three independent measurements performed from different samples. Each performed in triplicate. Results were given in the form of mean  $\pm$  SD (standard deviations). Correlations between clinical parameters and gene expression as measured by qPCR were analysed by Wilcoxon test. A value of  $P < 0.05$  was considered statistically significant. Data were analysed with SPSS 14.0 (SPSS, Chicago, IL).

### **3 Results**

#### **3.1 Expression of heme metabolism relevant enzymes in colorectal tissues**

$\delta$ -aminolevulinatase synthase<sub>1</sub> (ALAS<sub>1</sub>), porphobilinogen deaminase (PBGD), ferrochelatase (FECH), and heme oxygenase (HO) mRNA-expression were determined in microdissected specimens of colorectal carcinoma tissue and corresponding normal mucosa. Quantitative single-step multiplex RT-PCR in relation to that of the housekeeper gene  $\beta$ -Actin and in comparison with the colorectal cell line SW480 was used (Figure 3.1). Results showed that ALAS<sub>1</sub> mRNA-expression was reduced in colorectal carcinomas compared to that of normal tissue of the same patients ( $P < 0.031$ , Wilcoxon-test of matched pairs). No significant alterations in PBGD mRNA-expression between colorectal carcinomas and normal mucosa were detected. HO mRNA-expression was reduced in colorectal carcinomas compared to normal tissue of the same patients ( $P < 0.021$ , Wilcoxon-test of matched pairs). Ferrochelatase expression was significantly reduced in colorectal carcinomas compared to normal tissue of the same patients ( $P < 0.005$ , Wilcoxon test of matched pairs).

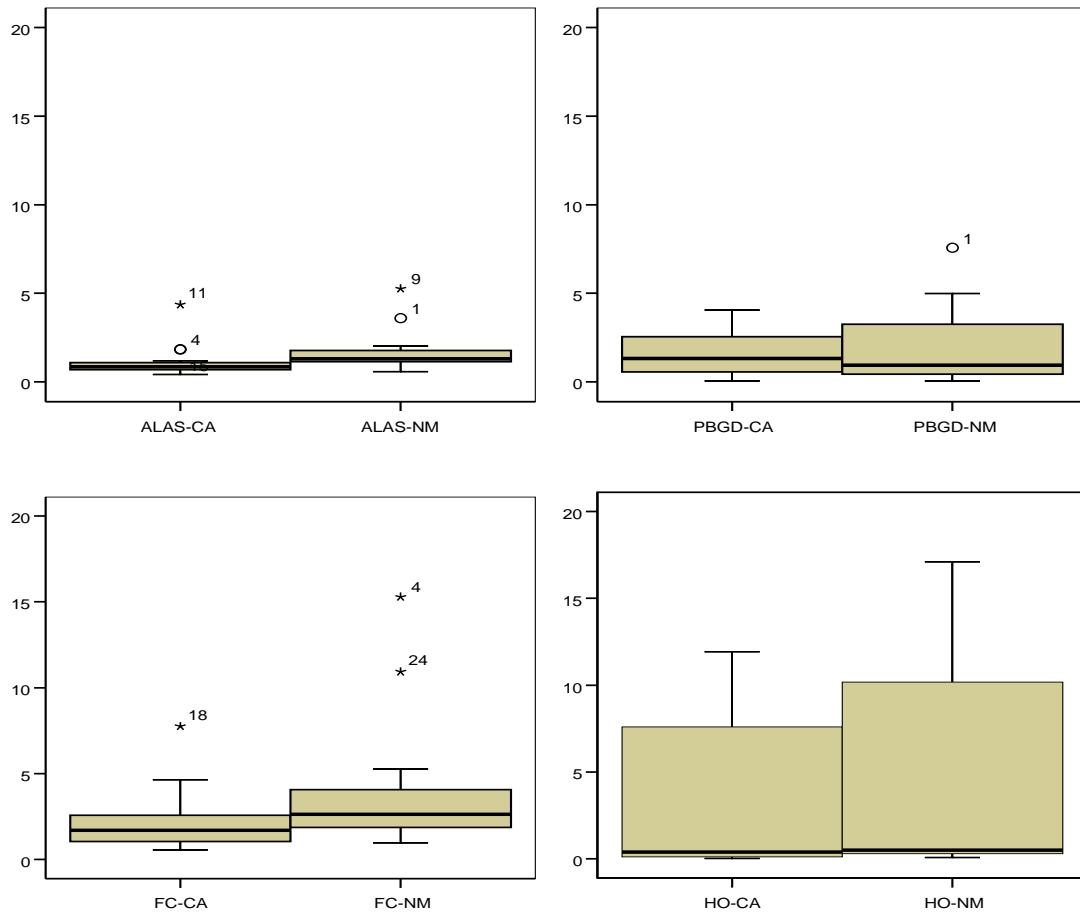


**Figure 3.1 Expression of heme metabolism enzymes in colorectal tissues**

The mRNA expression of  $\delta$ -aminolevulinate synthase (ALAS), porphobilinogen deaminase (PBGD), ferrochelatase (FC) and heme oxygenase (HO) in colorectal tumor tissue and corresponding normal mucosa were determined by using quantitative RT-PCR. A total of 30 cases of colorectal carcinomas were examined for each enzyme. Ferrochelatase mRNA expression was significantly higher in normal mucosa compared to carcinoma tissue ( $P < 0.005$ , Wilcoxon-test). Computational analysis of expression data was made by the  $\Delta\Delta C_t$ -method with reference to  $\beta$ -actin expression. Abbreviations: CA, carcinoma tissue; NM, normal mucosa. X-axis: tissue samples; Y-axis, relative amount of expression; \*, or  $^o$  depict samples which were rated as extremes or outliers.

### **3.2 FECH mRNA expression in different parts of the gastrointestinal tract**

Ferrochelatase mRNA-expression in microdissected samples of gastrointestinal tissue was determined by quantitative single-step multiplex RT-PCR as described above. In general, FECH expression is significantly reduced in gastrointestinal carcinomas in comparison to normal mucosa of the same patient. This decrease in FECH mRNA-expression was highly significant as well in gastric ( $P < 0.001$ ), colonic ( $P < 0.005$ ), and rectal ( $P < 0.031$ ) carcinomas compared to corresponding normal mucosa (Wilcoxon-test of matched pairs). FECH expression of esophageal carcinomas was also lower than that of corresponding normal mucosa. However, this difference was not significant, presumably because FECH expression in esophageal tissues showed higher variation (Figure 3. 2).

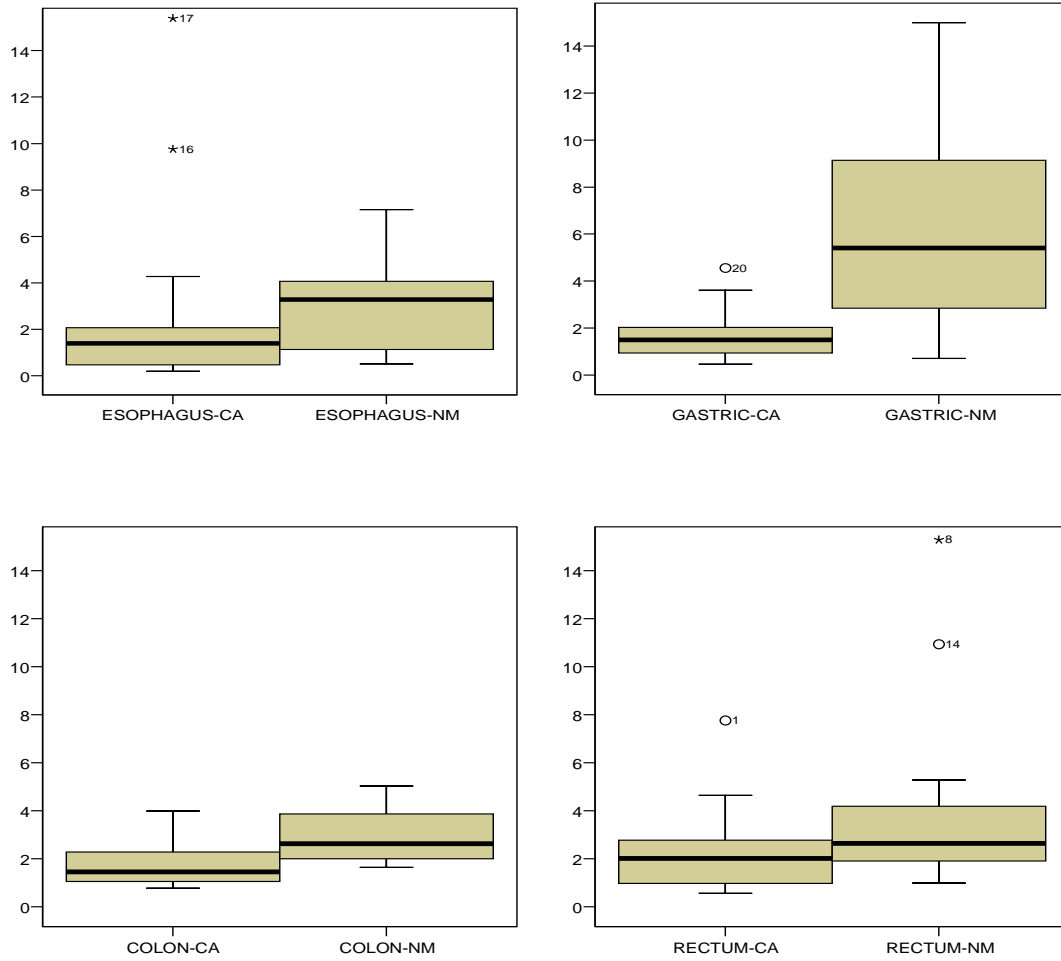


**Figure 3.2 Ferrochelatase mRNA expression in different parts of the gastrointestinal tract**

Ferrochelatase mRNA expression was determined by quantitative RT-PCR in different parts of the gastrointestinal tract. A panel of 18 cases with esophageal carcinomas, 20 cases with gastric carcinomas, 15 cases with colonic carcinomas, and 15 cases with rectal carcinomas, along with their non-malignant counterparts were examined. Throughout the gastrointestinal tract, except in esophageal tissue, ferrochelatase expression was significantly higher in normal mucosa compared to carcinoma tissue ( $p < 0.05$ ; Wilcoxon-test). Computational analysis of expression data was made by using the  $\Delta\Delta C_t$  method in comparison to  $\beta$ -actin expression (see Materials & Methods). Abbreviations: CA, carcinoma tissue; NM, normal mucosa. X-axis: tissue samples; Y-axis, relative amount of expression; \*, or  $^{\circ}$  depict samples which were rated as extremes or outliers.

### 3.3 FECH expression correlates with the potential to accumulate PpIX

In an *in vitro* model consisting of several carcinoma cell lines, FECH mRNA-expression and FECH enzyme activity were independently determined. FECH mRNA-expression was measured by quantitative single-step multiplex RT-PCR in relation to that of  $\beta$ -Actin. FECH enzyme activity was determined as described by van Hillegersberg<sup>147</sup>. FECH mRNA-expression correlated well with enzyme activity (Table 3.1). PpIX-accumulation was induced by exogenous ALA-stimulation with 0.1 mM ALA for 4 hours and determined by time-delayed fluorescence measurements as described above. Down-regulation of FECH expression in the carcinoma cell lines corresponded to their potential to accumulate PpIX after ALA-stimulation. The tendency for high PpIX content accompanied by low ferrochelatase expression and *vice versa* was observed.

**Table 3.1** Comparison of ferrochelatase mRNA-expression, enzyme activity, and concentration of protoporphyrin-IX in an *in vitro* model of several human carcinoma cell lines

Cell line	Ferrochelatase mRNA expression (relative amount)	Ferrochelatase enzyme activity (nU/mg)	PpIX (nmol /10 <sup>6</sup> cells)
HT29-P92	0.526±0.03	8.92±0.6	16.96±4.1
SW480	0.551±0.02	10.92±4.1	27.94±3.8
HT29-P37	0.696±0.02	12.33±3.8	19.15±3.2
MDA-MB-435	0.921±0.08	18.33±1.9	0.73±0.3
LS174T	1.000±0.05	23.54±6.3	1.76±0.3

Cells were cultured in 6-well plates for 5 days. Quantitative RT-PCR was used for determination of ferrochelatase mRNA-expression. Computational analysis of expression data was made by using the  $\Delta\Delta C_t$  method with reference to  $\beta$ -actin. Zn-Protoporphyrin was used as reaction product to determine ferrochelatase enzyme activity by HPLC-based fluorescence detection. Intracellular protoporphyrin-IX concentration was determined by time-resolved fluorescence spectroscopy using cells which were harvested after addition of 0.1 mM  $\delta$ -aminolevulinic acid for 4 hours. As depicted in column 2 and 3, FECH enzyme activity showed a strong correlation with mRNA expression ( $r^2=0.95$ ). Determination of PpIX showed that cell lines with high FECH enzyme activity displayed low PpIX-fluorescence ( $r^2=0.71$ ). Given are the means of five independent measurements. Cells used were colorectal carcinoma cells LS174T, SW480, HT29 (two different passages), and MDA-MB-435 cells, originally derived from a mammary carcinoma.

### 3.4 Silencing of FECH-expression by siRNA-treatment *in vitro*

For silencing of FECH gene expression by siRNA-treatment, the colorectal carcinoma cell line LS174T was chosen. These cells displayed relatively high amount of FECH

mRNA expression level and enzyme activity, and only a very low PpIX-fluorescence could be observed after ALA-addition. We used siRNAs directed towards three different coding regions of human ferrochelatase (EC 4.99.1.1), starting from base pairs 510, 1140, and 2107 of the FECH sequence (gene bank accession NM\_001012515.1) in a concentration of 50 nM. In addition, a 50 nM mixture composed of all 3 sequences was used. Cells of mock group were treated with a 50 nM of negative control siRNA, which was not related to heme biosynthesis and exhibited no target mRNA in the transcripts of FECH sequence. Among the three candidate siRNAs, the most effective working one was siRNA FECH-1140, which blocked about 65 % of the FECH expression found in mock-treated LS174T cells (Table 3.2).

**Table 3.2** Comparison of the efficacy of different siRNAs for silencing of FECH gene expression

siRNAs	FECH mRNA (relative amount)	Inhibition rate (%)
Mock siRNAs	1.000	
FECH-510 siRNAs	0.382 ( $\pm$ 0.12)	61.80
FECH-1140 siRNAs	0.354 ( $\pm$ 0.28)	64.60
FECH-2107 siRNAs	0.438 ( $\pm$ 0.13)	56.20
FECH-mixture siRNAs	0.323 ( $\pm$ 0.13)	67.70

$2 \times 10^5$  LS174T cells were treated twice (see Materials & Methods) with 50 nM siRNAs directed towards three different coding regions of human ferrochelatase (EC 4.99.1.1), starting from base pairs 510, 1140, and 2107 of the FECH gene sequence (gene bank accession NM\_001012515.1) in a concentration of 50 nM. In addition, a 50 nM mixture composed of all 3 candidate siRNAs as described above was used. Cells were also treated with a 50 nM of negative control siRNA, which was not related to heme biosynthesis and exhibited no target mRNA in the transcripts of FECH sequence. Quantitative RT-PCR was used for determination of ferrochelatase mRNA-expression. Computational analysis of expression data was made by using the  $\Delta\Delta C_t$  method with reference to  $\beta$ -actin. **Abbreviations:** mock-siRNAs: siRNA sequences which are not related to heme biosynthesis and exhibit no target mRNA in the transcripts of both NM\_001012515.1 and NM\_000140.2; FECH-510 siRNAs: siRNAs directed towards the ferrochelatase sequence starting at bp 510; FECH-1140 siRNAs: siRNAs directed towards the ferrochelatase sequence starting at bp 1140; FECH-2107 siRNAs: siRNAs directed towards the ferrochelatase sequence starting at bp 2107; FECH-mixture siRNAs: equal amounts of the mixture composed of all 3 candidate siRNAs as described above. Given are the means of five independent measurements.

### 3.5 PpIX accumulation in LS174T cells treated with FECH-siRNA

After treatment of LS174T cells with FECH-siRNA, cellular PpIX of the LS174T cells was quantitatively determined by a time-resolved fluorescence spectroscopy. Cellular concentration of PpIX in FECH-1140 siRNAs transfected LS174T cells was increased more than 20-fold compared to mock LS174T cells (Figure 3.3).

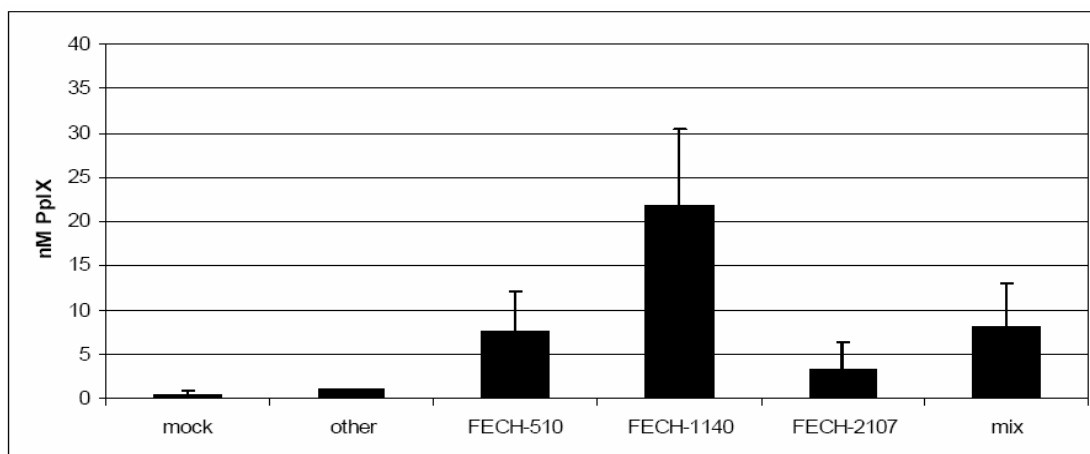


**Figure 3.3 PpIX accumulation in LS174T cells treated with siRNAs directed towards ferrochelatase mRNA**

LS174T cells were treated two times (see Materials & Methods) with 50 nM siRNA directed towards different regions of the ferrochelatase mRNA sequence (FECH mRNA, transcript variant 1, gene bank accession NM\_001012515.1). PpIX was quantitatively determined by time-resolved fluorescence spectroscopy.

**Abbreviations** mock: no siRNA-treatment; other: negative control siRNA; FECH-510: siRNA directed towards the ferrochelatase sequence starting at bp 510; FECH-1140: siRNA directed towards the ferrochelatase sequence starting at bp 1140; FECH-2107: siRNA directed towards the ferrochelatase sequence starting at bp 2107; FECH-mixture: equal amounts of the siRNAs directed towards different regions of the ferrochelatase mRNA sequence. X-axis: siRNA-treatment; Y-axis: nmol PpIX per  $10^6$  LS174T cells. Given are the means of five independent measurements.

### 3.6 PpIX accumulation after combined FECH-siRNA and ALA treatment

In order to study the effect of a combined treatment with FECH siRNA in conjunction with ALA, LS174T cells were treated twice with FECH-siRNA. Thereafter, ALA was added in a concentration of 0.1 mM for 240 min. As a consequence, PpIX fluorescence was increased more than 50-fold after combined FECH-1140 siRNAs treatment and ALA stimulation compared to ALA-treatment alone (Figure 3.4).

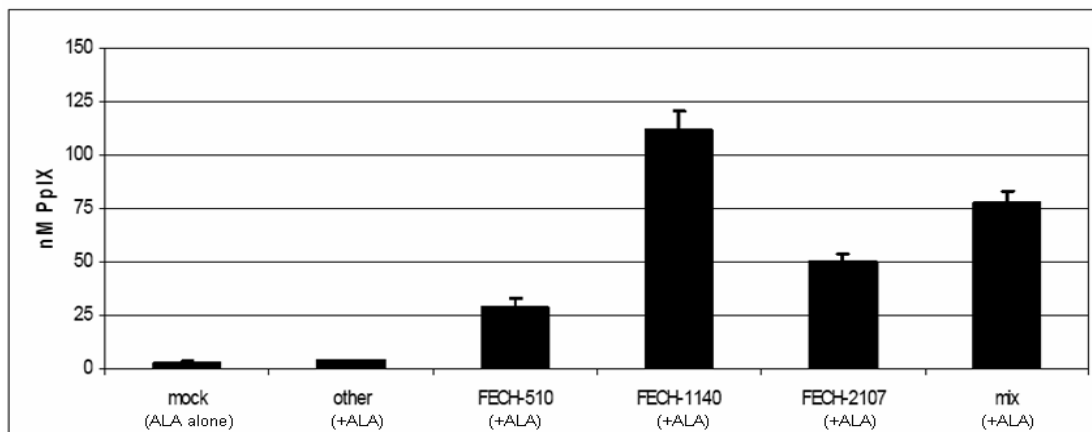


**Figure 3.4 PpIX accumulation in cells treated with FECH-siRNA and ALA**

LS174T cells were treated twice (see Materials & Methods) with 50 nM siRNA directed towards different regions of the ferrochelatase mRNA sequence (FECH mRNA, transcript variant 1, gene bank accession NM\_001012515.1). Thereafter, ALA was added in a concentration of 0.1 mM ALA for 4 hours. PpIX was quantitatively determined by time-resolved fluorescence spectroscopy. PpIX fluorescence was increased more than 50-fold after combined FECH-1140 siRNAs treatment and ALA stimulation compared to ALA-treatment alone (mock). **Abbreviations** mock: no siRNA-treatment; other: negative control siRNA; FECH-510: siRNA directed towards the ferrochelatase sequence starting at bp 510; FECH-1140: siRNA directed towards the ferrochelatase sequence starting at bp 1140; FECH-2107: siRNA directed towards the ferrochelatase sequence starting at bp 2107; FECH-mixture: equal amounts of the siRNAs directed towards different regions of the ferrochelatase mRNA sequence. X-axis: siRNA-treatment; Y-axis: nmol PpIX per  $10^6$  LS174T cells. Given are means of five independent measurements.

### 3.7 Two-photon microscopy for intracellular PpIX fluorescence imaging

Images of treated LS174T-cells were generated by two-photon microscopy. Due to the high depth of field of two-photon microscopy, the images showed sections through the LS174T cells, where the fluorescence light collected stems from a layer of approximately 1  $\mu\text{m}$  thickness. Imaging was performed 5  $\mu\text{m}$  above the cover slide surface. With cell diameters of approx. 10  $\mu\text{m}$ , the images are shown in figures (Figures 3.5) and (Figures 3.6) represent sections through the axial center of the cells. The images show the fluorescence detected in the PpIX channel reduced by the fluorescence intensity detected in the autofluorescence channel. Since endogenous fluorescence emission takes place in a broad wavelength range, almost identical autofluorescence intensities are detected in both channels. Therefore, the distribution of the autofluorescence signal in the PpIX channel can be compensated by subtracting the fluorescence intensities detected in the autofluorescence channel from the fluorescence signal detected in the PpIX channel. In addition, corresponding scatter plots show the correlation between the images detected at different detection

wavelengths, *i.e.*, PpIX at  $635\pm 20$  nm and endogenous fluorescence at  $535\pm 17.5$  nm. The use of scatter plots for signal decomposition was demonstrated by Moertelmaier *et al.* <sup>218</sup>. While mock-treated cells showed only weak fluorescence in the PpIX emission band (Figures 3.5 a,b), treatment of LS174T cells with 50 nM FECH-1140 siRNAs resulted in a strong increase in PpIX fluorescence, which showed increased brightness of the image and higher fluorescence intensity spots up to values of 250 counts PpIX/ms (Figures 3.5 c,d). Similarly, treatment of LS174T cells with 1 mM ALA alone led to a strong increase of PpIX fluorescence compared with mock treatment (Figures 3.6 a,b). However, PpIX fluorescence intensity was much higher up to 2500 counts PpIX/ms after combined FECH-1140 siRNAs treatment and ALA stimulation (Figures 3.6 c,d).

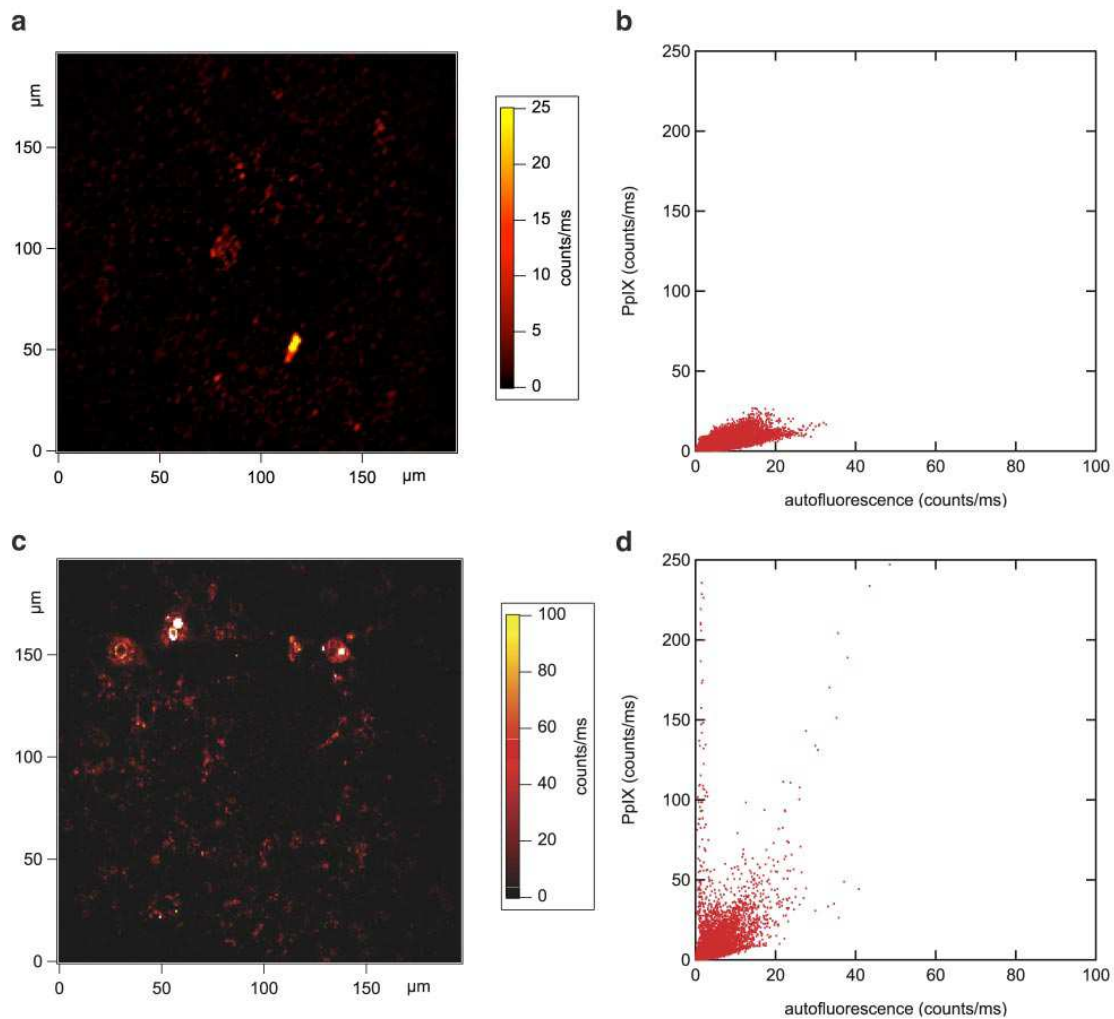


**Figure 3.5 Two-photon microscopy images of untreated cells and FECH-1140 siRNA treated LS174T cells**

In the images a) and c), cells fluorescently labeled by PpIX are displayed. Fluorescence is as detected in the PpIX channel, corrected for the fluorescence intensity of the autofluorescence channel. Please note that the intensity scale is cropped in false colors for better visibility and intensity. Values that exceed the scale are shown in white. The sharp yellow spot in image a) is an artefact. Corresponding scatter plots of two-photon-microscopy images of LS174T-cells b) and cells treated with FECH-1140 siRNA d) are presented as well. The scatter plots show the correlation pixel by pixel between images detected at different emission wavelengths. X-axis, endogenous autofluorescence at  $\lambda = 535 \pm 17.5$  nm; Y-axis, PpIX fluorescence at  $\lambda = 635 \pm 20$  nm; counts/ms, counts/millisecond.

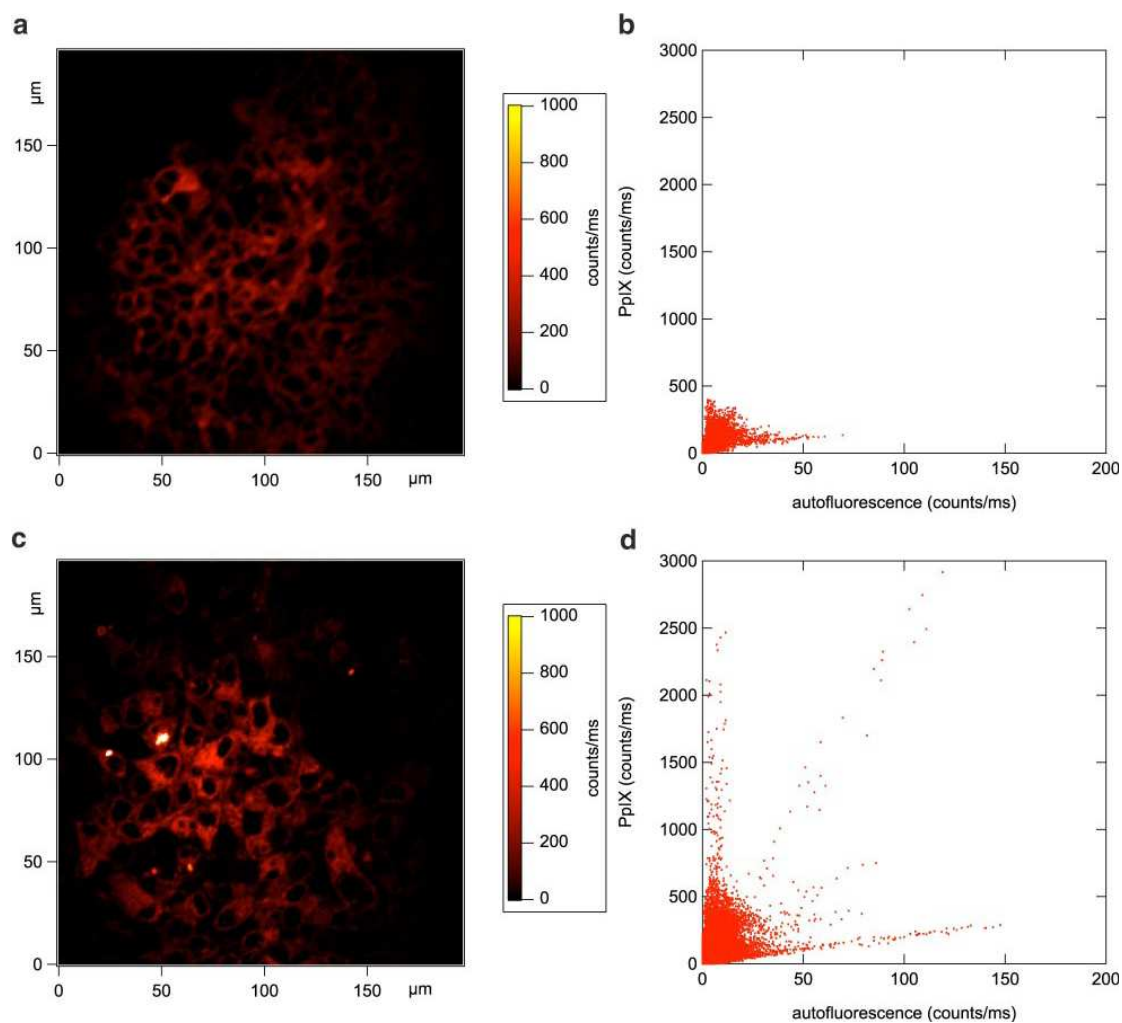
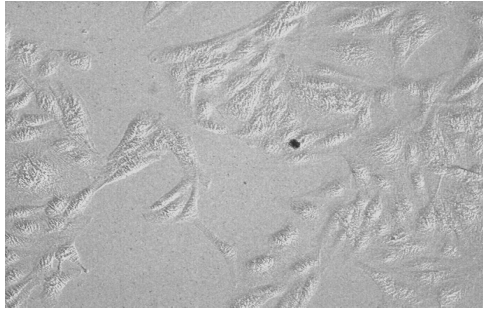


**Figure 3.6 Two-photon-microscopy images of cells treated with ALA and cells treated with FECH-1140 siRNA in conjunction with ALA**

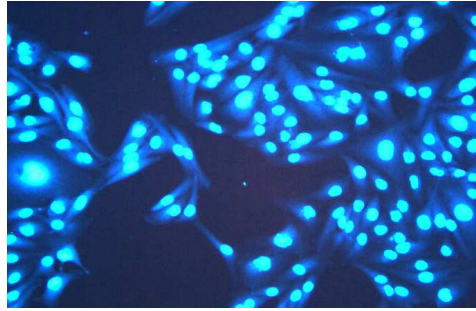
In the images a) and c), cells fluorescently labeled by PpIX are displayed. Fluorescence is as detected in the PpIX channel, corrected for the fluorescence intensity of the autofluorescence channel. Please note that the intensity scale is cropped in false colors for better visibility and intensity. Values that exceed the scale are shown in white. Corresponding scatter plots of two-photon-microscopy images of LS174T-cells treated for 4 h with 1 mM ALA alone b) and cells treated with FECH-1140 siRNA in conjunction with 1 mM ALA d) are presented as well. The scatter plots show the correlation pixel by pixel between images detected at different emission wavelengths. X-axis, endogenous autofluorescence at  $\lambda = 535 \pm 17.5$  nm; Y-axis, PpIX fluorescence at  $\lambda = 635 \pm 20$  nm; counts/ms, counts/ millisecond.

### **3.8 Visualization of the process of cationic liposomes mediated uptake of siRNAs**

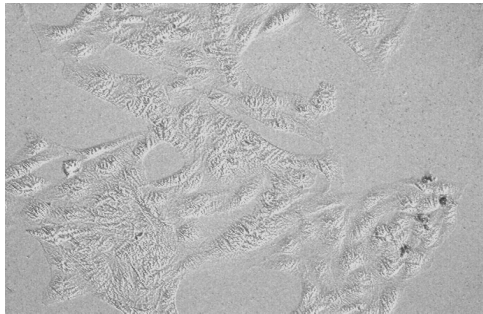
For evaluating the efficiency of PEG cationic liposomes and folate-PEG cationic liposomes mediated uptake of siRNAs, we used fluorescence micrography to observe the Cy3-labeled siRNAs (red) inside MDA MB 231 cells. After washing and fixing, cell nuclei were stained with the fluorescent marker DAPI (blue) to more accurately determine the location of the fluorescently labeled siRNA and to observe nuclear morphological structure. Fluorescent images and differential interference contrast (DIC) images are shown in (Figure 3.7).



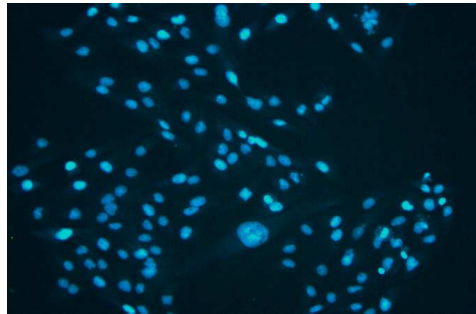
A: no-siRNA & no-liposome control DIC 100x



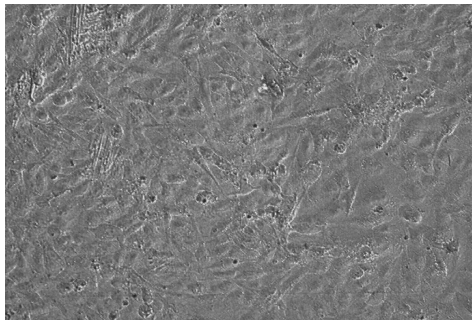
B: no-siRNA & no-liposome control TPF 100x



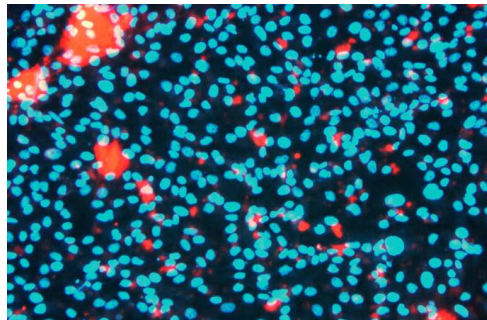
C: siRNA alone control DIC 100x



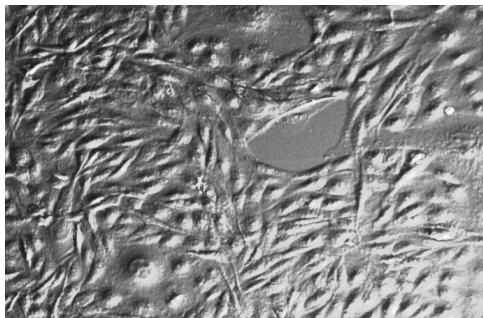
D: siRNA alone control TPF 100x



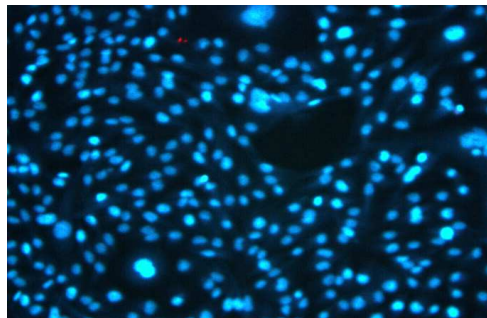
E: PEG liposome-siRNA DIC 100x



F: PEG liposome-siRNA TPF 100x



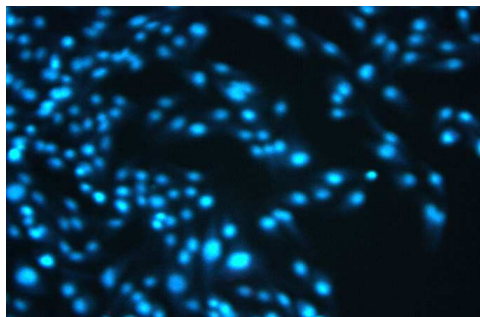
G: no-siRNA & no-liposome control DIC 100x



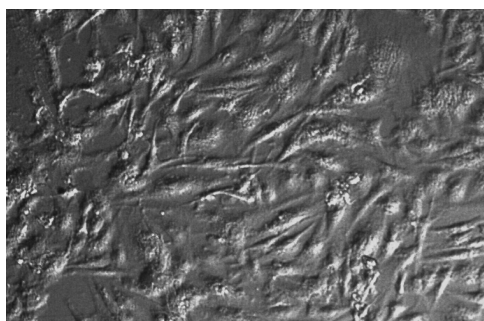
H: no-siRNA & no-liposome control TPF 100x



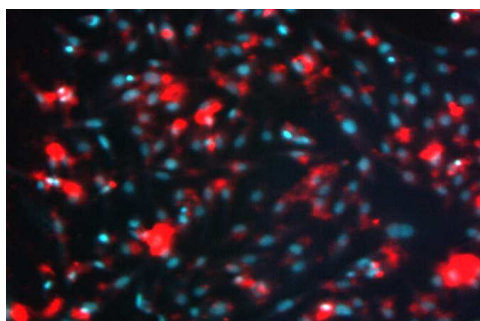
I: siRNA alone control DIC 100x



J: siRNA alone control TPF 100x



K: Folate-PEG liposome-siRNA DIC 100x



L: Folate-PEG liposome-siRNA TPF 100x

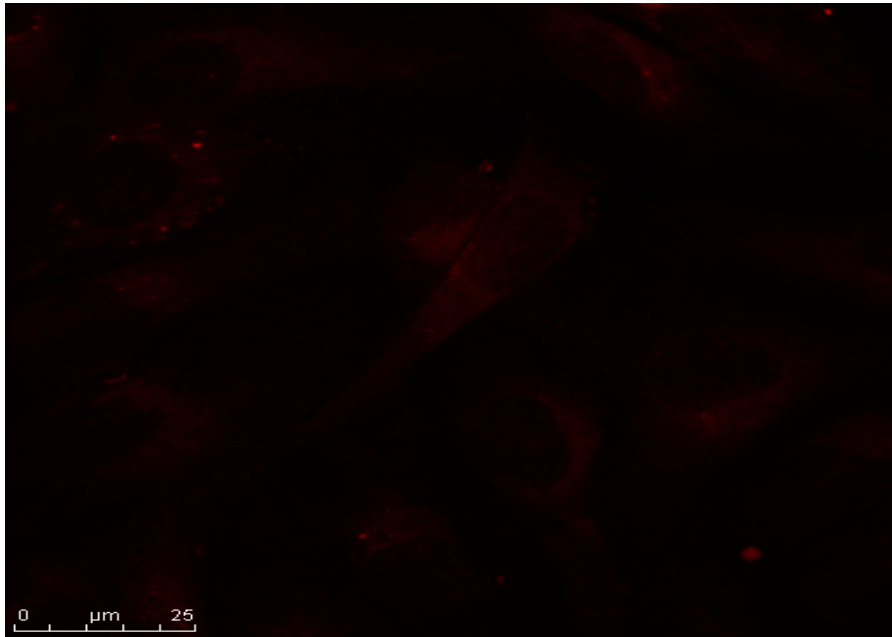
**Figure 3.7 Fluorescent microscopy of PEG-iposome and Folate-PEG-iposome-mediated uptake of Cy3 labeled siRNA:**

MDA MB 231 cells were seeded in 8-well chamber slide at a cells-plating density of  $1 \times 10^4$  /well. Cells were grown 24h in standard-culture conditions prior to transfection. Cy3-labeled siRNA-PEG cationic liposomal complexes or Cy3-labeled siRNA-folate PEG cationic liposomal complexes were applied to cells and incubated for 4 h. After washing and fixing, the cells were viewed by using an Olympus BX50 Microscope for fluorescence capabilities. Cell nuclei were stained with DAPI (blue). No-siRNA & no-liposome and naked Cy3-siRNA were used as negative controls.

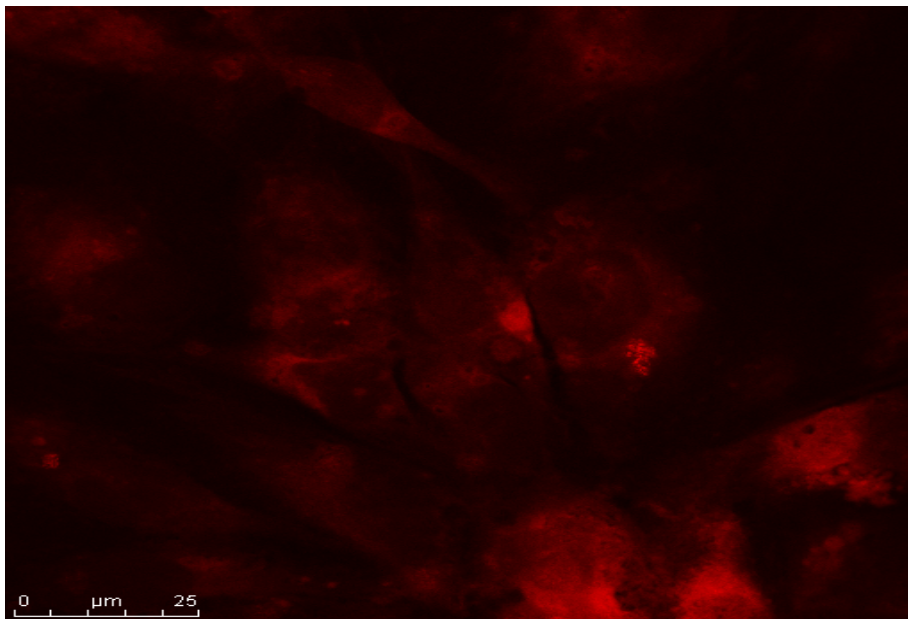
As can be seen from the photographs presented in Figure 3.7 F, in the field of view (Magnification 100x) about 40% of MDA MB 231 cells, in which the uptake of cy3-siRNA mediated by PEG cationic liposomes, bright-red fluorescence could be observed. Whereas in the case of the uptake of cy3-siRNA mediated by folate-PEG cationic liposomes (Figure 3.7 L), virtually all MDA MB 231 cells showed bright-red fluorescence in the field of view (Magnification 100x).

### **3.9 Silencing efficacy of FECH-siRNA transfected by folate-PEG cationic liposomes**

To evaluate the silencing efficacy of the FECH-siRNAs which were transfected by folate-coupled PEG cationic liposomes, confocal fluorescence-microscopy studies were performed on MDA MB 435 cells by using a Leica TCS SP5 confocal microscope for fluorescence detecting. Intracellular PpIX was excited with an excitation  $\lambda = 543$  nm, a programmable Leica Spectral-Photometer (SP detector) system setup allowed the acquisition of fluorescence emission spectra between 633 and 800 nm for detection. Confocal microscopy images confirmed that there was a considerable enhancement of PpIX fluorescence in FECH-siRNA transfected MDA MB 435 cells compared with mock-treated cells (Figure 3.8).



A. Mock-treated MDA MB 435 cells



B. FECH- siRNA transfected MDA MB 435 cells

**Figure 3.8 Silencing efficacy of FECH-siRNAs transfected by folate-PEG liposomes in MDA MB 435 cells**

MDA MB 435 cells were seeded in 8-well chamber slide at a cells-plating density of  $1 \times 10^4$  /well. Cells were grown in standard culture conditions prior to transfection. 24h after seeding, FECH-1140 siRNA (50nM) in Folate PEG cationic liposome-siRNA complex was applied to cells and incubated for 4 h. A second siRNA treatment was conducted on day 4. Cells were viewed at day 6 by using a Leica TCS SP5 confocal microscope for fluorescence capabilities. Folate PEG cationic liposome alone without siRNA treatment was used as negative controls. Confocal microscopy images showed a considerable enhancement of PpIX fluorescence in FECH-siRNA transfected cells compared with mock-treated cells.

### 3.10 Preliminary results for detecting millimeter-sized tumors in the mouse model

Xenografted tumor foci in nude mice were detected by probing the emission of PpIX fluorescence *in vivo*. Images were acquired with the fluorescence imaging system as described in materials and methods section. Results are shown in Table 3.3 and Figure 3.9.

**Table 3.3** Comparison of the detected positive xenografted tumor foci *in vivo* with respect to their fluorescence imaging for different treatment groups

Experimental groups	Inoculated xenograft tumor (n)	Fluorescence positive tumor (n)
(A) Liposome alone	2	0
(B) ALA alone	4	0
(C) siRNA alone	3	0
(D) siRNA- lipoplexes +ALA (15mg/kg)	5	3
(E) siRNA-PG SX141+ALA (5mg/kg)	3	3
(F) siRNA-PG SX141+ALA (10mg/kg)	3	3
(G) siRNA-PG SX141+ALA (15mg/kg)	3	2

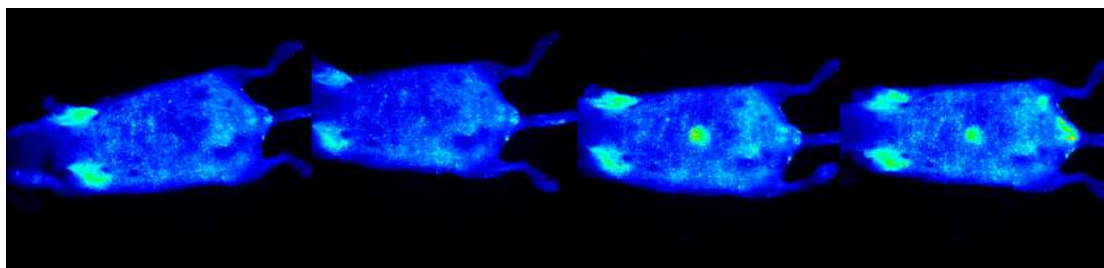
Immediately after ALA injection, no fluorescence increase was observed anywhere in all of the mice. The fluorescent signals from group A (Figure 3.9 A), mice were injected intratumorally with liposome alone, group B (Figure 3.9 B), mice were injected intratumorally with ALA at different drug concentrations: 5mg (1mouse), 10mg (1mouse), and 15mg/kg (2mice), and group C (Figure 3.9 C), mice were injected intratumorally with 0.067 nmol/gram of FECH-1140 siRNA alone were close to the background and showed little nonspecific fluorescent signals, which failed to detect the xenografted tumors in nude mice. In contrast, in group D (Figure 3.9 D<sub>1</sub>, D<sub>2</sub>, and D<sub>3</sub>), mice were treated with folate-PEG cationic lipoplexes containing FECH-1140 siRNAs at a dose of 0.067 nmol/gram followed by a single dose of 15mg/kg ALA, fluorescent signals started to increase in tumors 120 minutes after ALA injection. Dramatic enhancement of PpIX fluorescent signals from the areas of xenografted tumors were detected at 180 minutes and reached the highest level at 240 minutes after application of ALA. Xenografted tumors approximately 3 mm in diameter were easily recognized by detecting PpIX-dependent fluorescence emissions. Similarly, mice were injected intratumorally with siRNA-SX141 nanoparticles in conjunction with a low dose of ALA led to strong increase of PpIX-dependent fluorescence. Localized fluorescent hotspots were detected at the sites of the millimeter-sized tumors (Figure 3.9 E, F, and G). Circles indicate the xenografted tumors of the nude mice.

t=120min

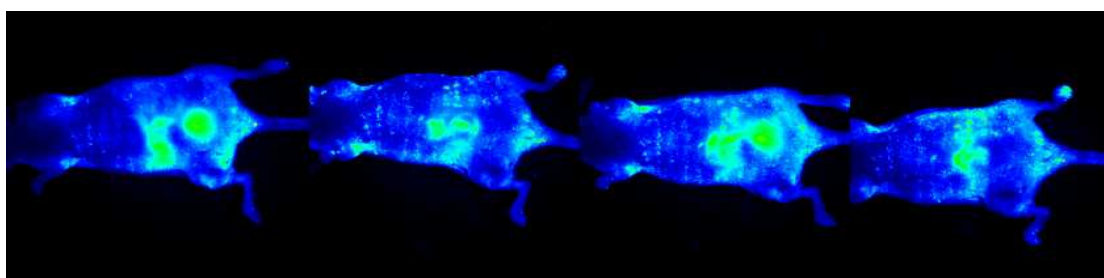
t=180min

t=240min

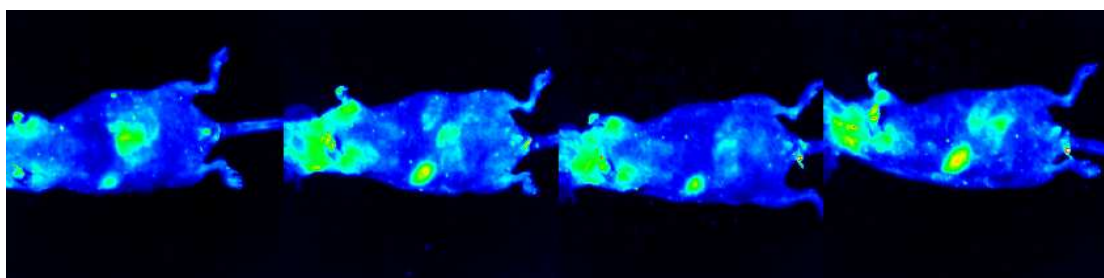
t=300min



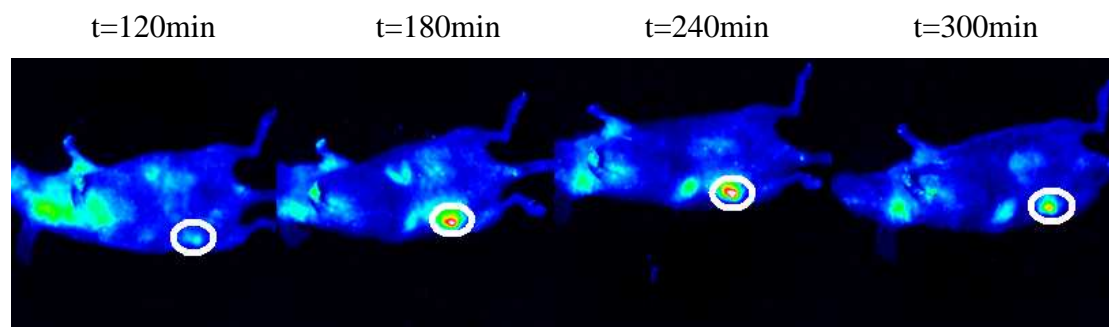
(A) Liposome treatment alone



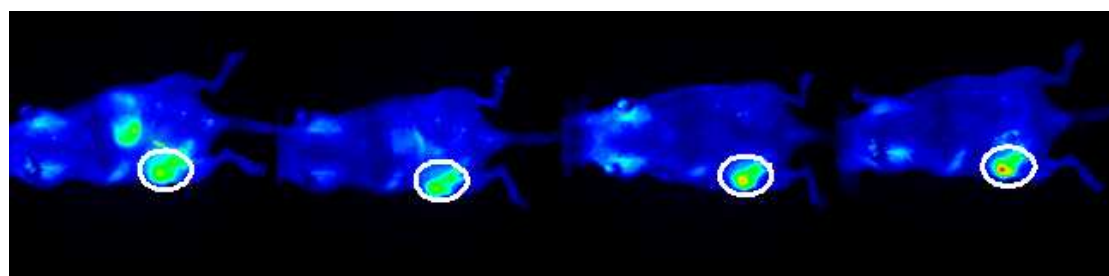
(B) ALA treatment alone



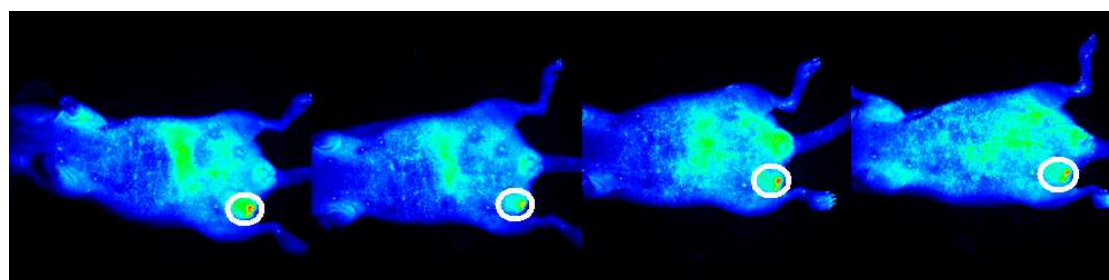
(C) siRNA treatment alone



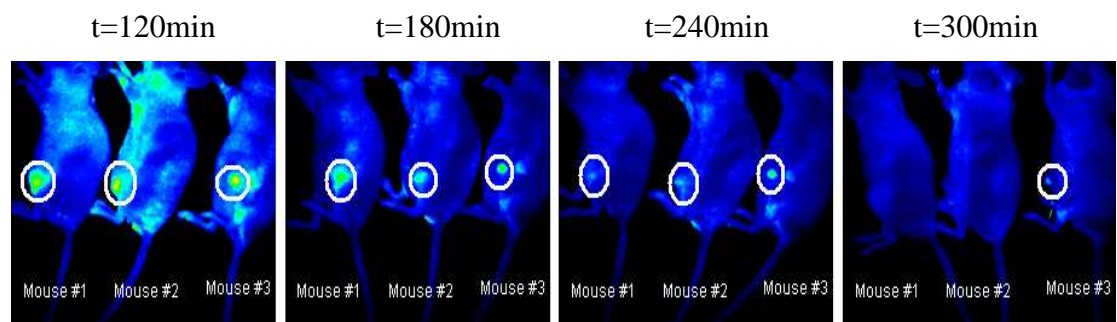
(D<sub>1</sub>) siRNA-lipoplexes +ALA 15 mg/kg (mouse#1)



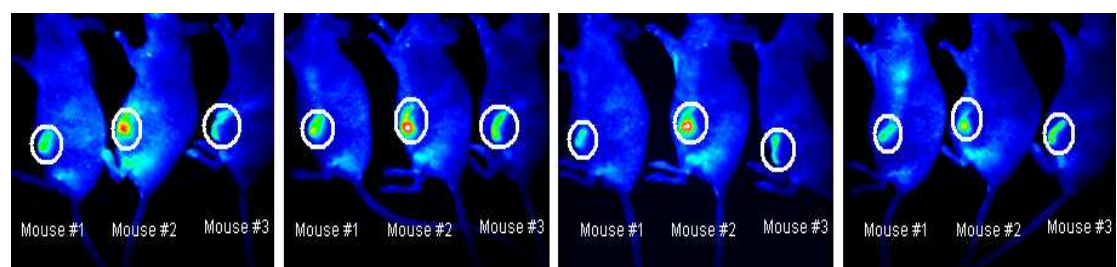
(D<sub>2</sub>) siRNA-lipoplexes +ALA 15 mg/kg (mouse#2)



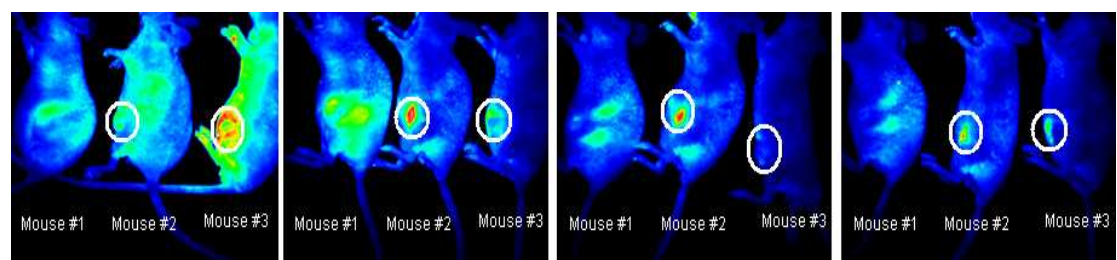
(D<sub>3</sub>) siRNA-lipoplexes +ALA 15 mg/kg (mouse#3)



(E) siRNA-PG SX141+ALA (5mg/kg)



(F) siRNA-PG SX141+ALA (10mg/kg)



(G) siRNA-PG SX141+ALA (15 mg/kg)

### Figure 3.9 Tumor fluorescent images in nude mice

The fluorescence signals from (A) Liposome treatment alone, (B) ALA treatment alone and (C) siRNA treatment alone, mice were close to the background and showed little nonspecific fluorescence signals which failed to detect the xenografted tumors in nude mice. In contrast, dramatic enhancement of PpIX fluorescent signals from the areas of xenografted tumors were detected in mice which were treated with folate-PEG cationic lipoplexes containing FECH-1140 siRNAs at a dose of 0.067 nmol/gram, followed by a single dose of 15 mg/kg ALA (D<sub>1</sub>, D<sub>2</sub>, D<sub>3</sub>). Similarly, mice were injected intratumorally with siRNA-SX141 nanoparticles in conjunction with different concentrations of ALA (5 mg, 10 mg, and 15 mg/kg), led to strong increase of PpIX-dependent fluorescence. Localized fluorescent hotspots were detected at the sites of the millimeter-sized tumors (E, F, G). Circles indicate the xenografted tumors.

## 4 Discussion

### 4.1 Relationship between FECH expression and PpIX formation

Tumor and surrounding normal tissue exhibit a different pattern of porphyrin metabolites. A better understanding of heme metabolism and the different expression levels of relevant enzymes between normal and malignant tissue is a key step in clarifying the molecular mechanisms leading to tumor-selective accumulation of endogenous PpIX.

We used quantitative RT-PCR to determine the mRNA expression levels of crucial enzymes in heme metabolism pathway, including  $\delta$ -Aminolevulinate synthase (ALAS), porphobilinogen deaminase (PBGD), ferrochelatase (FECH), and heme oxygenase (HO) in microdissected specimens of colorectal carcinoma tissue and corresponding normal mucosa (Figure 3.1). Ferrochelatase expression was significantly reduced in colorectal carcinomas compared to normal mucosa. Similarly, a significant down-regulation of FECH mRNA expression was shown in gastric, colonic and rectal carcinomas compared to normal tissue (Figure 3.2).

Among the heme metabolic relevant enzymes, PBGD and FECH are assumed to be the two most important regulatory molecules in ALA-induced PpIX formation. Previous investigations indicated that PBGD activity might be a strong regulatory factor in ALA-induced PpIX formation<sup>141, 142, 143, 144, 145</sup>. Hinnen suggested that a ratio of PBGD and FECH could be used as a diagnostic so-called PDT power index<sup>141</sup>. However, no significant alterations in PBGD mRNA-expression between colorectal carcinomas and normal mucosa were detected in this study. Our data confirmed the result seen previously by Hilf *et al.* who constructed plasmid vectors containing the PBGD DNA and demonstrated that transient transfection of cells with the cDNA of PBGD was successful in elevating enzyme activity in tumor cell lines, but this did not result in a comparable difference in the levels of PpIX<sup>220</sup>.

Our present results demonstrated that ALAS<sub>1</sub> mRNA was reduced in colorectal carcinomas compared to corresponding normal mucosa of the same patients. Although further investigation will be required to clarify the correlation between the mRNA expression and enzyme activity, our data support the previous observation by Kondo *et al.*<sup>143</sup> who found that hepatoma-derived cell lines exhibited decreased ALA synthase activity. The exact mechanisms involved in decreased ALAS<sub>1</sub> mRNA and HO mRNA expression in colorectal carcinomas are not yet clear.

Application of exogenous ALA is certainly an important factor for inducing accumulation of PpIX in cancerous cells. However, besides the uptake of the exogenous ALA, what is important for an increased PpIX formation seems to be the degree that heme cycle is activated in cells, and the degree to which it is altered. No matter how good the delivery of ALA may be, the formation of PpIX requires the activity of several enzymes (Figure 1.3). Moreover, selective accumulation of PpIX in cancerous tissues had been proved to occur under conditions without administration of exogenous ALA<sup>19, 20, 21</sup>. Thus, one of the main reasons for a selective accumulation of PpIX in cancerous tissues seems to be the difference in the metabolizing ability of the heme synthetic pathway between cancerous and normal tissues.

Previous investigations reported that the defects in FECH cause the accumulation of protoporphyrin in patients with erythropoietic protoporphyria<sup>116, 221</sup>. Data obtained from our studies agree with prior studies in showing that the selective porphyrins formation in human cancers was related to relatively lowered FECH enzyme activity<sup>15, 130, 143, 147, 222, 223</sup>. Moreover, our data revealed that a transcriptional down-regulation of FECH occurred in gastrointestinal malignant tissue (Figure 3. 1 and Figure 3. 2).

In an *in vitro* model, we also found a close correlation between FECH mRNA transcriptional level and enzyme activity. An increasing tendency for accumulation of PpIX was accompanied by a decrease in the expression of FECH, and *vice versa* (Table 3.1). Our data also showed that there were wide individual variations of the FECH expression levels among different cell-type origins, which might possibly be one of the causes for different capacity of the PpIX formation in different cancer-cell types.

The functional argument to prove the causal relationship between FECH expression and PpIX formation is now provided by the fact that the observed ALA resistance of LS174T cells which showed a relatively high level of FECH mRNA expression, can be overcome by functional application of siRNAs directed towards FECH gene. After knocking down FECH expression in siRNA-transfected LS174T cells, cellular PpIX was increased more than 20-fold compared to mock-treated cells (Figure 3.3). These results support that there is an inverse relationship between FECH-expression and PpIX-formation under the condition without exogenous ALA. The functional application of FECH-siRNA alone can lead to an obvious increase in accumulation of PpIX within colorectal cancerous cells by affecting the cellular heme metabolism.

Incubation of LS174T cells with 0.1 mM ALA for 4 hours did not induce significant accumulation of PpIX. However, if cells were treated with FECH-siRNA followed by 0.1 mM ALA, a dramatic enhancement of PpIX accumulation by a factor of 50 was achieved compared to ALA-treatment alone cells (Figure 3.4). Sharply red PpIX-dependent fluorescence could be observed in LS174T cells in which FECH-siRNA was transfected alone (Figures 3.5 c,d) or in conjunction with exogenous ALA (Figures 3.6 c,d).

We used siRNAs to block the translation of FECH in MDA MB 435 cells. Confocal-microscopy images revealed that there was an obvious increase of PpIX-fluorescence in siRNA-transfected cells (Figure 3.8), implying that the down-regulation of FECH-gene expression was associated with a considerable enhancement of PpIX accumulation in siRNA-transfected cells compared to untreated cells.

RNAi can act as a powerful tool to switch off a specific gene expression<sup>224</sup>. Although the expression of FECH varies widely from one cell line to another, functional application of siRNAs can achieve dramatic increase in the concentrations of PpIX in different tumor cells.

#### **4.2 Tumor targeting delivery of siRNAs mediated by nonviral vehicles**

Targeting delivery is the ability to preferentially direct the drug-loaded system to clinically relevant organs, tissues, cells or receptors. Tumor-specific delivery of drugs by carriers can be broadly categorized as passive and active targeting strategies according to drug transport mechanism. Passive targeting is the method determined by the physicochemical properties, e.g., molecular weight and electric charges of the macromolecular carriers relative to microvascular architecture characteristics of the healthy and malignant tissues. Active targeting is usually achieved by highly specific interactions between receptors on cell surface and targeting moieties conjugated to the drug carriers, which allow preferential accumulation of the drug in the tumor tissues. As far as tumor-targeting delivery of siRNA mediated by nonviral vehicle is concerned, there are at least three aspects, which have to be addressed: transfection efficiency, tumor selectivity, and biocompatibility.

##### **4.2.1 Transfection efficiency**

The first aspect involves the transfection efficiency. In the case of nonviral carriers for *in vivo* delivery of siRNA, the sufficient amounts of siRNAs should be delivered to the intended tissues and then to appropriate number of target cells selectively.

Furthermore, the siRNAs have to be delivered to their desired action site inside the targeted cells in sufficient concentration. The efficiency of RNAi in cell culture is often lost when siRNA is used *in vivo*. It is most likely due to rapid clearance of siRNAs by renal system<sup>177, 178</sup>, degradation by nucleases<sup>225</sup>, competitive uptake by nontarget cells<sup>178</sup>, difficulty in transporting across cell membranes once in the target tissues<sup>226</sup>, and endosomal trapping, *i.e.*, upon uptake via endocytosis, the siRNAs remain localized in the endosomes and/or lysosomes, failing to escape to the cytoplasm<sup>180</sup>.

A variety of nonviral vehicles have been used in nucleic acid delivery studies, but their effectiveness remains orders of magnitude poorer than viral vectors. Development of an effective delivery system is one of the most critical issues for using siRNA as a diagnostic agent.

Among the nonviral transfer technologies, lipofection is probably the most commonly used gene transfer method, providing safety of gene transfer associated with reasonable transfer efficiency *in vitro* and *in vivo*<sup>227</sup>. Although their gene transfer efficiency and *in vivo* stability need to be improved, cationic liposome transfection systems are considered relatively safe, simple to prepare and use, may be modified to enhance the internalization rate, and therefore can offer a safe alternative to their viral counterparts.

A chemically synthesized siRNA molecule is typically 21 nucleotides in length with 42 negative charges. This renders siRNA to be poly-anionic in nature. The electrostatic repulsion effect between the siRNA and cell membrane results in an extremely low membrane permeability for cellular uptake of naked siRNA. The positively charged amine groups of the cationic liposomes can help in the complexation and delivery of siRNA molecules. Dendritic polyglycerol-based nanocarriers, which incorporated with positively charged amine groups, may spontaneously form complexes with siRNAs, and facilitate the intracellular uptake of siRNAs by the same token.

In this study, folate-PEG cationic liposome and PG-based cationic polymers were selected as candidates for tumor-targeting delivery of siRNAs. MDA MB 231 cells transfected with Cy3-labeled siRNA were examined by fluorescence microscopy. There was a higher efficiency of uptake of Cy3-labeled siRNA in cells treated with folate-PEG cationic liposomal siRNA complex (Figure 3.7 L) compared to PEG cationic liposomal siRNA complex (Figure 3.7 F). Confocal microscopy confirmed

that the folate-PEG cationic liposome is efficient in delivering siRNA to tumor cells (Figure 3.8). FECH-siRNA transfected by folate-PEG cationic liposomes can selectively knock down FECH expression in MDA MB 435 cells, consequently leading to a higher accumulation of PpIX in those cells.

Folate-PEG cationic liposomes containing siRNAs were locally applied to xenografted tumors on nude mice. Neither application of a low dose of ALA alone (Figure 3.9 B) nor treated only with siRNA (Figure 3.9 C) can obtain sufficient fluorescent signals for *in vivo* detection of the xenografted tumors. The most likely explanation might be the different conditions between fluorescence detected *in vivo* and *in vitro*. In contrast, dramatic enhancement of PpIX fluorescent signals from the areas of xenografted tumors were detected in those of mice treated with siRNA followed by a low dose of ALA (Figure 3.9 D<sub>1</sub>, D<sub>2</sub>, and D<sub>3</sub>). Similarly, mice were injected intratumorally with siRNA-SX141 nanoparticles in conjunction with a low dose of ALA, which led to a strong increase of PpIX-dependent fluorescence. Localized fluorescent hotspots were observed at the sites of the millimeter-sized tumors (Figure 3.9 E, F, and G).

Although the precise mechanisms for folate-PEG cationic liposomes and PG-based cationic polymers mediated delivery of siRNAs to tumors are still not fully understood, it is likely that both of them contain positively charged groups to form lipoplexes/polyplexes with siRNAs, and further, gain the proper conformation and appropriate size to increase the contact between lipoplexes/polyplexes and tumor cells, finally, enter to tumor cells, then escape into cytoplasm to trigger RNAi to block FECH expression, because silencing efficiency of FECH-siRNA had been observed both *in vitro* (Figure 3.8 B) and *in vivo* (Figure 3.9 D<sub>1</sub>, D<sub>2</sub>, D<sub>3</sub>, E, F, and G).

Hyperbranched PG is one of the most important hyperbranched polymers, which can be used as the core unit and functionalized with amine groups to introduce DNA/siRNA transfection. Various parameters, such as molecular weight, amount of nitrogen atoms, their protonation behavior at certain pH values, degree of functionalisation (DF), and degrees of branching (DB) of a PG-based vector, influence the efficiency of this vector for DNA/siRNA transfection.

For successful DNA/RNA transfection, the nucleic acid molecules have to be released from endolysosomal vesicles before degradation of DNA/RNA starting. Polyplexes covered in positive charges interacting with the cell membrane will produce a high local concentration of polymers in endolysosomal vesicles, which renders these

vesicles to become more sensitive to osmotic stress <sup>228</sup>. On the other hand, the accumulated dendritic polymers can buffer the endosomal pH, causing the ATPase to transport more protons to reach the desired pH. However, the accumulation of protons in the vesicle must be balanced by an influx of counter ions, which leads to an influx of chloride anions. In the presence of dendritic polymers there will be a large increase in the ionic concentration within the endolysosome <sup>229</sup>. Moreover, the protonation of a large number of amines in the dendritic polymers will also expand their polymeric network by electrostatic repulsion of the internal positive charges <sup>228</sup>. The increased osmotic pressure ultimately causes swelling and rupture of the endolysosomal membrane <sup>228 229</sup>. Consequently, the DNA/RNA introduced by cationic polymers will be rapidly liberated from the damaging endolysosomal environment. This is known as “proton-sponge effect”. Shorter lifetime of the endocytic vesicles leads to faster release of the nucleic acid molecules. Thus, the degradation of DNA/RNA molecules could be avoided. However, whether there existed a similar phenomenon in the process of PG-based cationic polymers-mediated siRNA transfection remains unknown. Further basic research will be required, including precise measurements of the endosomal Cl<sup>-</sup> concentration, pH, and the volume of endosomes after internalization of polyplexes composed of siRNAs and dendritic PG cationic polymers, etc.

#### **4.2.2 Tumor selectivity**

The second problem relates to the cancer specificity of the synthetic vehicles. The size of the macromolecule is a crucial factor with respect to uptake by the tumor. An understanding of the functional size and physiological regulation of transvascular pathways is necessary to optimize the methods of delivery of siRNAs to tumors. Passively targeted liposomal nanocarriers for avoiding rapid reticular-endothelial system clearance and renal excretion have been suggested to be in the range of 70–200 nm in diameter <sup>230, 231, 232</sup>. The general trend for liposomes of similar composition is that increasing size translates into more rapid uptake by the RES <sup>232, 233, 234</sup>. On the other hand, small liposomes ( $\leq 60\text{nm}$ ) could be excreted out of kidney more rapidly than large ones. Liposomes of a defined size can be prepared by the extrusion of lipid suspensions through a polycarbonate filter containing pores of a similar size (e.g., 100 nm in diameter) to yield vesicles with their average diameter around the pore size of the filter used <sup>235, 236</sup>. Design of liposomal drug delivery system using such small particle size puts this branch of medicine within the regimen of nanotechnology.

Growing solid tumors have a higher vascular permeability than normal tissues. Stealth

liposomes of approx. 100 nm in size passively target solid tumors by extravasation into their extracellular space on intravenous administration. Extravasation is achieved due to the disorganized tumor vasculature<sup>237, 238, 239, 240</sup>.

Most normal tissues contain continuous capillaries with tight junctions<sup>241</sup>. The clefts between adjacent endothelial cells are usually 6-7 nm in width, which are impermeable to lipoplexes. However, there exist sinusoidal capillaries in liver, spleen, and bone marrow. Sinusoids are very large capillaries (diameter >30  $\mu\text{m}$ ) with numerous fenestrae and a discontinuous basal lamina because of the interruptions. Large compounds, even cells such as macrophages, can pass in and out of the blood through the sinusoidal capillaries. Therefore there is a tendency for accumulation of lipoplexes/polyplexes in those organs.

The homeostatic regulation of tissue and the growth of blood vessels are broken down in solid cancers. Tumor cells often have the potential for more rapid proliferation than normal cells<sup>242</sup>. Unlike normal blood vessels, tumor vessels are dilated and poorly differentiated<sup>133</sup>. Tumors are proved to have a poorly organized vascular architecture, irregular blood flow and the absence of functional lymphatic vessels. These immature vessels have wide interendothelial junctions, large number of fenestrae, discontinuous or absent basement membranes, and have leaky open gaps as large as 600 to 800 nm between adjacent endothelial cells<sup>243</sup>. The majority of tumors exhibited a characteristic vascular pore cutoff size between 380 and 780 nm<sup>134</sup>. These factors favor the movement of macromolecules across tumor vessels. A number of studies have confirmed passive accumulation of intravenously injected macromolecules in experimental and clinical cases of solid tumors<sup>191, 192, 193, 244</sup>. Macromolecules can extravasate through the leaky capillary walls into the tumor interstitial space in a size-dependent manner<sup>245</sup>. Furthermore, tumors have impaired lymphatic drainage<sup>191, 192, 193</sup>, which is exacerbated by the compression of lymphatic vessels by rapidly proliferative cancer cells<sup>242</sup>. Thus, the drug carriers concentrate in the tumor, and large increases in tumor-drug concentrations can be achieved<sup>242, 246</sup>.

The exact location of the filtration barrier of kidney is the glomerular capillary wall, which consists of thin endothelial cells with fenestrae measuring 60 – 80 nm in diameter<sup>247</sup>. As mentioned above, tumor vessels are proved to have leaky open gap. The liposomes that we used in animal experiments had been prepared with a mean size of 105 nm in diameter. Such liposomes would be able to avoid rapid RES clearance. Moreover, they are large enough to prevent rapid renal excretion yet small enough to extravasate into the tumor interstitial space through the leaky capillary

walls.

Naked siRNAs are poly-anionic in nature and have low membrane permeability. In order to facilitate the intracellular uptake of siRNAs, cationic functional groups are usually required for *in vivo* delivery of siRNA. Liposome-siRNA complexes protect siRNAs from rapid renal excretion by increasing their apparent size above the cut-off value as well as from nuclease degradation by sterically blocking the access of RNase. However, due to the positive charges, these complexes tend to form aggregates by binding to negatively charged biomolecules in the blood stream. Moreover, such positively charged complexes possess a propensity to interact with virtually any cell type they will encounter, creating a need to insulate the interactive surface of these complexes to promote the specificity of tumor targeting<sup>180</sup>.

Shielding of the cationic surfaces of these liposomes by engrafting polyethylene glycol on to the surfaces of the liposomes is supposed to gain a new conformational state, which is capable of facilitating the transfer of these liposomes/lipoplexes across the leaky tumor vessels and increasing the contact between lipoplexes and tumor cells. As coating liposomes with PEG renders their surface more hydrophilic, which inhibits the hydrophobic and electrostatic interactions between a wide variety of blood components, e.g., opsonins and the lipoplexes<sup>232</sup>, consequently prevents recognition by macrophages and reduces the rate of clearance of lipoplexes by reticular-endothelial system. These sterically stabilized liposomes can also reduce the rate of nonspecific binding of lipoplexes to non-target cells, so as to enable them to remain in the circulation longer<sup>232, 244</sup>. A longer liposomal blood-residence time will lead to repeated passages of these lipoplexes through the tumor microvascular bed, and result in a greater efficiency of the extravasation per unit volume of the convective current<sup>193</sup>. However, this solution may create another problem, i.e., the steric barrier imparted by PEG chains can interfere with the binding capacity of the PEG-liposomes. To circumvent this hurdle, ligands can be coupled to the distal terminus of the PEG chains. This strategy is expected to provide perfect accessibility to the ligand molecules for their target cells. Active targeting ligands are believed to restore the binding capacity of PEG-coated lipoplexes and lead to accumulation of these lipoplexes in tumor tissues with more precision than that the passive targeting processes will allow<sup>209</sup>.

Folates are essential for cell survival<sup>248</sup>. Tumor cells may have an increased demand for folic acid to meet their rapid division. Folate receptors are frequently over-expressed in a range of tumor tissues<sup>195, 196, 197, 198, 199, 200, 201</sup>. Thus, covalent

attachment of folic acid to PEG terminal possesses a recognition signal for specific interaction with folate-receptor-positive tumor cells, and guides the lipoplexes to enter into these cells via the same pathway as the free folic acid molecules. By combining both the EPR effect and receptor-mediated internalization pathway, more siRNA molecules are expected to be delivered into tumor cells. However, the requirement for targeting ligands may not be obligatory. In the way of using lipoplexes for delivery of siRNA to tumor, the most important reason seems to be the consequence of passive convective transport through a leaky endothelium<sup>249</sup>. Although active targeting is a very attractive approach, successful results often depend on the effective passive targeting, i.e., the success in passive targeting will help us achieve a successful result for tumor-targeted siRNA delivery. It could be the same reason for the preferential accumulation of siRNA-carrying dendritic PG nanoparticles in solid tumors.

Kainthan *et al.* used a hyperbranched polymer based on PG and PEG to bind DNA. Results showed that the multivalent cationic polymers were able to condense DNA to highly compact, stable, water-soluble nanoparticles in the range of 60 – 80 nm<sup>250</sup>. Polyplexes within the size range of 70 to 200 nm are small enough to extravasate into the tumor interstitial space through the leaky capillaries in the tumor tissue while cannot pass through the capillary walls with tight junctions in normal tissue. Differences in angiogenesis and microvascular architecture between the healthy and malignant tissues are responsible for the passive accumulation of macromolecules in tumors.

Based on our animal experimental results, despite their preliminary character, it is tempting to speculate that folate-PEG-cationic liposomal siRNA vehicle and dendritic PG nanoparticles could be able to improve local bioavailability of siRNAs within tumor tissue and facilitate the transfer of siRNAs across the tumor cell membrane. A considerable large part of siRNAs could have been released into the cytoplasm, as silencing efficiency of FECH-siRNA had been observed. Treatment of the mice with FECH-1140 siRNA containing lipoplexes/polyplexes in conjunction with a low dose of ALA led to strong increase of PpIX-dependent fluorescence, localized fluorescent hotspots were detected at the sites of the millimeter-sized tumors of the nude mice (Figure 3.9 D<sub>1</sub>, D<sub>2</sub>, D<sub>3</sub>, E, F, and G). In contrast, treatment of the same dose of ALA alone failed to detect the xenografted tumors in nude mice (Figure 3.9 B).

#### **4.2.3 Biocompatibility**

The third question refers to the biocompatibility of the synthetic vectors. Felgner *et al.* pioneered gene delivery with liposomes containing a synthetic cationic lipid

(DOTMA). These small unilamellar liposomes can interact spontaneously with DNA to form lipid-DNA complexes<sup>251</sup>. Cationic liposome-mediated transfection has been routinely applied as an efficient method in both *in vitro* and *in vivo* gene delivery studies, and in many human gene-therapy clinical trials<sup>252</sup>. Liposomal systems offer significant advantages over viral delivery options for *in vivo* delivery of nucleic acid molecules. The Doxil (liposomal doxorubicin) therapy is currently used to treat several human cancers. Many groups have already reported the usefulness of cationic liposomes or modified liposomes for *in vivo* use. A significant benefit of liposomal drug delivery systems for medical applications is that they are relatively safe (related to their lack of immunogenicity and integration) compared to viral systems<sup>246, 252</sup>, suggesting that liposome could be one of good candidates for *in vivo* delivery of siRNA.

In the same way, biocompatibility is one particularly advantageous characteristic of polyglycerol (PG). PG contains an inert polyether-backbone with functional hydroxyl-groups at every branch-end. This structural feature resembles the polyethylene glycol (PEG). As is well known, PEG is a synthetic non-toxic polymer. PG and its derivatives represent a versatile and promising class of materials for future biomedical applications<sup>214</sup>. Kainthan *et al.* synthesized a hyperbranched polymer based on polyglycerol and PEG and then studied the blood compatibility of these aminated PG-PEG polymers. Polymers showed insignificant effects on complement activation, platelet activation, coagulation, erythrocyte aggregation and hemolysis compared to polyethyleneimine (PEI). Cytotoxicity of these polymers is significantly lower than that of PEI<sup>250</sup>.

#### **4.3 The diagnostic application potential of the siRNA-based inhibitor of FECH for early cancer detection**

Most of invasive cancers are preceded by premalignant alterations, such as dysplasia or carcinoma *in situ*, and no anatomical imaging technique is available to detect such alterations<sup>253</sup>. PpIX-dependent fluorescence is associated with the early stages of carcinogenesis and correlated with the progression of cancerous lesions<sup>17, 19, 20, 63, 254</sup>. Certain cancerous and pre-malignant tissues selectively accumulated with PpIX and a significant tumor and normal (T/N) tissue contrast had been obtained following the addition of excessive amounts of exogenous ALA<sup>18, 255, 256</sup>. However, a significant hurdle remained for the development of this technique as a routine clinical diagnostic tool is that a fairly large dose of ALA must be applied for achieving sufficient cellular levels of PpIX for detection of tumors.

Although the success of using ALA-induced PpIX for early cancer detection depends on many factors such as the administration routes of ALA, excitation and detection modes, light wavelength, the location of the tumor, tissue type, and the concentration of ALA, in terms of safety, the dose of ALA is absolutely the most important factor.

Tumors located in deeper tissue layers will require a larger dose of ALA for PpIX-fluorescent detection. So far, using ALA-mediated PDD or PDT, fairly large doses of exogenous ALA (100-500mg/kg of body weight) have to be administered in order to achieve sufficient cellular levels of PpIX that are diagnostically or therapeutically relevant in clinical studies or animal experiments<sup>18, 36, 39, 47, 55, 255, 256</sup>. Obviously, under extremely high-dose conditions, the undesired side effects of exogenous ALA seem to be inevitable<sup>80, 81, 82, 83, 84, 85, 86, 87, 88, 96</sup>. Therefore, there is an urgent need for safe and efficient PpIX-inducing approach *in vivo*.

Here, we introduce a new concept for early cancerous tissues characterization. A siRNA-based inhibitor of FECH is capable of controlling PpIX fluorescence emission in cancerous cells. In conjunction with a very low dose of ALA (a single dose of 5 mg/kg) and encapsulated siRNA with dendritic PG nanoparticles, the siRNA-based inhibitor of FECH can identify the millimeter-sized tumor in a mouse model (Figure 3.9 E). This provides a distinct advantage over a singular ALA-induced PpIX mode in ensuring the safe use of ALA.

PpIX-mediated PDD is one type of the simplest imaging methods for viewing tumor-selective fluorescence. In connection with endoscopic visualization techniques, it is possible to utilize the investigator's naked eyes as a detector to find early stages of malignancies. Thus, to further explore this siRNA-based fluorescent approach holds a promising potential to distinguish cancerous tissues from normal tissues and obtain safer, more diagnostic accuracy for detecting cancers at their earlier stages.

Our data confirm a recent observation (2005) reported by Ohgari<sup>130</sup> who used an *in vitro* model to investigate the expression of FECH and uptake of ALA related to the accumulation of protoporphyrin. When mouse fibrosarcoma MethA cells, mouse fibroblast L929 cells and Balb/3T3 cells were treated with ALA, the greatest accumulation of protoporphyrin was observed in MethA cells, whereas the expression level of FECH was the lowest in MethA cells. They also examined the uptake of ALA by all three cell lines. The extent of ALA uptake by MethA and L929 cells was bigger than in the Balb/3T3 cells. Those results signified that not only the low level of FECH but also the exogenous ALA contributed to the accumulation of protoporphyrin IX in

cancer cells.

The relative contribution of the FECH-siRNA versus ALA to induce selectively PpIX accumulation within cancerous tissue is unknown. Even so, under the experimental conditions employed here, the cumulative effects of combined treatments could be a synergistic interaction. As showed in Figure 1.3, the final step of heme synthesis is the incorporation of ferrous iron into PpIX to form heme, which is catalyzed by FECH when sufficient cellular ferrous iron is available. It might become a “bottle-neck” for PpIX conversion if ALA is applied to heme-synthesis pathway exogenously. Under this condition, even a slight reduction of FECH activity in tumor cells may contribute to the selective accumulation of PpIX in tumor tissues. In other words, the approach that combines both the increased PpIX formation and reduced PpIX conversion may yield much stronger efficacy of PpIX accumulation than either the sole application of exogenous ALA (increasing formation of PpIX) or the siRNA treatment alone (reducing conversion of PpIX).

Despite the fact that the siRNA-based inhibitor of FECH was proved to work effectively *in vitro*, *e.g.*, treatment of FECH-siRNAs alone can obtain sufficient PpIX fluorescence signals to visualize cancerous cells (Figure 3.5 c and Figure 3.8 B), under the conditions employed in our animal experiments, the presence of a low dose of ALA was required for using siRNA-based inhibitor of FECH to identify the millimeter-sized tumor *in vivo*. However, these results do not necessarily contradict the hypothesis of inverse relationship between FECH-expression and PpIX-formation, but suggest that the detection of tumors located in relatively deeper tissue layers might require a much higher accumulation of PpIX in cancerous cells, which can be achieved by combining both manipulation of increased PpIX synthesis and reduced PpIX conversion.

The ability to accurately quantify the *in vivo* fluorescence is a critical step for evaluating the exact level of PpIX accumulation in tumor tissue. This is a major challenge. The detection of fluorescent signals *in vivo* is influenced by numerous factors other than the fluorescent marker only. The application of fluorescence-imaging techniques in living tissue is certainly complicated by the penetration depth of the excitation light, the absorption of light by endogenous tissue chromophores, and the multiple scattering feature of the excited fluorescence light.

The absorption of light by fluorophores is wavelength-dependent and the tissue penetration is greater at longer wavelengths. Porphyrin-related photosensitizers are

most efficiently activated by blue light since these wavelengths are generally absorbed most easily by this sort of compounds<sup>257, 258</sup>. However, blue-light tissue penetrance does not penetrate beyond depth as little as 0.45 mm. Penetration depth of 0.7 mm may be achieved by green light. Penetration depth of 1 mm can be achieved at a red light. Radiation with longer wavelengths penetrates more deeply into the tissues, *e.g.*, the penetration average values of near-infrared light (at 775 - 904 nm) ranged between 6.3 and 8.5 mm<sup>259</sup>. Since hemoglobin absorption diminishes at wavelengths >600 nm, red light can be used to photosensitize deeper tissue structures. However, porphyrin-related photosensitizers typically absorb red light less efficiently than blue light<sup>257</sup>. For example, their red absorption maxima at 630 nm are nearly 35 times less intense than blue peaks at 405 nm<sup>257, 258</sup>. When we used a LED with a peak-emission wavelength of 505 nm as excitation light source (see Materials & Methods), the penetration depth was limited within 1 mm and less the absorption intense than blue light.

On the other hand, PpIX fluorescence propagation in tissue decreases exponentially with distance due to part of the fluorescence will be reabsorbed, and the multiple scattering feature of excited fluorescence could strongly decrease the overall fluorescence intensity during its transportation to the detector. So that *in vivo* fluorescence image can be subject to various artifacts that can compromise the quantitative accuracy and lead to a negative *in vivo* fluorescence imaging result.

In contrast, when fluorescent images were acquired *in vitro*, for example, when applying confocal microscopy, the thickness of the cell sample was less than 50  $\mu\text{m}$  and such cells allowed forming a thin layer of the sample on the slide surface. The excitation laser beam penetrated the cells effectively and the returning fluorescence was directed to the confocal pinhole and photomultiplier undisturbed. Thus, it is quite feasible for the acquisition of a higher resolution PpIX fluorescence imaging compared to *in vivo* detecting methods.

Limited by its penetrating depth, PpIX-mediated PDD may be more suitable for detecting superficial macroscopically indiscernible malignancies rather than deep invasive lesions, as the excitation light penetrates only the superficial layers of tissue. However, most of human cancers originate from epithelial cells, which cover body surfaces and the interior of organs<sup>260</sup>. Many early malignancies occurred in areas of relatively superficial tissues, in intraepithelial layers at depths of a few hundred microns<sup>261, 262</sup>.

Therefore, early detection of carcinomas often relies on techniques to detect tissue abnormalities on these interior hollow-organs surface and the surface of the body cavities. Photodynamic diagnosis used in conjunction with conventional white-light endoscopy could offer a practical method for *in situ* detection of the PpIX fluorescence in the superficially transformed epithelial cells or neoplastic tissues of the accessible internal hollow organs, and thereby increase the sensitivity and specificity of endoscopic diagnosis for finding early malignancies.

Overall, the following conclusions can be drawn to sum up this dissertation:

- (1) A significant transcriptional down-regulation of FECH expression occurred in gastrointestinal malignant tissues.
- (2) FECH is the key player in PpIX conversion. Silencing of FECH by functional application of siRNA alone can lead to a dramatic enhancement of PpIX accumulation in LS174T colorectal carcinoma cells and MDA-MB-435 human mammary carcinoma cells.
- (3) In vivo application of siRNA-based inhibitor of FECH in conjunction with a very low dose of ALA leads to a significantly higher endogenous PpIX level at the site of the xenografted tumor in the mouse model. Either siRNAs encapsulated within folate-PEG cationic liposomes or bound to polyglycerol-based nanocarriers worked well in this regard, supporting the hypothesis that down-regulation of FECH expression plays a crucial role for selective accumulation of PpIX in cancerous tissues.

## 5 Prospects and future research directions

In the present work, the role played by FECH for the selective accumulation of PpIX in cancerous tissues and the possibilities of using siRNA-based inhibitor of FECH to induce accumulation of PpIX in cancerous tissues have been discussed. The main benefit of this approach lies in the fact that it may reduce the undesired side effects of exogenous ALA which are inevitable when fairly large doses currently must be used in a singular ALA-induced PpIX mode. Some of the results deserve to be further explored.

Although the siRNA-based inhibitor of FECH was proved to work effectively *in vitro* and resulted in encouraging results in the animal experiments, it cannot be claimed to be feasible *in vivo* now. Numerous challenges remain before this siRNA-based fluorescent approach can be translated into clinics to become a realistic tumor-diagnostic tool. The development of non-viral vectors for *in vivo* DNA/siRNA delivery, especially clinical applications, has suffered from low transfer efficiency, e.g., the cationic polymers are still lacking three orders of magnitude compared to viral systems, and therefore investigations have been focused on improvement of their delivery efficiency. The following criteria should be taken into account on the design of a synthetic vector for delivery of siRNAs *in vivo*: providing the ability to complex and compact the siRNAs, ensuring the good nuclease stability and reducing renal filtration, having the capacity of preventing recognition and clearance by the reticular-endothelial system, increasing the accessibility of the complexes to interact with the intended tissues and avoiding nonspecific cell binding, efficient endocytosis, with the capability of endolysosomal escape, ensuring siRNAs to be liberated from the complexes after endolysosomal escape, and lowering the cytotoxicity of the vector, etc.

As described above, for successful *in vivo* RNAi activation, siRNAs need to overcome multiple barriers to reach the sites of interest, e.g., the rapid renal excretion of naked siRNAs; nonspecific distribution of these siRNA-containing complexes throughout the body; degradation of siRNAs by nucleases and so on. Moreover, due to the positive charges, the siRNA-containing cationic complexes possess a propensity to interact with virtually any cell type they will encounter. The cationic complexes also tend to form aggregates by binding to negatively charged biomolecules in the blood stream, which may lead to more rapid clearance of these siRNA-containing complexes by reticular-endothelial system. Local injection of siRNAs at the site of pathology can avoid many of the difficulties that would be encountered after systemic administration. Thus, local application of siRNAs

becomes a popular approach to increase tumor tissue concentrations of siRNAs. Unfortunately, local administration of siRNAs can limit the effects on distance tissues and it is not always feasible because the target tissue cannot be reached or covers an area that is too large to be feasible for a local injection protocol<sup>180</sup>. Furthermore, in terms of early cancer diagnosis, the local application approach is difficult to obtain an ideal distribution of fluorescence for using PpIX as a diagnostic probe to scan early malignancies, because cancerous lesions could be located in different parts of the epithelial tissues inside the body. Thus, *in vivo* systemic siRNA-delivery approach will be required.

In addition, it is fair to assume that using FECH-siRNA to manipulate the heme synthetic pathway in tumor tissues is likely to affect other tissues. The nonspecific silencing effect could be reduced after having applied folate-PEG cationic liposomes or PG-based nanoparticles as tumor-targeting carriers to deliver FECH-siRNA. However, the extent of the selectivity for malignant cells *in vivo* remains unknown. Further studies based on animal models will be required to evaluate whether folate-PEG cationic liposomes and PG-based nanoparticles can act as the ideal vehicles for *in vivo* systemic delivery of siRNA as well as their stability and cytotoxicity. These will need to be performed in a series of separate experiments.

## List of references

1. Liotta LA, Kohn EC: Invasion and Metastases. In: Cancer Biology, Cancer Medicine, 5th Edition, BC Decker Inc, London (2000).
2. Liotta LA, Kohn EC: Invasion and Metastases. In: Cancer Biology, Cancer Medicine, 6th Edition, BC Decker Inc, London (2003).
3. Liotta LA, Stetler-Stevenson WG: Tumor invasion and metastasis: an imbalance of positive and negative regulation. *Cancer Res* 51: 5054s-5059s (1991).
4. Duffy MJ: Inhibiting tissue invasion and metastasis as targets for cancer therapy. *Biotherapy* 4: 45-52 (1992).
5. Fidler IJ: The organ microenvironment and cancer metastasis. *Differentiation* 70: 498-505 (2002).
6. Fidler IJ: Critical determinants of metastases. *Semin Cancer Biol* 12: 89-96 (2002).
7. Wittekind C, Neid M: Cancer Invasion and Metastasis. *Oncology* 69 (suppl 1): 14-16 (2005).
8. Weissleder R: Molecular Imaging in Cancer. *Science* 312(5777):1168-1171 (2006).
9. Orth K, Russ D, Steiner R, Beger HG: Fluorescence detection of small gastrointestinal tumours: principles, technique, first clinical experience. *Langenbeck's Arch Surg* 385: 488-494 (2000).
10. Kohn EC, Liotta LA: Molecular insights into cancer invasion: strategies for prevention and intervention. *Cancer Res* 55(9): 1856-1862 (1995).
11. Cho KR, Vogelstein B: Genetic alterations in the adenoma-carcinoma sequence. *Cancer* 70:1727-1731 (1992).
12. Weinberg RA: How cancer arises. *Sci Am* 275(3): 62-70 (1996).
13. Kerr KM: Pulmonary preinvasive neoplasia. *J Clin Pathol* 54: 257-271 (2001).
14. Pasanen AV, Vuopio P, Borgstrom GH, Tenhunen R: Haem biosynthesis in refractory sideroblastic anaemia associated with the preleukaemic syndrome. *Scand J Haematol* 27(1): 35-44 (1981).
15. el-Sharabasy MM, el-Waseef AM, Hafez MM, Salim SA: Porphyrin metabolism in some malignant diseases. *Br J Cancer* 65(3): 409-412 (1992).
16. Sokolov K, Follen M, Richards-Kortum R: Optical spectroscopy for detection of neoplasia. *Current Opinion in Chemical Biology* 6: 651-658 (2002).
17. Campbell DL, Gudgin Dickson EF, Forkert PG, Pottier RH, Kennedy JC: Detection of Early Stages of Carcinogenesis in Adenomas of Murine Lung by 5-Aminolevulinic Acid-Induced Protoporphyrin IX Fluorescence. *Photochemistry and Photobiology* 64 (4): 676-682 (1996).
18. Dorward AM, Fancher KS, Duffy TM, Beamer WG, Walt H: Early neoplastic and metastatic mammary tumours of transgenic mice detected by 5-aminolevulinic acid-stimulated protoporphyrin IX accumulation. *British Journal of Cancer* 93: 1137-1143 (2005).
19. Inaguma M, Hashimoto K: Porphyrin-Like Fluorescence in Oral Cancer. *Cancer* 86: 2201-2211 (1999).
20. Onizawa K, Okamura N, Saginoya H, Yoshida H: Characterization of autofluorescence in oral squamous cell carcinoma. *Oral Oncology* 39(2): 150-156 (2003).
21. Moesta KT, Ebert B, Handke T, Nolte D, Nowak C, Haensch WE, Pandey RK, Dougherty TJ, Rinneberg H, Schlag PM: Protoporphyrin IX Occurs Naturally in Colorectal Cancers and Their Metastases. *Cancer Research* 61: 991-999 (2001).
22. Weissleder R, Mahmood U: Molecular Imaging. *Radiology* 219: 316-333 (2001).
23. Allport JR, Weissleder R: *In vivo* imaging of gene and cell therapies. *Exp Hematol* 29(11): 1237-1246 (2001).
24. Palladino F, Canade A, Bianchi A, Lesti G, Antoniol OM, Macis G, Marano P: Molecular imaging: state of the art. *Rays* 28(1):

- 45-61 (2003).
25. Thakur M, Lentle BC: Report of a summit on molecular imaging. *Radiology* 236: 753-755 (2005).
  26. Profio AE, Doiron DR: A feasibility study of the use of fluorescence bronchoscopy for localization of small lung tumors. *Phys Med Biol* 22(5): 949-957 (1977).
  27. Kinsey JH, Cortese DA, Sanderson DR: Detection of hematoporphyrin fluorescence during fiberoptic bronchoscopy to localize early bronchogenic carcinoma. *Mayo Clin Proc* 53: 594-600 (1978).
  28. Dougherty TJ, Kaufman JE, Goldfarb A, Weishaupt KR, Boyle D, Mitteleman A: Photoradiation therapy for the treatment of malignant tumors. *Cancer Res* 38: 2628-2635 (1978).
  29. Harris DM, Wekhaven J: Endogenous Porphyrin fluorescence in tumors. *Lasers Surg Med* 7: 467-472 (1987).
  30. Weishaupt KR, Gomer CJ, Dougherty TJ: Identification of singlet oxygen as the cytotoxic agent in photoinactivation of murine tumor. *Cancer Res* 36: 2326-2329 (1976).
  31. Moan J, Sommer S: Oxygen dependence of the photosensitizing effect of haematoporphyrin derivative in NHIK 3025 cells. *Cancer Res* 45: 1608-1610 (1985).
  32. Pottier RH, Chow YF, LaPlante JP, Truscott TG, Kennedy JC, Beiner LA: Non-invasive technique for obtaining fluorescence excitation and emission spectra *in vivo*. *Photochem Photobiol* 44(5):679-687 (1986).
  33. de Villiers KA, Kaschula CH, Egan TJ, Marques HM: Speciation and structure of ferriprotoporphyrin IX in aqueous solution: spectroscopic and diffusion measurements demonstrate dimerization, but not  $\mu$ -oxo dimer formation. *J Biol Inorg Chem* 12:101-117 (2007).
  34. Peng Q, Warloe T, Berg K, Moan J, Kongshaug M, Giercksky KE, Nesland JM: 5-aminolevulinic acid-based photodynamic therapy: clinical research and future challenges. *Cancer* 79: 2282-2308 (1997).
  35. Lüdicke F: Photodynamic diagnosis of ovarian cancer using hexaminolaevulinate: a preclinical study. *British Journal of Cancer* 88: 1780-1784 (2003).
  36. Major AL, Rose GS, Chapman CF, Hiserodt JC, Tromberg BJ, Krasieva TB, Tadir Y, Haller U, DiSaia PJ, Berns MW: *In vivo* fluorescence detection of ovarian cancer in the NuTu-19 epithelial ovarian cancer animal model using 5-aminolevulinic acid (ALA). *Gynecol Oncol* 66: 122-132 (1997).
  37. Major AL, Rose GS, Svaasand LO, Ludicke F, Campana A, van Gemert MJ: Intraperitoneal photodynamic therapy in the Fischer 344 rat using 5-aminolevulinic acid and violet laser light: a toxicity study. *J Photochem Photobiol B* 66: 107-114 (2002b).
  38. Löning M, Diddens H, Küpker W, Diedrich K, Hüttmann G: Laparoscopic fluorescence detection of ovarian carcinoma metastases using 5-aminolevulinic acid-induced protoporphyrin IX. *Cancer* 100(8): 1650-1656 (2004).
  39. Hornung R, Major AL, McHale M, Liaw LH, Sabiniano LA, Tromberg BJ, Berns MW, Tadir Y: *In vivo* detection of metastatic ovarian cancer by means of 5-aminolevulinic acid-induced fluorescence in a rat model. *J Am Assoc Gynecol Laparosc* 5: 141-148 (1998).
  40. Löning MC, Diddens HC, Holl-Ulrich K, Löning U, Küpker W, Diedrich K, Hüttmann G: Fluorescence staining of human ovarian cancer tissue following application of 5-aminolevulinic acid: Fluorescence microscopy studies. *Lasers Surg Med* 38(5):549-554 (2006).
  41. Regis C, Collinet P, Farine MO, Mordon S: Comparison of aminolevulinic acid and hexylester aminolevulinate-induced protoporphyrin IX fluorescence for the detection of ovarian cancer in a rat model. *Photomed Laser Surg* 25(4): 304-311 (2007).

42. Na R, Stender IM, Wulf HC: Can autofluorescence demarcate basal cell carcinoma from normal skin? A comparison with protoporphyrin IX fluorescence. *Acta Derm Venereol* 81: 246-249 (2001).
43. Krieg RC, Messmann H, Rauch J, Seeger S, Knuechel R: Metabolic characterization of tumor cell-specific protoporphyrin IX accumulation after exposure to 5-aminolevulinic acid in human colonic cells. *Photochem Photobiol* 76(5): 518-25 (2002).
44. Berlin NI, Neuberger A, Scott JJ: The metabolism of  $\delta$ -aminolaevulinic acid. 1. Normal pathways, studied with the aid of  $^{15}\text{N}$ . *Biochem J* 64: 80-90 (1956).
45. Berlin NI, Neuberger A, Scott JJ: The metabolism of  $\delta$ -aminolaevulinic acid. 2. Normal pathways, studied with the aid of  $^{14}\text{C}$ . *Biochem J* 64: 90-100 (1956).
46. Novo M, Hüttmann G, Diddens H: Chemical instability of 5-aminolevulinic acid used in the fluorescence diagnosis of bladder tumours. *J Photochem Photobiol B* 34: 143-148 (1996).
47. Hua Z, Gibson SL, Foster TH, Hilf R: Effectiveness of delta-aminolevulinic acid-induced protoporphyrin as a photosensitizer for photodynamic therapy *in vivo*. *Cancer Res* 55: 1723-1731 (1995).
48. Gederas OA, Berg K, Romslo I: A comparative study of normal and reverse phase high pressure liquid chromatography for analysis of porphyrins accumulated after 5-aminolevulinic acid treatment of colon adenocarcinoma cells. *Cancer Lett* 150: 205-213 (2000).
49. Malik Z, Lugaci H: Destruction of erythroleukaemic cells by photoactivation of endogenous porphyrins. *Br J Cancer* 56(5): 589-595 (1987).
50. Divaris DXG, Kennedy JC, Pottier RH: Phototoxic damage to sebaceous glands and hair follicles of mice following systemic administration of 5-aminolevulinic acid correlates with localised protoporphyrin IX fluorescence. *American Journal of Pathology* 136(4): 891-897 (1990).
51. Kennedy JC, Pottier RH, Pross DC: Photodynamic therapy with endogenous protoporphyrin IX: Basic principles and present clinical experience. *J Photochem Photobiol B* 6: 143-148 (1990).
52. Kennedy JC, Pottier RH: New trends in photobiology Endogenous protoporphyrin IX, a clinically useful photosensitizer for photodynamic therapy. *Journal of Photochemistry and Photobiology B: Biology* 14(4): 275-292 (1992).
53. Moan J, Van Den Akker JTHM, Juzenas P, Ma LW, Angell-Petersen E, Gadmar ØB, Jani V: On the basis for tumor selectivity in the 5-aminolevulinic acid-induced synthesis of protoporphyrin IX. *Journal of Porphyrins and Phthalocyanines* 5(2): 170-176 (2001).
54. Stummer W, Stepp H, Möller G, Ehrhardt A, Leonhard M, Reulen HJ: Technical principles for protoporphyrin IX fluorescence guided microsurgical resection of malignant glioma tissue. *Acta Neurochir* 140: 995-1000 (1998).
55. Stummer W, Stocker S, Novotny A, Heimann A, Sauer O, Kempfski O, Plesnila N, Wietzorrek J, Reulen HJ: *In vitro* and *in vivo* porphyrin accumulation by C6 glioma cells after exposure to 5-aminolevulinic acid. *J Photochem Photobiol B* 45:160-169 (1998).
56. Leunig A, Betz CS, Mehlmann M, Stepp H, Arbogast S, Grevers G, Baumgartner R: Detection of squamous cell carcinoma of the oral cavity by imaging 5-aminolevulinic acid-induced protoporphyrin IX fluorescence. *Laryngoscope* 110: 78-83 (2000).
57. Betz CS, Stepp H, Janda P, Arbogast S, Grevers G, Baumgartner R, Leunig A: A comparative study of normal inspection, autofluorescence and 5-ALA-induced PpIX fluorescence for oral cancer diagnosis. *Int J Cancer* 97:245-252 (2002).
58. Gossner L, Stolte M, Sroka R, Rick K, May A, Hahn EG, Ell C: Photodynamic ablation of high-grade dysplasia and early cancer in Barrett's esophagus by means of 5-aminolevulinic acid. *Gastroenterology* 114: 448-455 (1998).
59. Mayinger B, Neidhardt S, Reh H, Martus P, Hahn EG: Fluorescence induced with 5-aminolevulinic acid for the endoscopic

- detection and follow-up of esophageal lesions. *Gastrointest Endosc* 54: 572-578 (2001).
60. Endlicher E, Knuechel R, Hauser T, Szeimis RM, Schölmerich J, Messmann H: Endoscopic fluorescence detection of low and high grade dysplasia in Barrett's esophagus using systemic or local 5-aminolevulinic acid sensitisation. *Gut* 48: 314-319 (2001).
  61. Messmann H: 5-Aminolevulinic acid-induced protoporphyrin IX for the detection of gastrointestinal dysplasia. *Gastrointest Endosc Clin N Am* 10: 497-512 (2000).
  62. Mayinger B, Horner P, Jordan M, Gerlach C, Horbach T, Hohenberger W, Hahn EG: Endoscopic fluorescence spectroscopy in the upper GI tract for the detection of GI cancer: initial experience. *Am J Gastroenterol* 96:2616-2621(2001).
  63. Baumgartner R, Huber RM, Schulz H, Stepp H, Rick K, Gamarra F, Leberig A, Roth C: Inhalation of 5-aminolevulinic acid: a new technique for fluorescence detection of early stage lung cancer. *J Photochem Photobiol B* 36:169-174 (1996).
  64. Hillemanns P, Weingandt H, Baumgartner R, Diebold J, Xiang W, Stepp H: Photodetection of cervical intraepithelial neoplasia using 5-aminolevulinic acid-induced porphyrin fluorescence. *Cancer* 88: 2275-2282 (2000).
  65. Duska LR, Wimberly J, Deutsch TF, Ortel B, Haas J, Houck K, Hasan T: Detection of female lower genital tract dysplasia using orally administered 5-aminolevulinic acid induced protoporphyrin IX: a preliminary study. *Gynecol Oncol* 85: 125-128 (2002).
  66. Kriegmair M, Baumgartner R, Knuechel R, Steinbach P, Ehsan A, Lumper W, Hofstädter F, Hofstetter A: Fluorescence photodetection of neoplastic urothelial lesions following intravesical instillation of 5-aminolevulinic acid. *Urology* 44(6): 836-841 (1994).
  67. Kriegmair M, Stepp H, Steinbach P, Lumper W, Ehsan A, Stepp HG, Rick K, Knüchel R, Baumgartner R, Hofstetter A: Fluorescence cystoscopy following intravesical instillation of 5-aminolevulinic acid: a new procedure with high sensitivity for detection of hardly visible urothelial neoplasias. *Urol Int* 55(4): 190-196 (1995).
  68. Kriegmair M, Baumgartner R, Knüchel R, Stepp H, Hofstädter F, Hofstetter A: Detection of early bladder cancer by 5-aminolevulinic acid induced porphyrin fluorescence. *J Urol* 155(1):105-110 (1996).
  69. Waidelich R, Hofstetter A, Stepp H, Baumgartner R, Weninger E, Kriegmair M: Early clinical experience with 5-aminolevulinic acid for the photodynamic therapy of upper tract urothelial tumors. *J Urol* 159: 401-404 (1998).
  70. Koenig F, McGovern FJ, Larne R, Enquist H, Schomacker KT, Deutsch TF: Diagnosis of bladder carcinoma using protoporphyrin IX fluorescence induced by 5-aminolaevulinic acid. *BJU Int* 83: 129-135 (1999).
  71. Riedl CR, Danilchenco D, Koenig F, Simak R, Loening SA, Pflueger H: Fluorescence endoscopy with 5-aminolevulinic acid reduces early recurrence rate in superficial bladder cancer. *J Urol* 165:1121-1123 (2001).
  72. Zaak D, Kriegmair M, Stepp H, Baumgartner R, Oberneder R, Schneede P, Corvin S, Frimberger D, Knuchel R, Hofstetter A: Endoscopic detection of transitional cell carcinoma with 5-aminolevulinic acid: results of 1012 fluorescence endoscopies. *Urology* 57: 690-694 (2001).
  73. Malik Z, Ehrenberg B, Faraggi A: Inactivation of erythrocytic, lymphocytic and myelocytic leukemic cells by photoexcitation of endogenous porphyrins. *J Photochem Photobiol B* 4: 195-205 (1989).
  74. Rittenhouse-Diakun K, Van Leengoed H, Morgan J, Hryhorenko E, Paszkiewicz G, Whitaker JE, Oseroff AR: The role of transferrin receptor (CD71) in photodynamic therapy of activated and malignant lymphocytes using the heme precursor  $\delta$ -aminolevulinic acid (ALA). *Photochem Photobiol* 61: 523-528 (1995).
  75. Bartosová J, Hrkal Z: Accumulation of protoporphyrin-IX (PpIX) in leukemic cell lines following induction by 5-aminolevulinic acid (ALA). *Comparative Biochemistry and Physiology Part C* 126: 245-252 (2000).

76. Gold MH: Aminolevulinic acid photodynamic therapy for actinic keratoses and photorejuvenation. *Expert Review of Dermatology* 2(4): 391-402 (2007).
77. Regula J, MacRobert AJ, Gorchein A, Buonaccorsi GA, Thorpe SM, Spencer GM, Hatfield AR, Bown SG: Photosensitisation and photodynamic therapy of oesophageal, duodenal, and colorectal tumors using 5 aminolaevulinic acid induced protoporphyrin IX: a pilot study. *Gut* 36: 67-75 (1995).
78. Gorchein A, Webber R:  $\delta$ -Aminolevulinic acid in plasma, cerebrospinal fluid, saliva and erythrocytes: studies in normal, uraemic and porphyric subjects. *Clin Sci* 72: 103-112 (1987).
79. Floderus Y, Sardh E, Möller C, Andersson C, Rejkaer L, Andersson DEH, Harper P: Variations in Porphobilinogen and 5-Aminolevulinic Acid Concentrations in Plasma and Urine from Asymptomatic Carriers of the Acute Intermittent Porphyria Gene with Increased Porphyrin Precursor Excretion. *Clinical Chemistry* 52: 701-707 (2006).
80. Feldman DS, Levere RD, Lieberman JS: Presynaptic neuromuscular inhibition by delta-aminolevulinic acid, a porphyrin precursor. *Trans Amer Neurol Assoc* 93: 206-208 (1968).
81. Goldberg A, McGillion FB: Proceedings: Central uptake and cardiovascular effects of delta-aminolaevulinic acid. *Br J Pharmacol* 49(1): 178P (1973).
82. Shanley BC, Neethling AC, Percy VA, Carstens M: Neurochemical aspects of porphyria. Studies on the possible neurotoxicity of delta-aminolevulinic acid. *S Afr Med J* 49: 576-580 (1975).
83. Helson L, Braverman S, Mangiardi J:  $\delta$ -Aminolevulinic acid effects on neuronal and glial tumor cell lines. *Neurochemical Research* 18(12): 1255-1258 (1993).
84. Russell VA, Lamm MCL, Taljaard JF: Inhibition of Na<sup>+</sup>, K<sup>+</sup>-ATPase activity by delta-aminolevulinic acid. *Neurochem Res* 8: 1407-1415 (1983).
85. Percy VA, Lamm MCL, Taljaard JF: d-Aminolevulinic acid uptake, toxicity, and effect on [14C] g-aminobutyric acid uptake into neurons and glia in culture. *J Neurochem* 36: 69-76 (1981).
86. Emanuelli T, Pagel FW, Alves LB, Regner A, Souza DO: Inhibition of adenylate cyclase activity by 5-aminolevulinic acid in rat and human brain. *Neurochem Int* 38: 213-218 (2001).
87. Mitchell G, Larochelle J, Lambert M, Michaud J, Grenier A, Ogier H, Gauthier M, Lacroix J, Vanasse M, Larbrisseau A: Neurologic crises in hereditary tyrosinemia. *N Engl J Med* 49: 432-437 (1990).
88. Novotny A, Xiang J, Stummer W, Teuscher NS, Smith DE, Keep RF: Mechanisms of 5-Aminolevulinic Acid Uptake at the Choroid Plexus. *Journal of Neurochemistry* 75: 321-328 (2000).
89. Brennan MJW, Cantrill RC: The effect of delta-aminolaevulinic acid on the uptake and efflux of amino acid neurotransmitters in rat brain synaptosomes. *Journal of Neurochemistry* 33: 721-725 (1979).
90. Albert C, Yeung LW, Moore MR, Goldberg A: Pathogenesis of Acute Porphyria. *Quarterly Journal of Medicine, New Series* 63(241): 377-392 (1987).
91. Cutler MG, Moore MR, Dick JM: Effects of delta-aminolaevulinic acid on contractile activity of rabbit duodenum. *Eur J Pharmacol* 64: 221-230 (1980).
92. Cutler MG, McLaughlin M, McNeil E, Moore MR: Effects of delta-aminolaevulinic acid on contractile activity in the isolated small intestine of the rabbit. *Neuropharmacology* 24: 1005-1009 (1985).
93. Krnjevic K, Schwartz S: The action of gamma-aminobutyric acid on cortical neurons. *Exp Brain Res* 3: 320-336 (1967).
94. Walker JE: Glutamate, GABA and CNS disease: a review. *Neurochem Res* 8: 521-550 (1983).
95. Dichter HN, Taddeini L, Lin S, Ayala GF: Delta-aminolaevulinic acid. Effect of a porphyrin precursor on an isolated

- neuronal preparation. *Brain Res* 126: 189-195 (1977).
96. Becker DM, Viljoen D, Kramer S: The inhibition of red cell and brain ATPase by deltaaminolaevulinic acid. *Biochim Biophys Acta* 225: 26-34 (1971).
97. McGillion FB, Thompson GG, Moore MR, Goldberg A: The passage of  $\delta$ -aminolevulinic acid across the blood-brain barrier of the rat. *Biochem Pharmacol* 23: 472-474 (1974).
98. Princ FG, Juknat AA, deI Carmen Batlle AM: Porphyrinogenesis in rat cerebellum: effect of high  $\delta$ -aminolevulinic acid concentration. *Gen Pharmac* 25: 761-766 (1994).
99. Juknat AA, Kotler ML, deI Carmen Batlle AM: High  $\delta$ -aminolevulinic acid uptake in rat cerebral cortex: effect on porphyrin biosynthesis. *Comp Biochem Physiol* 111C: 143-150 (1995).
100. Mustajoki P, Koskelo P: Hereditary hepatic porphyrias in Finland. *Acta Med Scand* 200: 171-178 (1976).
101. Webber J, Kessel D, Fromm D: Side effects and photosensitization of human tissues after aminolevulinic acid. *J Surg Res* 68: 31-37 (1997).
102. Radin, NS, Rittenberg D, Shemin D: The role of glycine in the biosynthesis of heme. *J Biol Chem* 184: 745-754 (1950).
103. Wittenberg J, Shemin D: The location in protoporphyrin of the carbon atoms derived from the  $\alpha$ -carbon atom of glycine. *J Biol Chem* 103-116 (1950).
104. May BK, Bawden MJ: Control of heme biosynthesis in animals. *Semin Hematol* 26: 150-156 (1989).
105. Scotto AW, Chang LF, Beattie DS: The characterization and submitochondrial localization of delta-aminolevulinic acid synthase and an associated amidase in rat liver mitochondria using an improved assay for both enzymes. *J Biol Chem* 258: 81-90 (1983).
106. Shemin D: On the synthesis of heme. *Naturwissenschaften* 57: 185-190 (1970).
107. Xu W, Kozak CA, Desnick RJ: Uroporphyrinogen-III synthase, molecular cloning, nucleotide sequence, expression of a mouse full-length cDNA, and its localization on mouse chromosome 7. *Genomics* 26: 556-562 (1995).
108. Elder GH, Evans JO: Evidence that the coproporphyrinogen oxidase activity of rat liver is situated in the intermembrane space of mitochondria. *Biochem J* 172: 345-347 (1978).
109. Grandchamp B, Phung N, Nordmann Y: The mitochondrial localization of coproporphyrinogen III oxidase. *Biochem J* 176: 97-102 (1978).
110. Snot S, Granick S: Mitochondrial Coproporphyrinogen Oxidase and Protoporphyrin Formation. *J Biol Chem* 236(4): 1173-1180 (1961).
111. Ferreira GC, Andrew TL, Karr SW, Dailey HA: Organization of the terminal two enzymes of the heme biosynthetic pathway: orientation of protoporphyrinogen oxidase and evidence for a membrane complex. *J Biol Chem* 263: 3835-3839 (1988).
112. Jones MS, Jones OTG: The structural organization of haem synthesis in rat liver mitochondria. *Biochem J* 113: 507-514 (1969).
113. Maines MD: The heme oxygenase system: Update 2005. *Antiox Redox Signal* 7: 1761-1766 (2005).
114. Maines MD, Gibbs PEM: 30 some years of heme oxygenase: from a "molecular wrecking ball" to a "mesmerizing" trigger of cellular events. *Biochem Biophys Res Commun* 338: 568-577 (2005).
115. Whitcombe DM, Carter NP, Albertson DG, Smith SJ, Rhodes DA, Cox TM: Assignment of the human ferrochelatase gene (FECH) and a locus for protoporphyria to chromosome 18q22. *Genomics* 11(4): 1152-1154 (1991).
116. Brenner DA, Didier JM, Frasier F, Christensen SR, Evans GA, Dailey HA: A molecular defect in human protoporphyria. *Am J Hum Genet* 50(6):1203-1210 (1992).

117. Taketani S, Adachi Y, Nakahashi Y: Regulation of the expression of human ferrochelatase by intracellular iron levels. *Eur J Biochem* 267: 4685–4692 (2000).
118. Taketani S, Kakimoto K, Ueta H, Masaki R, Furukawa T: Involvement of ABC7 in the biosynthesis of heme in erythroid cells: Interaction of ABC7 with ferrochelatase. *Blood* 101(8): 3274-3280 (2003).
119. Ferreira GC, Franco R, Lloyd SG, Moura I, Moura JGG, Huynh BH: Structure and function of ferrochelatase. *J Bioenerg Biomembr* 27: 221-229 (1995).
120. Camadro JM, Ibrahim NG, Levere RD: Kinetic studies of human liver ferrochelatase. Role of endogenous metals. *J Biol Chem* 259(9): 5678-5682 (1984).
121. Camadro JM, Labbe P: Kinetic studies of ferrochelatase in yeast. Zinc or iron as competing substrates. *Biochim Biophys Acta* 707: 280-288 (1982).
122. Dailey HA: Metal inhibition of ferrochelatase. *Ann NY Acad Sci* 514: 81-86 (1987).
123. Porra R, Jones OTG: Studies on ferrochelatase. 1. Assay and properties of ferrochelatase from a pig-liver mitochondrial extract. *Biochem J* 87: 181-185 (1963).
124. Rand EB, Bunin N, Cochran W, Ruchelli E, Olthoff KM, Bloomer JR: Sequential Liver and Bone Marrow Transplantation for Treatment of Erythropoietic Protoporphyrin. *Pediatrics* 118(6):e1894-1897 (2006).
125. Karr SR, Dailey HA: The synthesis of murine ferrochelatase *in vitro* and *in vivo*. *Biochem J* 254: 799–803 (1988).
126. Camadro JM, Labbe P: Purification and properties of ferrochelatase from the yeast *Saccharomyces cerevisiae*. Evidence for a precursor form of the protein. *J Biol Chem* 263: 11675-11682 (1988).
127. Dailey HA, Finnegan MG, Johnson MK: Human Ferrochelatase Is an Iron-Sulfur Protein. *Biochemistry* 33: 403–407 (1994).
128. Burden AE: Human ferrochelatase: crystallization, characterization of the [2Fe-2S] cluster and determination that the enzyme is a homodimer. *Biochimica et Biophysica Acta (BBA)* 1435(1-2): 191-197 (1999).
129. Koenig F, Knittel J, Stepp H: Diagnosing Cancer *in Vivo*. *Science* 292(5520): 1401-1403 (2001).
130. Ohgari Y, Nakayasu Y, Kitajima S, Sawamoto M, Mori H, Shimokawa O, Matsui H, Taketani S: Mechanisms involved in  $\delta$ -aminolevulinic acid (ALA)-induced photosensitivity of tumor cells: Relation of ferrochelatase and uptake of ALA to the accumulation of protoporphyrin. *Biochemical Pharmacology* 71(1-2): 42-49 (2005).
131. Jain RK: Transport of molecules in the tumor interstitium: a review. *Cancer Res* 47(12): 3039-3051 (1987).
132. Rud E, Gederaas O, Hogset A, Berg K: 5-aminolevulinic acid, but not 5-aminolevulinic acid esters, is transported into adenocarcinoma cells by system BETA transporters. *Photochem Photobiol* 71: 640–647 (2000).
133. Dreher MR, Liu W, Michelich CR, Dewhirst MW, Yuan F, Chilkoti A: Tumor Vascular Permeability, Accumulation, and Penetration of Macromolecular Drug Carriers. *JNCI Journal of the National Cancer Institute* 98(5): 335-344 (2006).
134. Hobbs SK, Monsky WL, Yuan F, Roberts WG, Griffith L, Torchilin VP, Jain RK: Regulation of transport pathways in tumor vessels: Role of tumor type and microenvironment. *Proc Natl Acad Sci USA* 95: 4607–4612 (1998).
135. Baish JW, Gazit Y, Berk DA, Nozue M, Baxter LT, Jain RK: Role of tumor vascular architecture in nutrient and drug-delivery: An Invasion Percolation-Based Network Model. *Microvascular Research* 51(3): 327-346 (1996).
136. Andersson-Engels S, Brun A, Kjellén E, Salford LG, Svanberg K, Svanberg S: Identification of brain tumours in rats using laser-induced fluorescence and haematoporphyrin derivative. *Lasers Med Sci* 4: 241-249 (1989).
137. Abels C, Heil P, Dellian M, Kuhnle GE, Baumgartner R, Goetz AE: *In vivo* kinetics and spectra of 5-aminolaevulinic acid-induced fluorescence in an amelanotic melanoma of the hamster. *Br J Cancer* 70(5): 826-833 (1994).
138. Gaullier JM, Berg K, Peng Q, Anholt H, Selbo PK, Moan J: Use of 5-aminolevulinic acid esters to improve photodynamic

- therapy on cells in culture. *Cancer Res* 57: 1481–1486 (1997).
139. Gederaas OA, Holroyd A, Brown SB, Vernon D, Moan J, Berg K: 5-aminolevulinic acid methyl ester transport on amino acid carriers in a human colon adenocarcinoma cell line. *Photochem Photobiol* 73: 164–169 (2001).
  140. Brunner H, Hausmann F, Krieg RC, Endlicher E, Schölmerich J, Knuechel R, Messmann H: The effects of 5-aminolevulinic acid esters on protoporphyrin IX production in human adenocarcinoma cell lines. *Photochem Photobiol* 74: 721–725 (2001).
  141. Hinnen P, de Rooij FW, van Velthuysen ML, Edixhoven A, van Hillegersberg R, Tilanus HW, Wilson JH, Siersema PD: Biochemical basis of 5-aminolaevulinic acid-induced protoporphyrin IX accumulation: a study in patients with (pre)malignant lesions of the oesophagus. *Br J Cancer* 78(5): 679-682 (1998).
  142. Gibson SL, Cupriks DJ, Havens JJ, Nguyen ML, Hilf R: A regulatory role for porphobilinogen deaminase (PBGD) in delta-aminolaevulinic acid (delta-ALA)-induced photosensitization. *Br J Cancer* 77(2): 235-242 (1998).
  143. Kondo M, Hirota N, Takaoka T, Kajiwara M: Heme-biosynthetic enzyme activities and porphyrin accumulation in normal liver and hepatoma cell line of rats. *Cell Biol Toxicol* 9: 95-105 (1993).
  144. Leibovici L, Schoenfeld N, Yehoshua HA, Mamet R, Rakowsky E, Shindel A, Atsmon A: Activity of porphobilinogen deaminase in peripheral blood mononuclear cells of patients with metastatic cancer. *Cancer* 62: 2297-2300 (1988).
  145. Navone N, Polo C, Frisardi A, Batlle A: Mouse mammary carcinoma porphobilinogenase and hydroxymethylbilane synthetase. *Comp Biochem Physiol B* 98: 67-71 (1991).
  146. Krieg RC, Fickweiler S, Wolfbeis OS, Knuechel R: Cell-type specific protoporphyrin IX metabolism in human bladder cancer *in vitro*. *Photochem Photobiol* 72: 226-233 (2000).
  147. van Hillegersberg R, van den Berg JWO, Kort WJ, Terpstra OT, Wilson JHP: Selective accumulation of endogenously produced porphyrins in a liver metastasis model in rats. *Gastroenterology* 103: 647-651 (1992).
  148. Berg K, Anholt H, Bech O, Moan J: The influence of iron chelators on the accumulation of protoporphyrin IX in 5-aminolaevulinic acid-treated cells. *Br J Cancer* 74: 688–697 (1996).
  149. Iinuma S, Farshi SS, Ortel B, Hasan T: A mechanistic study of cellular photodestruction with 5-aminolaevulinic acid-induced porphyrin. *Br J Cancer* 70(1): 21-28 (1994).
  150. Pourzand C, Reelfs O, Kvam E, Tyrrell RM: The iron regulatory protein can determine the effectiveness of 5-aminolevulinic acid in inducing protoporphyrin IX in human primary skin fibroblasts. *J Invest Dermatol* 112: 419-425 (1999).
  151. Lash A, Saleem A: Iron metabolism and its regulation. A review. *Ann Clin Lab Sci* 25: 20-30 (1995).
  152. Kauppi B, Nielsen BB, Ramaswamy S, Larsen IK, Thelander M, Thelander L, Eklund H: The three-dimensional structure of mammalian ribonucleotide reductase protein R2 reveals a more-accessible iron-radical site than *Escherichia coli* R2. *J Mol Biol* 262: 706-720 (1996).
  153. Boshier JM, Labouesse M: RNA interference: genetic wand and genetic watchdog. *Nature Cell Biology* 2: E31-E36 (2000).
  154. McManus MT, Sharp PA: Gene silencing in mammals by small interfering RNAs. *Nature Reviews Genetics* 3: 737-747 (2002).
  155. van der Krol AR, Mur LA, Beld M, Mol JN, Stuitje AR: Flavonoid genes in *Petunia*: addition of a limited number of gene copies may lead to a suppression of gene expression. *Plant Cell* 2: 291–299 (1990).
  156. Napoli C, Lemieux C, Jorgensen R: Introduction of a chalcone synthase gene into *Petunia* results in reversible co-suppression of homologous genes in trans. *Plant Cell* 2: 279–289 (1990).
  157. Bingham PM: Cosuppression comes to the animals. *Cell* 90: 385–387 (1997).
  158. Guo S, Kempfues KJ: par-1, a gene required for establishing polarity in *C. elegans* embryos, encodes a putative Ser/Thr

- kinase that is asymmetrically distributed. *Cell* 81: 611-620 (1995).
159. Fire A, Xu S, Montgomery MK, Kostas SA, Driver SE, Mello CC: Potent and specific genetic interference by double-stranded RNA in *Caenorhabditis elegans*. *Nature* 391: 806-811 (1998).
  160. Tuschl T, Zamore PD, Lehmann R, Bartler DP, Sharp PA: Targeted mRNA degradation by double-stranded RNA *in vitro*. *Genes & Dev* 13: 3191-3197 (1999).
  161. Hammond SM, Bernstein E, Beach D, Hannon GJ: An RNA-directed nuclease mediates posttranscriptional gene silencing in *Drosophila* cells. *Nature* 404: 293-296 (2000).
  162. Hamilton AJ, Baulcombe DC: A species of small antisense RNA in posttranscriptional gene silencing in plants. *Science* 286: 950-952 (1999).
  163. Zamore PD, Tuschl T, Sharp PA, Bartel DP: RNAi: Double-stranded RNA directs the ATP-dependent cleavage of mRNA at 21 to 23 nucleotide intervals. *Cell* 101: 25-33 (2000).
  164. Bernstein E, Caudy AA, Hammond SM, Hannon GJ: Role for a bidentate ribonuclease in the initiation step of RNA interference. *Nature* 409: 363-366 (2001).
  165. Hammond SM, Boettcher S, Caudy AA, Kobayashi R, Hannon GJ: Argonaute2, a link between genetic and biochemical analyses of RNAi. *Science* 293: 1146-1150 (2001).
  166. Manche L, Green SR, Schmedt C, Mathews MB: Interactions between doublestranded RNA regulators and the protein kinase DAI. *Mol. Cell Biol* 12: 5238-5248 (1992).
  167. Williams BR: Role of the double-stranded RNA-activated protein kinase (PKR) in cell regulation. *Biochem. Soc. Trans.* 25: 509-513 (1997).
  168. Minks MA, West DK, Benveniste S, Baglioni C: Structural requirements of doublestranded RNA for the activation of 2',5'-oligo(A) polymerase and protein kinase of interferon-treated HeLa cells. *J Biol Chem* 254: 10180-10183 (1979).
  169. Elbashir SM, Harborth J, Lendeckel W, Yalcin A, Weber K, Tuschl T: Duplexes of 21-nucleotide RNAs mediate RNA interference in cultured mammalian cells. *Nature* 411: 494-498 (2001).
  170. Donze O, Picard D: RNA interference in mammalian cells using siRNAs synthesized with T7 RNA polymerase. *Nucleic Acids Res* 30: e46 (2002).
  171. Marshall E: Gene Therapy Death Prompts Review of Adenovirus Vector. *Science* 286: 2244-2245, (1999).
  172. Kohn DB, Sadelain M, Dunbar C, Bodine D, Kiem HP, Candotti F, Tisdale J, Riviere I, Blau CA, Richman RE: American society of gene therapy (ASGT) ad hoc subcommittee on retroviral-mediated gene transfer to hematopoietic stem cells. *Molecular Therapy* 8:180-187 (2003).
  173. Hacein-Bey-Abina S, von Kalle C, Schmidt M, Le Deist F, Wulffraat N, McIntyre E, Radford I, Villeval JL, Fraser CC, Cavazzana-Calvo M, Fischer A: A serious adverse event after successful gene therapy for X-linked severe combined immunodeficiency. *N Engl J Med* 348:255-256 (2003).
  174. Anson DS: The use of retroviral vectors for gene therapy-what are the risks? A review of retroviral pathogenesis and its relevance to retroviral vector-mediated gene delivery. *Genet Vaccines Ther* 2 (1): 9 (2004).
  175. Dykxhoorn DM, Novina CD, Sharp PA: Killing the messenger: Short RNAs that silence gene expression. *Nat. Rev. Mol. Cell Biol* 4: 457-467 (2003).
  176. Khanna D, Balgir PP, Gurloveen K: RNA interference: An Ancient Mechanism for Novel Therapeutics. *The Internet Journal of Genomics and Proteomics* 2: 1540-2630 (2007).
  177. Santel A, Aleku M, Keil O, Endruschat J, Esche V, Fisch G, Dames S, Löffler K, Fechtner M, Arnold W, Giese K, Klippel A,

- Kaufmann J: A novel siRNA-lipoplex technology for RNA interference in the mouse vascular endothelium. *Gene Ther* 13: 1222–1234 (2006).
178. van de Water FM, Boerman OC, Wouterse AC, Peters JG, Russel FG, Masereeuw R: Intravenously administered short interfering RNA accumulates in the kidney and selectively suppresses gene function in renal proximal tubules. *Drug Metab Dispos* 34: 1393–1397 (2006).
179. Haag R, Kratz F: *Polymer Therapeutics: Concepts and Applications*. *Angewandte Chemie International Edition* 45: 1198–1215 (2006).
180. Oliveira S, Storm G, Schiffelers RM: Targeted Delivery of siRNA. *Journal of Biomedicine and Biotechnology*, Article ID 63675:1–9 (2006).
181. Luger K, Mäder AW, Richmond RK, Sargent DF, Richmond TJ: Crystal structure of the nucleosome core particle at 2.8 Å resolution. *Nature* 389: 251–260 (1997).
182. Wagner E, Cotten M, Foisner R, Birnstiel ML: Transferrin–polycation–DNA complexes: the effect of polycations on the structure of the complex and DNA delivery to cells. *Proc. Natl Acad. Sci. USA* 88: 4255–4259 (1991).
183. Hansma HG, Golan R, Hsieh W, Lollo CP, Mullen-Ley P, Kwoh D: DNA condensation for gene therapy as monitored by atomic force microscopy. *Nucleic Acids Res* 26: 2481–2487 (1998).
184. Sørensen DR, Leirdal M, and Sioud M: Gene silencing by systemic delivery of synthetic siRNAs in adult mice. *J Mol Biol*, 327: 761–766 (2003).
185. Landen CN Jr, Chavez-Reyes A, Bucana C, Schmandt R, Deavers MT, Lopez-Berestein G, Sood AK: Therapeutic EphA2 gene targeting *in vivo* using neutral liposomal small interfering RNA delivery. *Cancer Res* 65: 6910–6918 (2005).
186. Zimmermann TS, Lee AC, Akinc A, Bramlage B, Bumcrot D, Fedoruk MN, Harborth J, Heyes JA, Ješs LB, John M, Judge AD, Lam K, McClintock K, Nechev LV, Palmer LR, Racie T, Rohl I, Seišert S, Shanmugam S, Sood V, Soutschek J, Toudjarska I, Wheat AJ, Yaworski E, Zedalis W, Koteliansky V, Manoharan M, Vornlocher HP and MacLachlan I: RNAi-mediated gene silencing in non-human primates. *Nature* 441: 111–114 (2006).
187. Zhang C, Tang N, Liu XJ, Liang W, Xu W, Torchilin VP: siRNA-containing liposomes modified with polyarginine effectively silence the targeted gene. *Journal of Controlled Release* 112: 229–239 (2006).
188. Gregoriadis G, Wills EJ, Swain CP, Tavill AS: Drug-carrier potential of liposomes in cancer chemotherapy. *Lancet*, I: 1313–1316 (1974).
189. Ishida T, Harashima H, Kiwada H: Liposome Clearance. *Bioscience Reports* 22(2):197–224 (2002).
190. Zelphati O, Uyechi LS, Barron LG, Szoka FC Jr: Effect of serum components on the physico-chemical properties of cationic lipid/oligonucleotide complexes and on their interactions with cells. *Biochimica et Biophysica Acta* 1390:119–133 (1998).
191. Matsumura Y, Maeda H: A new concept for macromolecular therapeutics in cancer chemotherapy: mechanism of tumorotropic accumulation of proteins and the antitumor agent smancs. *Cancer Res* 46:6387–6392 (1986).
192. Seymour LW: Passive tumor targeting of soluble macromolecules and drug conjugates. *Crit Rev Ther Drug Carrier Syst* 9:135–187 (1992).
193. Maeda H, Wu J, Sawa T, Matsumura Y, Hori K: Tumor vascular permeability and the EPR effect in macromolecular therapeutics: a review. *J. Controlled Release* 65: 271–284 (2000).
194. Rijnboutt S, Jansen G, Posthuma G, Hynes JB, Schornagel JH, Strous GJ: Endocytosis of GPI-linked membrane folate receptor  $\alpha$ . *J Cell Biol* 132:35–47 (1996).
195. Wu M, Gunning W, Ratnam M: Expression of folate receptor type in relation to cell type, malignancy, and differentiation in

- ovary, uterus, and cervix. *Cancer Epidemiol Biomarkers Prev* 8:775–782 (1999).
196. Weitman SD, Lark RH, Coney LR, Fort DW, Frasca V, Zurawski VR Jr, Kamen BA: Distribution of the folate receptor GP38 in normal and malignant cell lines and tissues. *Cancer Res* 52:3396–3401 (1992).
197. Garin-Chesa P, Campbell I, Saigo PE, Lewis JL, Old LJ, Rettig WJ: Trophoblast and ovarian cancer antigen LK26. Sensitivity and specificity in immunopathology and molecular identification as a folate-binding protein. *Am J Pathol* 142:557-567 (1993).
198. Ross JF, Chaudhuri PK, Ratnam M: Differential regulation of folate receptor isoforms in normal and malignant tissues *in vivo* and in established cell lines. Physiologic and clinical implications. *Cancer* 73:2432–2443 (1994).
199. Goren D, Horowitz AT, Tzemach D, Tarshish M, Zalipsky S, Gabizon A: Nuclear delivery of doxorubicin via folate targeted liposomes with bypass of multidrug-resistance efflux pump. *Clin. Cancer Res* 6 : 1949-1957 (2000).
200. Weitman SD, Weinberg AG, Coney LR, Zurawski VR, Jennings DS, Kamen BA: Cellular localization of the folate receptor: potential role in drug toxicity and folate homeostasis. *Cancer Res* 52: 6708-6711 (1992).
201. Melani C, Figini M, Nicosia D, Luison E, Ramakrishna V, Casorati G, Parmiani G, Eshhar Z, Canevari S, Colombo MP: Targeting of interleukin 2 to human ovarian carcinoma by fusion with a single-chain FR of antifolate receptor antibody. *Cancer Res* 58: 4146-4154 (1998).
202. Leamon CP, Low PS: Delivery of macromolecules into living cells: a method that exploits folate receptor endocytosis. *Proc. Natl Acad. Sci. USA* 88:5572–5576 (1991).
203. Lee RJ, Low PS: Delivery of liposomes into cultured KB cells via folate receptor-mediated endocytosis. *J Biol Chem* 269: 3198–3204 (1994).
204. Lu Y, Low PS: Folate-mediated delivery of macromolecular anticancer therapeutic agents. *Adv. Drug Deliv. Rev* 54: 675-693 (2002).
205. Gabizon A, Shmeeda H, Horowitz AT, Zalipsky S: Tumor cell targeting of liposome-entrapped drugs with phospholipid-anchored folic acid-PEG conjugates. *Adv. Drug Deliv. Rev* 56: 1177-1192 (2004).
206. Reddy JA, Abburi C, Hofland H, Howard SJ, Vlahov I, Wils P, Leamon CP: Folate-targeted, cationic liposomemediated gene transfer into disseminated peritoneal tumors. *Gene Ther* 9: 1542-1550 (2002).
207. Leamon CP, Cooper SR, Hardee GE: Folate liposome-mediated antisense oligodeoxynucleotide targeting to cancer cells: evaluation *in vitro* and *in vivo*. *Bioconjug. Chem* 14: 738-747 (2003).
208. Ni S, Stephenson SM, Lee RJ: Folate receptor targeted delivery of liposomal daunorubicin into tumor cells. *Anticancer Res* 22: 2131–2135 (2002).
209. Pan XQ, Wang H, Lee RJ: Antitumor activity of folate receptor-targeted liposomal doxorubicin in a KB oral carcinoma murine xenograft model. *Pharm. Res* 20: 417–422 (2003).
210. Pan XQ, Zheng X, Shi G, Wang H, Ratnam M, Lee RJ: Strategy for the treatment of acute myelogenous leukemia based on folate receptor  $\beta$ -targeted liposomal doxorubicin combined with receptor induction using all-trans retinoic acid. *Blood* 100: 594–602 (2002).
211. Lu Y, Low PS: Folate targeting of haptens to cancer cell surfaces mediates immunotherapy of syngeneic murine tumors. *Cancer Immunol. Immunother* 51: 153–162 (2002).
212. Stephenson SM, Yang W, Stevens PJ, Tjarks W, Barth RF, Lee RJ: Folate receptor-targeted liposomes as possible delivery vehicles for boron neutron capture therapy. *Anticancer Res* 23: 3341-3345 (2003).
213. Kim SH, Mok H, Jeong JH, Kim SW, Park TG: Comparative Evaluation of Target-Specific GFP Gene Silencing Efficiencies

- for Antisense ODN, Synthetic siRNA, and siRNA Plasmid Complexed with PEI-PEG-FOL Conjugate. *Bioconjugate Chem* 17 (1): 241-244 (2006).
214. Frey H, Haag R: Dendritic polyglycerol: a new versatile biocompatible Material. *Reviews in Molecular Biotechnology* 90: 257-267 (2002).
215. Gottschalk C, Wolf F, Frey H: Multi-Arm Star Poly(L-lactide) with Hyperbranched Polyglycerol Core. *Macromolecular Chemistry and Physics* 208: 1657-1665 (2007).
216. Tziveleka LA, Kontoyianni C, Sideratou Z, Tsiourvas D, Paleos CM: Novel functional Hyperbranched Polyether Polyols as Prospected Drug Delivery Systems. *Macromol. Biosci* 6: 161-169 (2006).
217. Livak KJ, Schmittgen TD: Analysis of relative gene expression data using real-time quantitative PCR and the 2(-Delta Delta C(T)) Method. *Methods* 25: 402-408 (2001).
218. Mörtelmaier M, Kögler DJ, Hesse J, Sonnleitner M, Huber LA, Schutz GJ: Single molecule microscopy in living cells: Subtraction of autofluorescence based on two color recording. *Single Mol* 3: 225-231 (2003).
219. Huwyler J, Wu D, Partridge WM: Brain drug delivery of small molecules using immunoliposomes, *Proc Natl Acad Sci USA* 93: 14164-14169 (1996).
220. Hilf R, Havens JJ, Gibson SL: Effect of delta-aminolevulinic acid on protoporphyrin IX accumulation in tumor cells transfected with plasmids containing porphobilinogen deaminase DNA. *Photochem Photobiol* 70: 334-340 (1999).
221. Ferreira GC: Ferrochelatase. *Int. J. Biochem. Cell Biol* 31: 995-1000 (1999).
222. Schoenfeld N, Epstein O, Lahav M, Mamet R, Shaklai M, Atsmon A: The heme biosynthetic pathway in lymphocytes of patients with malignant lymphoproliferative disorders. *Cancer Letters (Shannon, Ireland)* 43: 43-48 (1988).
223. Dailey HA, Smith A: Differential interaction of porphyrins used in photoradiation therapy with Ferrochelatase. *Biochem J* 223: 441-445 (1984).
224. Heidersbach A, Gaspar-Maia A, McManus MT, Ramalho-Santos M: RNA interference in embryonic stem cells and the prospects for future therapies. *Gene Therapy* 13: 478-486 (2006).
225. Agostini F, Dapas B, Farra R, Grassi M, Racchi G, Klingel K, Kardolf R, Heindenreich O, Mercatanti A, Rainaldi G, Altamura N, Guarnieri G, Grassi G: Potential applications of small interfering RNAs in the cardiovascular field. *Drugs of the Future* 31(6): 513-525 (2006).
226. Ragusa A, García I, Penadés S: Nanoparticles as Nonviral Gene Delivery Vectors. *NanoBioscience, IEEE* 6: 319-330 (2007).
227. Lasic DD: Recent developments in medical applications of liposomes: sterically stabilized liposomes in cancer therapy and gene delivery. *J Controlled Release* 48:203-222 (1997).
228. Behr JP: The proton sponge: a trick to enter cells the viruses did not exploit. *Chimia* 51: 34-36 (1997).
229. Sonawane ND, Szoka RC, Verkman AS: Chloride accumulation and swelling in endosomes enhances DNA transfer by polyamine-DNA polyplexes. *J Biol Chem* 278: 44826-44831 (2003).
230. Harashima H, Hiraiwa T, Ochi Y, Kiwada H: Size dependent liposome degradation in blood: *in vivo/in vitro* correlation by kinetic modelling. *J Drug Target* 3:253-261 (1995).
231. Litzinger DC, Buiting AMJ, Rooijen NV, Huang L: Effect of liposome size on the circulation time and intraorgan distribution of amphipathic poly(ethylene glycol)-containing liposomes. *Biochim Biophys. Acta* 1190:99-107 (1994).
232. Drummond DC, Meyer O, Hong K, Kirpotin DB, Papahadjopoulos D: Optimizing Liposomes for Delivery of Chemotherapeutic Agents to Solid Tumors. *Pharmacol Rev* 51: 691-744 (1999).

233. Abra RM, Hunt CA: Liposome disposition *in vivo*. III. Dose and vesicle-size effects. *Biochim Biophys Acta* 666: 493-503 (1981).
234. Senior JH: Fate and behaviour of liposomes *in vivo*: A review of controlling factors. *CRC Crit Rev Ther Drug Carrier Syst* 3: 123-193 (1987).
235. Olson F, Hunt CA, Szoka FC, Vail WJ, Papahadjopoulos D: Preparation of liposomes of defined size distribution by extrusion through polycarbonate membranes. *Biochim Biophys Acta* 557: 9-23 (1979).
236. Szoka F, Olson F, Heath T, Vail W, Mayhew E, Papahadjopoulos D: Preparation of unilamellar liposomes of intermediate size (0.1-0.2  $\mu\text{m}$ ) by a combination of reverse phase evaporation and extrusion through polycarbonate membranes. *Biochim Biophys Acta* 601: 559-571 (1980).
237. Gabizon A, Price DC, Huberty J, Bresalier RS, Papahadjopoulos D: Effect of liposome composition and other factors on the targeting of liposomes to experimental tumours: biodistribution and imaging studies. *Cancer Res* 50:6371-6378 (1990).
238. Papahadjopoulos D, Allen TM, Gabizon A, Mayhew E, Matthay K, Huang SK, Lee KD, Woodle MC, Lasic DD, Redemann C, Martin FJ: Sterically stabilized liposomes: improvements in pharmacokinetics and antitumour therapeutic efficacy. *Proc Natl Acad Sci USA* 88:11460-11464 (1991).
239. Wu NZ, Da D, Rudoll TL, Needham D, Whorton AR, Dewhirst MW: Increased microvascular permeability contributes to preferential accumulation of stealth liposomes in tumor-tissue. *Cancer Res* 53:3765-3770 (1993).
240. Huang SK, Lee KD, Hong K, Friend DS, Papahadjopoulos D: Microscopic localization of sterically stabilized liposomes in colon carcinoma-bearing mice. *Cancer Res* 52: 5135-5143 (1992).
241. Lum H, Malik A: Regulation of vascular endothelial barrier function. *Am. J. Physiol* 267: L223-L241 (1994).
242. Minchinton AI, Tannock IF: Drug penetration in solid tumours. *Nature Reviews Cancer* 6: 583-592 (2006).
243. Allen TM, Cullis PR: Drug Delivery Systems: Entering the Mainstream. *Science* 303:1818-1822 (2004).
244. Moein Moghimi S, Christy Hunter A, Clifford Murray J: Long-Circulating and Target-Specific Nanoparticles: Theory to Practice. *Pharmacol. Rev* 53: 283-318 (2001).
245. Jain RK: Transport of molecules across tumor vasculature. *Cancer Metastasis Rev* 6(4):559-593 (1987).
246. Northfelt DW, Martin FJ, Working P, Volberding PA, Russell J, Newman M, Amantea MA, Kaplan LD: Doxorubicin encapsulated in liposomes containing surface-bound polyethylene glycol: pharmacokinetics, tumor localization, and safety in patients with AIDS-related Kaposi's sarcoma. *J. Clin. Pharmacol* 36: 55-63 (1996).
247. Rostgaard J, Qvortrup K: Sieve Plugs in Fenestrae of Glomerular Capillaries - Site of the Filtration Barrier? *Cells Tissues Organs* 170(2-3):132-138 (2002).
248. Jhaveri MS, Rait AS, Chung KN, Trepel JB, Chang EH: Antisense oligonucleotides targeted to the human  $\alpha$ folate receptor inhibit breast cancer cell growth and sensitize the cells to doxorubicin treatment. *Mol Cancer Ther* 3:1505-1512 (2004).
249. Gabizon AA: Stealth Liposomes and Tumor Targeting: One Step Further in the Quest for the Magic Bullet. *Clinical Cancer Research* 7: 223-225 (2001).
250. Kainthana RK, Gnanamanib M, Ganguli M, Ghosh T, Brooks DE, Maiti S, Kizhakkedathu JN: Blood compatibility of novel water soluble hyperbranched polyglycerol-based multivalent cationic polymers and their interaction with DNA. *Biomaterials* 27: 5377-5390 (2006).
251. Felgner PL, Gadek TR, Holm M, Roman R, Chan HW, Wenz M, Northrop JP, Ringold GM, Danielsen M: Lipofection: a highly efficient, lipidmediated DNA-transfection procedure. *Proc. Natl Acad. Sci. USA* 84: 7413-7417 (1987).
252. Gene Therapy Clinical Trials. The Journal of Gene Medicine online. <http://www.wiley.co.uk/genetherapy/clinical/>

253. Chaudhury NK, Chandra S, Mathew TL: Oncologic Applications of Biophotonics: Prospects and Problems. Applied Biochemistry and Biotechnology 96: 183-204 (2001).
254. Mehlmann M, Betz CS, Stepp H, Arbogast S, Baumgartner R, Grevers G, Leunig A: Fluorescence staining of laryngeal neoplasms after topical application of 5-aminolevulinic acid: preliminary results. Lasers Surg Med 25(5):414-420 (1999).
255. Otake M, Nishiwaki M, Kobayashi Y, Baba S, Kohno E, Kawasaki T, Fujise Y, Nakamura H: Selective accumulation of ALA-induced PpIX and photodynamic effect in chemically induced hepatocellular carcinoma. British Journal of Cancer 89: 730-736 (2003).
256. Henderson BW, Vaughan L, Bellnier DA, van Leengoed H, Johnson PG, Oseroff AR: Photosensitization of murine tumor, vasculature and skin by using 5-aminolevulinic acid-induced porphyrin. Photochem Photobiol 62: 780-789 (1995).
257. Wyss P, Svaasand LO, Tadir Y, Haller U, Berns MW, Wyss MT, Tromberg BJ: Photomedicine of the endometrium: experimental concepts. Hum Reprod 10(1):221-226 (1995).
258. Kimel S, Tromberg BJ, Roberts WG, Berns MW: Singlet oxygen generation of porphyrins, chlorins and phthalocyanines. Photochem. Photobiol 50:175-183 (1989).
259. Faris F, Thorniley M, Wickramasinghe Y, Houston R, Rolfe P, Livera N, Spencer A: Non-invasive *in vivo* near-infrared optical measurement of the penetration depth in the neonatal head. Clin Phys Physiol Meas 12(4):353-358 (1991).
260. Yamada KM and Clark K: Cell biology: Survival in three dimensions. Nature 419: 790-791 (2002).
261. Frank SA: Dynamics of Cancer. Princeton University Press, Princeton and Oxford (2007).
262. Fléjou JF: Barrett's oesophagus: from metaplasia to dysplasia and cancer. Gut 54 Suppl 1:i6-12 (2005).

## Abbreviations

<b>AKs</b>	Actinic keratoses
<b>ALA</b>	$\delta$ -Aminolevulinic acid
<b>ALAS</b>	$\delta$ -Aminolevulinate synthase
<b>ALAD</b>	$\delta$ -Aminolevulinate dehydratase
<b>2', 5'AS</b>	2', 5' Adenylate Synthetase
<b>BSA</b>	Bovine serum albumin
<b>CCD</b>	Charge-coupled device
<b>CIS</b>	Carcinoma <i>in situ</i>
<b>CO</b>	Carbon monoxide
<b>CSF</b>	Cerebrospinal fluid
<b>CT</b>	Computerized tomography
<b>DB</b>	Degree of branching
<b>DF</b>	Degree of functionalisation
<b>DMEM</b>	Dulbecco's modified Eagle's medium
<b>dsRNA</b>	Double strand RNA
<b>EDTA</b>	Ethylenediaminetetraacetic acid
<b>eIF2<math>\alpha</math></b>	Elongation initiation factor 2 $\alpha$
<b>EPR effect</b>	Enhanced permeability and retention effect
<b>FBS</b>	Fetal bovine serum
<b>FDA</b>	Food and Drug Administration
<b>FECH</b>	Ferrochelatase
<b>Fe/S cluster</b>	[2Fe-2S] iron-sulfur clusters
<b>FR</b>	Folate receptor
<b>GABA</b>	G-aminobutyric acid
<b>GI</b>	Gastro-intestinal tract
<b>HO</b>	Heme oxygenase
<b>HPD</b>	Hematoporphyrin Derivative
<b>HPLC</b>	High performance liquid chromatography
<b>IR</b>	Infrared
<b>MRI</b>	Magnetic resonance imaging
<b>NADH</b>	Nicotinamide adenine dinucleotide
<b>NADPH</b>	Nicotinamide adenine dinucleotide phosphate
<b>Na<sup>+</sup> K<sup>+</sup>ATPase</b>	Sodium potassium ATPase
<b>NIR</b>	Near infrared
<b>NO</b>	Nitric oxide
<b>PAMAM</b>	Polyamidoamine
<b>PBS</b>	Phosphate buffered saline

<b>PBGD</b>	Porphobilinogen deaminase
<b>PDD</b>	Photodynamic diagnosis
<b>PDT</b>	Photodynamic therapy
<b>PEG</b>	Polyethylene glycols
<b>PEI</b>	Polyethylenimine
<b>PG</b>	Polyglycerol
<b>PKR</b>	Protein Kinase R
<b>PLL</b>	Poly-L-lysine
<b>PpIX</b>	Protoporphyrin IX
<b>RNAi</b>	RNA interference
<b>RES</b>	Reticuloendothelial system
<b>RISC</b>	RNA-induced silencing complex
<b>RT-PCR</b>	Reverse transcription polymerase chain reaction
<b>SD</b>	Standard deviations
<b>siRNA</b>	small interfering RNA
<b>shRNA</b>	small hairpins RNA
<b>UV</b>	Ultraviolet
$\lambda_{ex}$	Excitation wavelength
$\lambda_{em}$	Emission wavelength